FLUTTER AND FORCED RESPONSE OF MISTUNED ROTORS USING STANDING WAVE ANALYSIS

David J. Bundas

John Dugundji

GT&PDL Report No. 170 March 1983

ABSTRACT

The torsion flutter and forced response of tuned and mistuned cascades is examined using a standing wave approach, as opposed to the traditional traveling wave approach used in cascades aerodynamic models. The motion of the blades and the corresponding cascade aerodynamic loads are expressed in terms of standing wave modes and arbitrary transient motion, by fitting the sinusoidal force coefficients in terms of ratios of polynomials in the Laplace transform variable, sometimes referred to as Padé approximants. Whitehead's two dimensional, incompressible aerodynamic model is expressed in this transient form and is used to solve the flutter and forced response problems. Results obtained with the transient, standing wave analysis for the flutter and forced response are similar to those obtained by traveling wave analyses, but they yield the transient decay rate associated with vibrations of the blades, as opposed to the structural damping required for flutter obtained by the traveling method.

The standing wave analysis presented here may prove to be more versatile for dealing with certain applications such as mistuned rotors, "localized" blade flutter, low engine order excitation, transient impulses on the rotor, and coupling in with forced response and dynamic shaft problems.

ACKNOWLEDGEMENTS

The authors would also like to acknowledge helpful discussions with Professor Edward Crawley, Ken Hall, and Dinkar Mokadam during the preparation of this thesis. This work was supported by NASA Grant No. NAG3-214, with NASA Lewis Research Center. Dr. Robert E. Kielb was the Technical officer.

The present document constitutes for the most part, an M.S. thesis by the first author.

TABLE OF CONTENTS

NOMENCLATURE

A_A, A_B, A_C, A_D	nondimensional traveling wave force coefficients as they enter (2-40) and (2-41), $= (A_{AR} + iA_{AI})$, etc.
A^+, A^-	nondimensional aerodynamic coefficients associated with forward and backward traveling waves, $= (A^+_{AR} + iA^+_{AI})$, etc.
$\bar{A}_R, \bar{A}_I, \bar{\bar{A}}_R, \bar{\bar{A}}_I$	defined by (2-10)
$\underset{\sim}{A}, \underset{\sim}{B}$	matrices of first order form of equations of motion, defined by (3-18) for the tuned cascade, and by (3-33) for the mistuned cascade
A, B, C, D	coefficients of cubic equation, (3-8)
a	real part of eigenvalue
a	elastic axis location in semichords aft of midchord
$B_2, B_1, B_0, \tilde{B}_2, \tilde{B}_1, \tilde{B}_0$	coefficients of transient, standing wave form of airloads
$\underset{\sim}{B}_2, \underset{\sim}{B}_1, \underset{\sim}{B}_0$	matrices of coefficients of transient, standing wave form of airloads, defined by (2-38) for the tuned cascade, and by (2-42) for the mistuned cascade
b	semichord
$C_{Fq}, C_{F\alpha}, C_{Mq}, C_{M\alpha}$	force and moment coefficients as defined

by Whitehead [2]

$C(k)$	Theodorsen Function
$\underset{\sim}{C}$	matrix defined by (3-17)
$\underset{\sim}{D}$	matrix defined by (3-31)
G	imaginary part of Theodorsen Function
$\underset{\sim}{E}$	vector of applied loads in first order form of equations of motion
f_{cn}, f_{sn}	nondimensional coefficients associated with components of engine order excitation
F	real part of Theodorsen Function
$G_1, g_0, \tilde{G}_1$	coefficients of transient form of airloads
$\underset{\sim}{G}_1, \underset{\sim}{g}_0$	matrices of coefficients of transient, standing wave form of airloads, defined by (2-38) for the tuned cascade, and by (2-42) for the mistuned cascade
h	displacement of blade
$\bar{h}$	magnitude of blade displacement
$\underset{\sim}{I}$	identity matrix
I_α	mass moment of inertia
I_{AVG}	average mass moment of inertia
I_o	reference mass moment of inertia
I_{high}, I_{low}	inertia associated with the high and low frequency blades of a mistuned cascade, respectively
j	blade number
k	reduced frequency, $\omega b / U$

$k_{\alpha j}$	torsional stiffness of blade j
$\mathcal{L}[\ ]$	Laplace transform
l	lift on section of isolated airfoil
m	aerodynamic moment acting on section of isolated airfoil
m_j	aerodynamic moment acting on section of blade j
m_j^D	disturbance moment acting on blade j
m_j^{D*}	nondimensional disturbance moment acting on blade j
N	number of blades
n	engine order
$\underset{\sim}{P}$	transformation matrix of blade coordinates and multiblade coordinates
$\tilde{p}$	nondimensional eigenvalue, $= \alpha/\omega_0 + i\,\omega/\omega_0$
q_{cr}, q_{sr}	multiblade coordinates
$\underset{\sim}{q}$	vector of multiblade coordinates
$\underset{\sim}{\bar{q}}$	eigenvector of multiblade coordinates
r	mode number, number of nodal diameters
s'	Laplace transform variable
R	radius of rotor to section of blade under consideration
$\underset{\sim}{T}$	matrix defined by (4-7)
t	time
u	velocity at blade
$\bar{u}$	reduced velocity, $u/\omega_0 b$

$\underset{\sim}{X}$	vector of modal coordinates of first order form of equations of motion
Y_{cr}, Y_{sr}	coordinates associated with augmented equation of standing wave form of airloads
$\underset{\sim}{Y}$	vector of coordinates, Y_{cr}, Y_{sr}
α	rotation of isolated airfoil
α_j	rotation of blade j
$\bar{\alpha}$	complex magnitude of torsional vibration
$\bar{\alpha}_r$	modal coordinate associated with traveling wave having interblade phase angle
$\lvert\alpha\rvert$	magnitude of torsional vibration of blade j
β_r	interblade phase angle, $= 2\pi r/N$
γ_α	undamped natural frequency ratio, $=\omega_\alpha/\omega_b$
γ	frequency ratio of vibration, $=\omega/\omega_b$
δ_{rn}	Kronecker delta
g	structural damping
g_A	aerodynamic damping
η	elastic axis location in % chord aft of leading edge
$\bar{\theta}_j$	position of blade j with respect to fixed, non-rotating axes
θ_j	position of blade j with respect to axes fixed to disk

ν	inertia ratio
ξ	stagger angle
ρ	density of air
τ	nondimensional time
ϕ_j	phase angle of vibration of blade j
ψ	Küssner Function
ω	frequency of vibration
$\omega_{\alpha j}$	natural torsional frequency of vibration of blade j
$\omega_{high}, \omega_{low}$	natural frequencies of high and low frequency blades of a mistuned cascade
ω_o	reference frequency, average frequency
Ω	angular velocity of rotor

Subscripts

$\underset{\sim}{(\ )}$	matrix
$(\dot{\ })$	d/dt
$(\overset{o}{\ })$	d/dτ
j	blade number

1. Introduction

Most work involving the aeroelastic stability and response of cascades makes use of cascade aerodynamic models which assume that all blade motions are sinusoidal. Modes of motion are represented by waves traveling around the circumference of the rotor. Dugundji [1] has shown that the traveling wave modes can be expressed in terms of standing wave modes, which are traditionally used in solving the fixed wing flutter problem. One advantage of this method is that the equations of motion for rotating structures and "static" structures can be easily joined. Eventually, problems of blade-disk coupling and shaft motions can be more easily handled by this method. The casting of the cascade traveling wave airloads into standing wave form is detailed in Chapter 2.

Whitehead [2] gives a good history of the early development of cascade aerodynamic models. His model for a two-dimensional, incompressible fluid with flat plate airfoils is used in this work. Smith [3] has extended to subsonic compressible flow, and Adamczyck and Goldstein [4], among others, to the supersonic cascade with subsonic axial flow. More recently, computational fluid dynamics has been used by Whitehead [5] to obtain the airforces for the two-dimensional high deflection cascade with subsonic axial flow. In each of these models, the force coefficients can be expressed as a complex number depending on the frequency of vibration and other flight and geometric parameters. Using these methods to generate airload coefficients requires a lengthy computation for each frequency of vibration desired. To solve the flutter problem the V-g method is used, whereby the structural damping required

for flutter is obtained.

When control and aeroelastic interactions of fixed wing aircraft are being examined, the airloads must be in a form suitable for general motions of the airfoil. Edwards, Ashley and Breakwell [6] have shown that through the use of Laplace Transforms, the complete unsteady airloads acting on an isolated airfoil can be approximated by a ratio of polynomials, and that a transient form of the airloads can be expressed. The present work extends these ideas to cascade aerodynamics, expressing the airloads in a transient form so that the airloads due to general motions of the airfoils can be determined. In solving the flutter problem, it is no longer necessary to know the frequency of vibration when computing coefficients. In addition, the actual transient decay of the motion is obtained. In Chapter 3, the transient form of the airloads is applied to solving the torsion flutter problem. The isolated airfoil stability is compared to the tuned cascade stability, and the effect of mistuning is introduced.

Mistuning, or differences in natural frequencies, stiffnesses, and inertias between blades is being studied as a possible passive control of turbomachinery flutter and forced response. Srinivasan [7] has demonstrated the beneficial effect of mistuning on torsion flutter and Kaza and Kielb [8] have shown that mistuning often has a beneficial effect on the bending-torsion flutter speed and an adverse effect on the forced response of the cascade. The present work duplicates these results for the torsion degree of freedom using airforces expressed in a transient, standing wave form.

The effects of mistuning on the forced response are discussed in Chapter 4. The fact that the airloads are expressed in terms of general motion allows a quick solution of the response problem. If the airloads were expressed in terms of traveling waves, then the airloads must be recalculated for each frequency. To demonstrate the transient form of the airloads, the response of a cascade to an impulsive loading of one blade is calculated.

Chapter 5 deals with the extensions of these standing wave methods to deal with flexible disk rotors. Also these methods are applied to give the cascade aerodynamic influence coefficients, that is, the effect of the motions of one blade on the forces produced at another blade.

2. Transient Cascade Airforces

Unsteady cascade aerodynamic theories have been under development since the early 1950's. Each of these theories makes the assumption that the airfoil motion is sinusoidal. Edwards et. al. [6], and Vepa [9] give a method for obtaining airloads due to general motions of an airfoil using the Theodorsen function. This method was developed to study active control of aeroelastic structures, and is based on the approximation of the unsteady air loads by ratios of polynomials in the Laplace transform variable, sometimes refered to as Padé approximants.

2.1 Standing Wave Representation

The cascade aerodynamic theories were developed for harmonic vibrations that can be represented by traveling waves moving around the circumference of the disk. For a tuned rotor, each of the blades will have the same amplitude and interblade phase angle for a given mode of vibration. The torsional amplitude, α_j, of each blade in such a cascade can be written in terms of a traveling wave mode as,

$$\alpha_j = \bar{\alpha}_r e^{i(\omega t + j\beta_r)} \qquad (2\text{-}1)$$

where

$\beta_r = \frac{2\pi r}{N}$, interblade phase angle

j = blade number

N = number of blades

r = mode number, number of nodal diameters

$\bar{\alpha}_r$ = modal amplitude

See figure 1.

The airforces corresponding to such a vibration can be expressed as,

$$m_j = 2\pi\rho U^2 b^2 (A_R + iA_I)_r \bar{\alpha}_r e^{i(\omega t + j\beta_r)} \qquad (2\text{-}2)$$

Here the aerodynamic moment per unit span due to pitching motion, m_j, of each blade is given in terms of a traveling wave mode, where the nondimensional complex aerodynamic coefficient (A_R+iA_I) is associated with the interblade phase angle β_r. For a mistuned cascade, the blades no longer vibrate with the same amplitude or constant interblade phase angle. In order to specify the N magnitudes and N phase angles of the motion of each blade of an arbitrarily mistuned N-bladed rotor, the solution must contain 2xN constants. To obtain solutions, then, one sums over all nodal diameter traveling wave modes,

$$\alpha_j = \sum_{r=0}^{N-1} \bar{\alpha}_r e^{i(\omega t + j\beta_r)} \qquad (2-3)$$

Here, there are N modal amplitudes, $\bar{\alpha}_r$, and N modal phase angles, β_r. When summed, the blade amplitudes and blade phase angles are reconstructed. The corresponding airforces are summed also as follows,

$$m_j = 2\pi\rho U^2 b^2 \sum_{r=0}^{N-1} (A_R + iA_I)_r \bar{\alpha}_r e^{i(\omega t + j\beta_r)} \qquad (2-4)$$

An alternative, based on standing wave modes is discussed by Dugundji [1]. The use of standing wave analysis is traditional when studying the flutter of aircraft wings. In the present analysis, deflections are represented by standing wave modes of the form

$$\alpha_j = q_{cr}(t) \cos j\beta_r \qquad (2-5)$$

where q_{cr} is a generalized coordinate, and is in general a function of time. For example, if $\beta_r = 0$ the motion represented would be the "umbrella" mode, where all blades move in unison. To show that the traveling wave representation and the standing wave representation are equivalent, add two traveling waves of the form (2-1), traveling in opposite directions (+j and -j) with equal amplitudes $\bar{\alpha}_r$, and take the real part,

$$\alpha_j = \frac{\bar{\alpha}_r}{2}\cos(\omega t + j\beta_r) + \frac{\bar{\alpha}_r}{2}\cos(\omega t - j\beta_r) \qquad (2\text{-}6)$$

Expanding and combining terms leaves

$$\alpha_j = \bar{\alpha}_r \cos\omega t \cos j\beta_r \qquad (2\text{-}7)$$

which is of the form (2-5) for $q_{bc_r}(t)=\bar{\alpha}_r\cos\omega t$. The form of the standing wave airforces can be determined in a similar manner. Adding the traveling wave airforces associated with +j and -j directions gives,

$$m_j = 2\pi\rho u^2 b^2\left[(A_R^+ + iA_I^+)\frac{\bar{\alpha}_r}{2}e^{i(\omega t + j\beta_r)} + (\bar{A}_R + i\bar{A}_I)\frac{\bar{\alpha}_r}{2}e^{i(\omega t - j\beta_r)}\right] \qquad (2\text{-}8)$$

Here, $(A_R^+ + iA_I^+)$ refers to the complex aerodynamic coefficients associated with the traveling wave having an interblade phase angle β_r, while the coefficient $(\bar{A}_R + i\bar{A}_I)$ is associated with the traveling wave having an interblade phase angle $-\beta_r$, or $(360-\beta_r)$. By examining the motion associated with these traveling waves, the direction of the wave can be determined. Interblade phase angles between $\beta_r = 0$ degrees and $\beta_r = 180$ degrees are associated with forward (in the direction of rotation) traveling waves, while interblade phase angles between $\beta_r = -180$ degrees and $\beta_r = 0$ degrees are associated with backward traveling waves. Expanding (2-8), taking only the real part and combining terms, yields

$$m_j = 2\pi\rho u^2 b^2 \{[\bar{A}_R \bar{\alpha}_r \cos\omega t - \bar{A}_I \bar{\alpha}_r \sin\omega t]\cos j\beta_r$$

$$+[-\bar{\bar{A}}_I \bar{\alpha}_r \cos\omega t - \bar{\bar{A}}_R \bar{\alpha}_r \sin\omega t]\sin j\beta_r\} \qquad (2\text{-}9)$$

where

$$\bar{A}_R = \tfrac{1}{2}(A_R^+ + A_R^-)$$
$$\bar{A}_I = \tfrac{1}{2}(A_I^+ + A_I^-)$$
$$\bar{\bar{A}}_R = \tfrac{1}{2}(A_R^+ - A_R^-)$$
$$\bar{\bar{A}}_I = \tfrac{1}{2}(A_I^+ - A_I^-) \qquad (2\text{-}10)$$

As has already been shown, by comparing (2-7) and (2-5) the expression for the torsional displacement of blade j can be written in terms of an arbitrary function of time and a standing wave mode as,

$$\alpha_j = q_{cr}(t)\cos j\beta_r \qquad (2\text{-}11)$$

The corresponding standing wave form of the moment acting on blade j can be written as,

$$m_j = 2\pi\rho U^2 b^2 \left\{ \left[B_1 \frac{b}{U} \dot{q}_{cr} + B_0 q_{cr} \right] \cos j\beta_r + \left[\tilde{B}_1 \frac{b}{U} \dot{q}_{cr} + \tilde{B}_0 q_{cr} \right] \sin j\beta_r \right\} \qquad (2\text{-}12)$$

Here the aerodynamic moment is given as a function of the displacement and velocity of the generalized coordinate, q_{cr}. By assuming the solution $q_{cr} = \bar{\alpha}_r \cos\omega t$, and comparing (2-9) and (2-12), one can see that the standing wave coefficents B_1, B_0, $\tilde{B}_1$, $\tilde{B}_0$, are related to the traveling wave coefficients $\bar{A}_R$, $\bar{A}_I$, $\bar{\bar{A}}_R$, $\bar{\bar{A}}_I$, by the following relations:

$$\begin{aligned} B_0 &= \bar{A}_R \\ k B_1 &= \bar{A}_I \\ \tilde{B}_0 &= -\bar{\bar{A}}_I \\ k \tilde{B}_1 &= \bar{\bar{A}}_R \end{aligned} \qquad (2\text{-}13)$$

Since the traveling wave coefficients $\bar{A}_R$, $\bar{A}_I$, $\bar{\bar{A}}_R$, and $\bar{\bar{A}}_I$ vary with reduced frequency $k = \omega b/U$, the standing wave coefficients B_1, B_0, $\tilde{B}_1$, and $\tilde{B}_0$ can be used to fit the traveling wave data over a range of frequencies. Equations (2-13) can be solved for the standing wave coefficients. The general motion form of the standing wave aerodynamic moment (2-12) contains information about how the moment would vary for different frequencies of sinusoidal motion, as well as for any arbitrary

motion. The generalized coordinate q_{bcr} is an arbitrary function of time. Again, the standing wave coefficients are in general a function of the interblade phase angle, β_r, gap-to-chord ratio, s/c, and stagger angle, ξ. As an example, coefficients from Whitehead's [2] incompressible, two-dimensional theory were fit using this simple approximation. The approximation to the Whitehead moment using (2-12) is shown by the dashed line in figure 2. In this example, the stagger angle is zero degrees and the forward and backward traveling wave coefficients are identical. Thus, $\bar{\bar{A}}_R$, and $\bar{\bar{A}}_I$ are each equal to zero. The remaining standing wave coefficients are related to the Whitehead coefficient $C_{M\alpha}$ by

$$\bar{A}_R + i\bar{A}_I = 2C_{M\alpha} \tag{2-14}$$

As can be seen in figure 2 this fit (2-13) might be acceptable for low values of reduced frequency, but is poor at higher reduced frequencies. For a more accurate fit of the data the moment acting on blade j can be more generally expressed as,

$$m_j = 2\pi\rho U^2 b^2 \left\{ \left[B_2 \frac{b^2}{U^2}\ddot{q}_{bcr} + B_1 \frac{b}{U}\dot{q}_{bcr} + B_0 q_{bcr} + G_1 Y_{cr} \right] \cos j\beta_r \right.$$
$$\left. + \left[\tilde{B}_2 \frac{b^2}{U^2}\ddot{q}_{bcr} + \tilde{B}_1 \frac{b}{U}\dot{q}_{bcr} + \tilde{B}_0 q_{bcr} + \tilde{G}_1 Y_{cr} \right] \sin j\beta_r \right\} \tag{2-15}$$

$$\frac{b}{U}\dot{Y}_{cr} + g_0 Y_{cr} = \frac{b}{U}\dot{q}_{bcr} \tag{2-16}$$

This representation was motivated by the complete unsteady airforces acting on an isolated airfoil (see [10]). If the coefficient $G_1 = 0$, then B_2 represents a virtual modal mass, B_1 a modal aerodynamic damping, and B_0 a modal aerodynamic stiffness. The coefficient G_1 represents the unsteady aerodynamic effect, or the amount of aerodynamic lag, since by solving (2-16) for Y_{cr} one obtains

$$Y_{cr}(t) = \int_0^t e^{-\frac{q_0 u}{b}(t-\tau)} \dot{q}_{bcr}(\tau)\, d\tau \qquad (2\text{-}17)$$

For a value of $\dot{q}_{cr}$ at time τ, where τ is any time back to 0, the effect on the moment (2-15) increases as t is taken closer and closer to τ. In the limit as $t = \tau$, the term $G_1 Y_{cr}(t)$ reduces to $G_1 q_{bcr}(t)$, another term of the form of an aerodynamic stiffness. That is, the farther in the past the motion $\dot{q}_{cr}$ occurred, the less effect there is on the aerodynamic moment. Hence, an aerodynamic "memory" or "lag" effect. In general, G_1 and $\tilde{G}_1$ contribute to the stiffness and damping, so that B_1 and B_0 alone do not represent the level of modal aerodynamic damping and stiffness, respectively. Note that only one augmented equation is used. Another possible augmented equation for Y_{cr} with $\tilde{q}_c$ is neglected. This does not result in a significant error and it reduces the number of equations describing the moment acting on the blades. Thus for each second order equation expressing the aerodynamic moment for general motions of the airfoil, there is only one first order augmented equation. Solving (2-16) by Laplace transform and substituting into (2-15) gives

$$\mathcal{L}[m_j] = 2\pi\rho U^2 b^2 \left\{ \left[B_2 s^2 + B_1 s + B_0 + \frac{G_1 s}{s+g_0} \right] \cos j\beta_r + \left[\tilde{B}_2 s^2 + \tilde{B}_1 s + \tilde{B}_0 + \frac{\tilde{G}_1 s}{s+g_0} \right] \sin j\beta_r \right\} \mathcal{L}[q_{cr}] \qquad (2\text{-}18)$$

where $s = s'b/u$, and s' is the Laplace transform variable corresponding to time, t. The unsteady effect is contained in the Padé approximants, $G_1 s/s+g_0$ and $\tilde{G}_1 s/s+g_0$.

To obtain the relations between the standing wave coefficients B_2, B_1, B_0, G_1, g_0, $\tilde{B}_2$, $\tilde{B}_1$, $\tilde{B}_0$, and $\tilde{G}_1$, and the given aerodynamic coefficients $\bar{A}_R$, $\bar{A}_I$, $\bar{\bar{A}}_R$, and $\bar{\bar{A}}_I$, in terms of reduced frequency, k, solve (2-16) by substituting $Y_{cr} = Y_{ccr}\cos\omega t + Y_{csr}\sin\omega t$. Then solve for Y_{ccr} and Y_{csr} and substitute back into (2-15). Use the solution $q_{cr} = \bar{\alpha}_r \cos\omega t$ in (2-15) and compare terms with (2-9) to give the new relations between the standing wave coefficients and the traveling wave coefficients as follows,

$$-k^2 B_2 + B_0 + \frac{k^2 G_1}{k^2+g_0^2} = \bar{A}_R$$

$$k B_1 + \frac{k g_0 G_1}{k^2+g_0^2} = \bar{A}_I$$

$$-k^2 \tilde{B}_2 + \tilde{B}_0 + \frac{k^2 \tilde{G}_1}{k^2+g_0^2} = -\bar{\bar{A}}_I$$

$$k \tilde{B}_1 + \frac{k g_0 \tilde{G}_1}{k^2+g_0^2} = \bar{\bar{A}}_R \qquad (2\text{-}19)$$

There are many methods to obtain fits to the traveling wave coefficients using the nine standing wave coefficients B_2, B_1, B_0, G_1, g_0, $\tilde{B}_2$, $\tilde{B}_1$, $\tilde{B}_0$, and $\tilde{G}_1$. Since reduced frequencies at which flutter usually occurs are in the range k = 0 to k = 1, that was the range chosen as the one over which to fit the data. To obtain the standing wave coefficients, the traveling wave coefficients $\bar{A}_R$, $\bar{A}_I$, $\bar{\bar{A}}_R$, and $\bar{\bar{A}}_I$, were fit at k = 0, k = 0.1, and k = 1, and (2-19) was used to solve for the standing wave coefficients. Appendix A has a more complete description of the fitting process. Relations (2-19) give a much better approximation to the Whitehead coefficients than the simpler relations (2-13). (See figure 2.) The coefficients $\bar{A}_R$, $\bar{A}_I$, $\bar{\bar{A}}_R$, and $\bar{\bar{A}}_I$ are related to the forward and backward traveling wave coefficients by the relations (2-10).

The solution for mistuned rotors requires a summing over all the

nodal diameter modes. In addition to the $\cos(j\beta_r)$ modes, the standing wave modes $\sin(j\beta_r)$ must also be represented for a complete solution. The standing wave deflection for $\sin(j\beta_r)$ can be obtained similarly by subtracting the two traveling waves that were added to give (2-7). Reducing leaves,

$$\alpha_j = \bar{\alpha}_r \sin\omega t \sin j\beta_r \qquad (2\text{-}20)$$

which is just a special case of the standing wave deflection pattern,

$$\alpha_j = q_{sr}(t) \sin j\beta_r \qquad (2\text{-}21)$$

The representation of deflections as a pair of waves traveling in opposite direction has been shown equivalent to a pair of standing waves. Corresponding airforces give results of the form (2-15), (2-16), and (2-19).

Summarizing, to represent arbitrary motion and corresponding airforces for a cascade using standing wave modes, the deflections and corresponding airforces can be expressed in the following form,

$$\alpha_j(t) = q_{cr}(t)\cos j\beta_r + q_{sr}(t)\sin j\beta_r \qquad (2\text{-}22)$$

$$m_j = 2\pi\rho u^2 b^2 \Big\{ \Big[B_2 \frac{b^2}{u^2} \ddot{q}_{cr} + B_1 \frac{b}{u} \dot{q}_{cr} + B_0 q_{cr} + G_1 Y_{cr} - \tilde{B}_2 \frac{b^2}{u^2} \ddot{q}_{sr} - \tilde{B}_1 \frac{b}{u} \dot{q}_{sr} - \tilde{B}_0 q_{sr} - \tilde{G}_1 Y_{sr} \Big] \cos j\beta_r + \Big[B_2 \frac{b^2}{u^2} \ddot{q}_{sr} + B_1 \frac{b}{u} \dot{q}_{sr} + B_0 q_{sr} + G_1 Y_{sr} + \tilde{B}_2 \frac{b^2}{u^2} \ddot{q}_{cr} + \tilde{B}_1 \frac{b}{u} \dot{q}_{cr} + \tilde{B}_0 q_{cr} + \tilde{G}_1 Y_{cr} \Big] \sin j\beta_r \Big\} \qquad (2\text{-}23)$$

$$\frac{b}{u} \dot{Y}_{cr} + g_0 Y_{cr} = \frac{b}{u} \dot{q}_{cr} \qquad (2\text{-}24)$$

$$\frac{b}{u} \dot{Y}_{sr} + g_0 Y_{sr} = \frac{b}{u} \dot{q}_{sr} \qquad (2\text{-}25)$$

where B_2, B_1, B_0, G_1, g_0, $\tilde{B}_2$, $\tilde{B}_1$, $\tilde{B}_0$, and $\tilde{G}_1$, are constants obtained by fitting the given sinusoidal traveling wave coefficients by (2-19) and (2-10).

The above procedure can be extended to both bending and torsional motion of the airfoils by expressing the traveling wave deflections, h_j, and rotations, α_j, and the corresponding traveling wave lift, l_j, and moment, m_j, as,

$$\begin{Bmatrix} h_j/b \\ \alpha_j \end{Bmatrix} = \begin{Bmatrix} \bar{h}_r/b \\ \bar{\alpha}_r \end{Bmatrix} e^{i(\omega t + j\beta_r)} \qquad (2-26)$$

$$\begin{Bmatrix} l_j \\ m_j/b \end{Bmatrix} = 2\pi\rho U^2 b \begin{bmatrix} A_A & A_B \\ A_C & A_D \end{bmatrix} \begin{Bmatrix} \bar{h}_r/b \\ \bar{\alpha}_r \end{Bmatrix} e^{i(\omega t + j\beta_r)}$$

where $\bar{h}_r$ and $\bar{\alpha}_r$ are generalized coordinates associated with the traveling wave mode r, and A_A, A_B, A_C, and A_D are nondimensional aerodynamic coefficients for lift due to deflection, lift due to rotation, etc. The coefficient A_A refers to either $(A^+_{AR}+iA^+_{AI})$ or $(A^-_{AR}+iA^-_{AI})$ (depending on the direction of the traveling wave), as they appeared in (2-8). The sign conventions are defined at the leading edge as in figure 3. The relations between the traveling wave coefficients defined above and Whitehead traveling wave coefficients are as follows,

$$\begin{aligned} A_A &= ikC_{Fq} \\ A_B &= -C_{F\alpha} \\ A_C &= -2ikC_{Mq} \\ A_D &= 2C_{M\alpha} \end{aligned} \qquad (2-27)$$

The transient form of the deflections and the corresponding lift and moment acting on blade j for a single pair of standing wave modes can be

expressed as follows,

$$h_j = h_{cr} \cos j\beta_r + h_{sr} \sin j\beta_r$$

$$\alpha_j = \alpha_{cr} \cos j\beta_r + \alpha_{sr} \sin j\beta_r \qquad (2\text{-}28)$$

$$
\begin{aligned}
\ell_j = 2\pi\rho U^2 b \Big\{ \Big[& B_{2A}\frac{b^2}{U^2}\frac{\ddot{h}_{cr}}{b} + B_{1A}\frac{b}{U}\frac{\dot{h}_{cr}}{b} + B_{0A}\frac{h_{cr}}{b} + G_{1A}Y_{hcr} \\
& - \tilde{B}_{2A}\frac{b^2}{U^2}\frac{\ddot{h}_{sr}}{b} - \tilde{B}_{1A}\frac{b}{U}\frac{\dot{h}_{sr}}{b} - \tilde{B}_{0A}\frac{h_{sr}}{b} - \tilde{G}_{1A}Y_{hsr} \\
& + B_{2B}\frac{b^2}{U^2}\ddot{\alpha}_{cr} + B_{1B}\frac{b}{U}\dot{\alpha}_{cr} + B_{0B}\alpha_{cr} + G_{1B}Y_{\alpha cr} \\
& - \tilde{B}_{2B}\frac{b^2}{U^2}\ddot{\alpha}_{sr} - \tilde{B}_{1B}\frac{b}{U}\dot{\alpha}_{sr} - \tilde{B}_{0B}\alpha_{sr} - \tilde{G}_{1B}Y_{\alpha sr}\Big]\cos j\beta_r \\
& + \Big[B_{2A}\frac{b^2}{U^2}\frac{\ddot{h}_{sr}}{b} + B_{1A}\frac{b}{U}\frac{\dot{h}_{sr}}{b} + B_{0A}\frac{h_{sr}}{b} + G_{1A}Y_{hsr} \\
& + \tilde{B}_{2A}\frac{b^2}{U^2}\frac{\ddot{h}_{cr}}{b} + \tilde{B}_{1A}\frac{b}{U}\frac{\dot{h}_{cr}}{b} + \tilde{B}_{0A}\frac{h_{cr}}{b} + \tilde{G}_{1A}Y_{hcr} \\
& + B_{2B}\frac{b^2}{U^2}\ddot{\alpha}_{sr} + B_{1B}\frac{b}{U}\dot{\alpha}_{sr} + B_{0B}\alpha_{sr} + G_{1B}Y_{\alpha sr} \\
& + \tilde{B}_{2B}\frac{b^2}{U^2}\ddot{\alpha}_{cr} + \tilde{B}_{1B}\frac{b}{U}\dot{\alpha}_{cr} + \tilde{B}_{0B}\alpha_{cr} + \tilde{G}_{1B}Y_{\alpha cr}\Big]\sin j\beta_r \Big\}
\end{aligned}
\tag{2-29}
$$

$$
m_j/b = 2\pi\rho U^2 b\left\{\left[B_{2C}\frac{b^2}{U^2}\frac{\ddot{h}_{cr}}{b} + B_{1C}\frac{b}{U}\frac{\dot{h}_{cr}}{b} + \cdots\right]\cos j\beta_r + \cdots\right\}
$$

$$\frac{b}{u}\dot{Y}_{hcr} + g_0 Y_{hcr} = \frac{b}{u}\dot{h}_{cr}$$

$$\frac{b}{u}\dot{Y}_{\alpha cr} + g_c Y_{\alpha cr} = \frac{b}{u}\dot{\alpha}_{cr} \qquad (2-30)$$

$$\vdots$$

The form of m_j/b is similar to the form of l_j. By replacing all the B_{iA} by B_{iC}, and all B_{iB} by B_{iD}, one can obtain the expression for moment m_j/b from the expression for lift, l_j. There is one augmented equation (2-30) for each of the four coordinates, h_{cr}, h_{sr}, α_{cr}, and α_{sr}. The equations for lift and moment can be written more compactly in matrix form as follows,

$$\begin{Bmatrix} h_j/b \\ \alpha_j \end{Bmatrix} = \underset{\sim}{P}\,\underset{\sim}{q} \qquad (2-31)$$

$$\begin{Bmatrix} l_j \\ m_j/b \end{Bmatrix} = 2\pi\rho U^2 b \underset{\sim}{P} \left\{ \underset{\sim}{B}_2 \frac{b^2}{U^2} \ddot{\underset{\sim}{q}}_b + \underset{\sim}{B}_1 \frac{b}{U} \dot{\underset{\sim}{q}}_b + \underset{\sim}{B}_0 \underset{\sim}{q}_b + \underset{\sim}{G}_1 \underset{\sim}{Y} \right\}$$

$$\frac{b}{U} \dot{\underset{\sim}{Y}} + \underset{\sim}{g}_0 \underset{\sim}{Y} = \frac{b}{U} \dot{\underset{\sim}{q}} \qquad (2\text{-}32)$$

where the matrices have been defined as

$$\underset{\sim}{q} = \begin{Bmatrix} h_{cr}/b \\ \alpha_{cr} \\ h_{sr}/b \\ \alpha_{sr} \end{Bmatrix} \qquad \underset{\sim}{Y} = \begin{Bmatrix} Y_{hcr} \\ Y_{\alpha cr} \\ Y_{hsr} \\ Y_{\alpha sr} \end{Bmatrix} \qquad (2\text{-}33)$$

$$\underset{\sim}{P} = \begin{bmatrix} \cos j\beta_r & 0 & \sin j\beta_r & 0 \\ 0 & \cos j\beta_r & 0 & \sin j\beta_r \end{bmatrix}$$

$$\underset{\sim}{B_2} = \left[\begin{array}{cc|cc} B_{2A} & B_{2B} & -\tilde{B}_{2A} & -\tilde{B}_{2B} \\ B_{2C} & B_{2D} & -\tilde{B}_{2C} & -\tilde{B}_{2D} \\ \hline \tilde{B}_{2A} & \tilde{B}_{2B} & B_{2A} & B_{2B} \\ \tilde{B}_{2C} & \tilde{B}_{2D} & B_{2C} & B_{2D} \end{array}\right]$$

$$\underset{\sim}{g_0} = \left[\begin{array}{cc|cc} g_0 & 0 & 0 & 0 \\ 0 & g_0 & 0 & 0 \\ \hline 0 & 0 & g_0 & 0 \\ 0 & 0 & 0 & g_0 \end{array}\right]$$

The matrices $\underset{\sim}{B_1}$, $\underset{\sim}{B_0}$, and $\underset{\sim}{G}$, are similar to $\underset{\sim}{B_2}$.

This work involves only the torsion degree of freedom, and only the coefficient A_D is used directly. The constants required above were

obtained using Whitehead's [2] two-dimensional, incompressible aerodynamics. Equations (2-19)) were used to solve for the standing wave coefficients, and their values are listed in Tables 1 and 2 for stagger angles of $\gamma = 0$ degrees and $\gamma = 45$ degrees and gap-to-chord ratio, s/c = 1. The values listed in the table refer to an axis system located at the leading edge. Figures 4 and 5 show the fits of the Whitehead traveling wave coefficients at the leading edge. Tables 3 and 4 list the exact values of the Whitehead coefficients versus the approximate values. To transfer information to any axis, located a distance η per cent chord behind the leading edge, one finds the following relations. (See figure 3.)

$$
\begin{aligned}
(A_A)_\eta &= (A_A)_o \\
(A_B)_\eta &= (A_B)_o + 2\eta (A_A)_o \\
(A_C)_\eta &= (A_C)_o + 2\eta (A_A)_o \\
(A_D)_\eta &= (A_D)_o + 2\eta[(A_B)_o + (A_C)_o] + 4\eta^2 (A_A)_o
\end{aligned}
\qquad (2\text{-}34)
$$

where $(\ )_o$ represents a quantity evaluated at the leading edge. The same transformations are used when transfering standing wave coefficients to any axis η. By substituting B_{2D}, B_{2C}, etc. into the above for

A_b, A_c, etc. one can obtain the appropriate transferred coefficients.

Returning to the cascade torsion problem, expressions (2-22), (2-23), (2-24), and (2-25) can be written more compactly in matrix form as follows

$$\alpha_j = \underset{\sim}{P}\ \underset{\sim}{q} \tag{2-35}$$

$$m_j = 2\pi\rho U^2 b^2 \underset{\sim}{P}\left\{\underset{\sim}{B}_2 \frac{b^2}{U^2}\ddot{\underset{\sim}{q}} + \underset{\sim}{B}_1 \frac{b}{U}\dot{\underset{\sim}{q}} + \underset{\sim}{B}_0 \underset{\sim}{q} + \underset{\sim}{G}_1 \underset{\sim}{Y}\right\} \tag{2-36}$$

$$\frac{b}{U}\dot{\underset{\sim}{Y}} + \underset{\sim}{g}_0 \underset{\sim}{Y} = \frac{b}{U}\dot{\underset{\sim}{q}} \tag{2-37}$$

where the matrices have been defined as

$$\underset{\sim}{P} = \left[\cos j\beta_r \quad \sin j\beta_r\right] \qquad \underset{\sim}{q} = \begin{Bmatrix} q_{cr} \\ q_{sr} \end{Bmatrix} \qquad \underset{\sim}{Y} = \begin{Bmatrix} Y_{cr} \\ Y_{sr} \end{Bmatrix}$$

$$\underset{\sim}{B}_2 = \begin{bmatrix} B_{2D} & -\tilde{B}_{2D} \\ \tilde{B}_{2D} & B_{2D} \end{bmatrix} \qquad \underset{\sim}{g}_0 = \begin{bmatrix} g_0 & 0 \\ 0 & g_0 \end{bmatrix} \tag{2-38}$$

The matrices $\underset{\sim}{B}_1$, $\underset{\sim}{B}_0$, and $\underset{\sim}{G}_1$ are similar to $\underset{\sim}{B}_2$, and all the entries of all the matrices depend on the interblade phase angle. To represent mistuned cascade aerodynamics it is necessary to include all nodal

diameter standing wave modes from $r = 0$ to $r = (N-1)/2$. Now the deflections and corresponding moments can be represented by

$$\underset{\sim}{\alpha} = \underset{\sim}{P}\,\underset{\sim}{q} \tag{2-39}$$

$$\underset{\sim}{m} = 2\pi\rho U^2 b^2 \underset{\sim}{P}\left\{\underset{\sim}{B}_2 \frac{b^2}{U^2}\ddot{\underset{\sim}{q}} + \underset{\sim}{B}_1 \frac{b}{U}\dot{\underset{\sim}{q}} + \underset{\sim}{B}_0\,\underset{\sim}{q} + \underset{\sim}{G}_1\,\underset{\sim}{Y}\right\} \tag{2-40}$$

$$\frac{b}{U}\dot{\underset{\sim}{Y}} + \underset{\sim}{g}_0\,\underset{\sim}{Y} = \frac{b}{U}\dot{\underset{\sim}{q}} \tag{2-41}$$

where the new matrices have been defined

$$\underset{N\times 1}{\underset{\sim}{\alpha}} = \begin{Bmatrix} \alpha_0 \\ \alpha_1 \\ \alpha_2 \\ \vdots \\ \alpha_{N-1} \end{Bmatrix} \quad \underset{N\times 1}{\underset{\sim}{q}} = \begin{Bmatrix} q_{c0} \\ q_{c1} \\ q_{s1} \\ q_{c2} \\ q_{s2} \\ \vdots \\ q_{c\frac{N-1}{2}} \\ q_{s\frac{N-1}{2}} \end{Bmatrix} \quad \underset{N\times 1}{\underset{\sim}{Y}} = \begin{Bmatrix} Y_{c0} \\ Y_{c1} \\ Y_{s1} \\ Y_{c2} \\ Y_{s2} \\ \vdots \\ Y_{c\frac{N-1}{2}} \\ Y_{s\frac{N-1}{2}} \end{Bmatrix} \tag{2-42}$$

$$\underset{\sim}{B}_2 = \begin{bmatrix} B_{2D}(r=0) & 0 & 0 & 0 & \cdots & \cdots & \cdots \\ 0 & B_{2D}(r=1) & -\tilde{B}_{2D}(1) & 0 & 0 & \cdots & \cdots \\ 0 & \tilde{B}_{2D}(1) & B_{2D}(1) & 0 & 0 & \cdots & \cdots \\ \vdots & 0 & 0 & \ddots & \vdots & & \\ & 0 & 0 & \cdots & B_{2D}\left(r=\frac{N-1}{2}\right) & -\tilde{B}_{2D}(\;) & \\ & \vdots & \vdots & \cdots & \tilde{B}_{2D}(\;) & B_{2D}(\;) & \end{bmatrix}$$

$$\underset{\sim}{g_o} = \begin{bmatrix} g_o(r=0) & 0 & 0 & \cdots & & & \\ 0 & g_o(1) & 0 & 0 & \cdots & & \\ 0 & 0 & g_o(1) & 0 & \cdots & & \\ \vdots & \vdots & 0 & \ddots & & & \\ \vdots & \vdots & \vdots & & \ddots & & \\ \vdots & \vdots & \vdots & & & g_o\left(\frac{N-1}{2}\right) & 0 \\ \cdots & \cdots & \cdots & \cdots & \cdots & 0 & g_o\left(\frac{N-1}{2}\right) \end{bmatrix}$$

$$\underset{N\times N}{\underset{\sim}{P}} = \begin{bmatrix} c0\beta_0 & c0\beta_1 & s0\beta_1 & c0\beta_2 & s0\beta_2 & \cdots & c0\beta_{\frac{N-1}{2}} & s0\beta_{\frac{N-1}{2}} \\ c1\beta_0 & c1\beta_1 & s1\beta_1 & \vdots & \vdots & \vdots & \vdots & \vdots \\ c2\beta_0 & c2\beta_1 & s2\beta_1 & \vdots & \vdots & \vdots & \vdots & \vdots \\ \vdots & \vdots & \vdots & \vdots & \vdots & \vdots & \vdots & \vdots \\ c(N-1)\beta_0 & c(N-1)\beta_1 & s(N-1)\beta_1 & \cdots & \cdots & \cdots & \cdots & s(N-1)\beta_{\frac{N-1}{2}} \end{bmatrix}$$

$$cj\beta_r \equiv \cos j\beta_r \ , \quad sj\beta_r \equiv \sin j\beta_r$$

where, for $r = 0$, there is no contribution from the $\sin j\beta_r$ mode, and so it is neglected. Since the standing waves appear in pairs and the $\sin j\beta_r$ mode is a non-mode, odd numbers of blades are easier to handle. To model an even number of blades, an extra set of modes would be required. The mode number r would be $N/2$, and the $\sin j\beta_r$ mode is always zero, since N is an even number. Only one mode, the $\cos j\beta_r$ mode, representing 180 degrees of phase separation of the motion of adjacent blades, is added. For simplicity, only odd numbers of blades are used in this work. The matrices $\underset{\sim}{B}_1$, $\underset{\sim}{B}_0$, and $\underset{\sim}{G}_1$, are similar to $\underset{\sim}{B}_2$.

2.2 Application to Isolated Airfoil

For comparison, the complete unsteady airforces acting on a typical section of an isolated airfoil have been expressed in terms of the general motion of standing wave modes, and the standing wave coefficients B_2, B_1, B_0, G_1, and $\mathcal{J}_0$, have been determined. These airforces are given by

$$\ell = 2\pi\rho U^2 b\left\{\left[-\frac{1}{2}\frac{b^2}{U^2}\frac{\ddot{h}}{b} + \frac{1}{2}\frac{b}{U}\dot{\alpha} - \frac{1}{2}a\frac{b^2}{U^2}\ddot{\alpha}\right] + C(k)\left[-\frac{b}{U}\frac{\dot{h}}{b} + \alpha + \left(\frac{1}{2}-a\right)\frac{b}{U}\dot{\alpha}\right]\right\} \qquad (2\text{-}43)$$

$$m/b = 2\pi\rho U^2 b\left\{\left[-\frac{a}{2}\frac{b^2}{U^2}\frac{\ddot{h}}{b} - \frac{1}{2}\left(\frac{1}{2}-a\right)\frac{b}{U}\dot{\alpha} - \frac{1}{2}\left(\frac{1}{8}+a^2\right)\frac{b^2}{U^2}\ddot{\alpha}\right] + C(k)\left(a+\frac{1}{2}\right)\left[-\frac{b}{U}\frac{\dot{h}}{b} + \alpha + \left(\frac{1}{2}-a\right)\frac{b}{U}\dot{\alpha}\right]\right\} \qquad (2\text{-}44)$$

where C(k) is the Theodorsen function (derived in terms of sinusoidal motion), and a is the elastic axis location in semichords aft of midchord. See reference [10]. To obtain the traveling wave coefficients in the proper form, assume solutions of the form

$$h = \mathrm{Re}\{\bar{h}\, e^{i\omega t}\}$$
$$\alpha = \mathrm{Re}\{\bar{\alpha} e^{i\omega t}\} \qquad (2\text{-}45)$$

Now the airforces (2-43) and (2-44) can be represented by

$$\ell = 2\pi\rho U^2 b\left\{A_A \frac{\bar{h}}{b} + A_B \bar{\alpha}\right\} e^{i\omega t} \qquad (2\text{-}46)$$

$$m/b = 2\pi\rho U^2 b\left\{A_C \frac{\bar{h}}{b} + A_D \bar{\alpha}\right\} e^{i\omega t} \qquad (2\text{-}47)$$

where for these isolated airforces the nondimensional aerodynamic coefficients have been defined as follows,

$$\begin{aligned}
A_A &= \tfrac{1}{2}k^2 - ikC(k) \\
A_B &= \tfrac{1}{2}ak^2 + i\tfrac{1}{2}k + C(k)\left[1 + i(\tfrac{1}{2}-a)k\right] \\
A_C &= \tfrac{1}{2}ak^2 - ik(a+\tfrac{1}{2})C(k) \\
A_D &= \tfrac{1}{2}(\tfrac{1}{8}+a^2)k^2 - i\tfrac{1}{2}(\tfrac{1}{2}-a)k + (a+\tfrac{1}{2})C(k)\left[1 + ik(\tfrac{1}{2}-a)\right]
\end{aligned} \qquad (2\text{-}48)$$

If the Theodorsen function is written $C(k)=F(k)+iG(k)$, then we find the following

$$\begin{aligned}
A_{AR} &= \tfrac{1}{2}k^2 + kG \\
A_{AI} &= -kF \\
A_{BR} &= \tfrac{1}{2}ak^2 + F - (\tfrac{1}{2}-a)kG \\
A_{BI} &= \tfrac{1}{2}k + G + (\tfrac{1}{2}-a)kF \\
A_{CR} &= \tfrac{1}{2}ak^2 + (a+\tfrac{1}{2})kG \\
A_{CI} &= -(a+\tfrac{1}{2})kF \\
A_{DR} &= \tfrac{1}{2}(\tfrac{1}{8}+a^2)k^2 + (a+\tfrac{1}{2})F - (\tfrac{1}{4}-a^2)kG \\
A_{DI} &= -\tfrac{1}{2}(\tfrac{1}{2}-a)k + (a+\tfrac{1}{2})G + (\tfrac{1}{4}-a^2)kF
\end{aligned} \qquad (2\text{-}49)$$

Now these coefficients can be fit using the first two equations of (2-19) as the Theodorsen function $C(k) = F + iG$ is a known function of reduced frequency. The transient coefficients can be solved for from (2-19) as shown in Appendix A. The values of the transient coefficients are shown in Table 5 for $a = -1$ (elastic axis at the leading edge). For the isolated airfoil, the modal displacements are equal to the blade displacements, and (2-28) becomes,

$$h_j = h(t)$$
$$\alpha_j = \alpha(t) \qquad (2\text{-}50)$$

The corresponding transient lift and moment are obtained from (2-29) as follows,

$$\ell_j = 2\pi\rho U^2 b \left\{ B_{2A} \frac{b^2}{U^2} \frac{\ddot{h}}{b} + B_{1A} \frac{b}{U} \frac{\dot{h}}{b} + B_{0A} \frac{h}{b} + G_{1A} Y_h + B_{2B} \frac{b^2}{U^2} \ddot{\alpha} + B_{1B} \frac{b}{U} \dot{\alpha} + B_{0B} \alpha + G_{1B} Y_\alpha \right\}$$

$$m_j/b = 2\pi\rho U^2 b \left\{ B_{2C} \frac{b^2}{U^2} \frac{\ddot{h}}{b} + B_{1C} \frac{b}{U} \frac{\dot{h}}{b} + B_{0C} \frac{h}{b} + G_{1C} Y_h + B_{2D} \frac{b^2}{U^2} \ddot{\alpha} + B_{1D} \frac{b}{U} \dot{\alpha} + B_{0D} \alpha + G_{1D} Y_\alpha \right\}$$

$$\frac{b}{U} \dot{Y}_h + g_0 Y_h = \frac{b}{U} \dot{h}$$
$$\frac{b}{U} \dot{Y}_\alpha + g_0 Y_\alpha = \frac{b}{U} \dot{\alpha} \qquad (2\text{-}51)$$

where the modal cross-coupling terms do not appear for the isolated

airfoil case. The approximate aerodynamic coefficients are compared to the Whitehead values in figure 8, and their numerical values for several reduced frequencies are compared in table 6.

Notice that the fits to the isolated airfoil aerodynamic coefficients are not quite as accurate as the fits to the cascade aerodynamic coefficients. Rock and DeBra [11] have shown that for an isolated airfoil in a wind tunnel, the accuracy of the approximation depends on the ratio of the wall spacing to the semichord of the airfoil. They have indicated that to keep the same level of accuracy the order of the approximation must be increased as the wall-spacing-to-semichord ratio increases. This implies that for a given order of approximation, the aerodynamics for a cascade with a gap-to-chord ratio of one will be more accurately represented than those of an isolated airfoil, which has an effective gap-to-chord ratio of infinity.

3. Application to Torsion Flutter

3.1 Isolated Airfoil

For an isolated airfoil, the torsional equation of motion can be written

$$I_\alpha \ddot{\alpha} + 2\zeta\omega_\alpha I_\alpha \dot{\alpha} + \omega_\alpha^2 I_\alpha \alpha = m + m^D \qquad (3\text{-}1)$$

where m is the aerodynamic moment and m^D is a disturbance moment acting on a section of the airfoil. Sign conventions at the leading edge are shown in figure 3. From the fitting of the isolated airfoil unsteady airforces, the moment m can be expressed in the form of (2-15) and (2-16) as,

$$m = 2\pi\rho U^2 b^2 \left\{ B_{2D} \frac{b^2}{U^2} \ddot{\alpha} + B_{1D} \frac{b}{U} \dot{\alpha} + B_{0D} \alpha + G_{1D} Y \right\} \qquad (3\text{-}2)$$

$$\frac{b}{U} \dot{Y} + g_0 Y = \frac{b}{U} \dot{\alpha} \qquad (3\text{-}3)$$

where the standing wave coefficients shown in Table 3 have been transferred to the midchord are as follows,

$$(B_{2D})_{\eta=.5} = -.015 \;,\; (B_{1D})_{\eta=.5} = -.148 \;,$$

$$(B_{0D})_{\eta=.5} = .500 \;,\; (G_{1D})_{\eta=.5} = -.158 \;,$$

$$g_0 = .130$$

Since there is only one degree of freedom, there is a single multiblade coordinate which is equal to the rotation of the airfoil (i.e., $q_{bcr} = \alpha$). By placing (3-2) into (3-1) and dividing by $\pi \rho b^4 \omega_0^2$, the nondimensional equation of motion can be obtained

$$\nu \ddot{\alpha} + 2\zeta_\alpha \nu \dot{\alpha} + \nu \gamma_\alpha^2 \alpha = 2B_{2D}\ddot{\alpha} + 2\bar{u}B_{1D}\dot{\alpha} + 2\bar{u}^2 B_{0D}\alpha + 2\bar{u}^2 G_{1D} Y \qquad (3\text{-}4)$$

$$\dot{Y} + \bar{u} g_0 Y = \dot{\alpha} \qquad (3\text{-}5)$$

where the following nondimensional quantities have been defined,

$$\nu = \frac{I\alpha}{\pi\rho b^4} \quad , \quad \omega_o t = \tau \quad , \quad \frac{d}{dt}(\ ) = (\dot{}), \quad \frac{d}{d\tau}(\ ) = (^{o}),$$

$$\gamma_\alpha = \frac{\omega_\alpha}{\omega_o} \quad , \quad \bar{u} = \frac{u}{\omega_o b} \qquad (3-6)$$

To look at the flutter problem, m^D has been set to zero. The subscript D, denoting a moment coefficient due to blade angle of attack, will be dropped at this time.

To study the aeroelastic stability, assume a solution of the form

$$\alpha = \bar{\alpha} e^{\tilde{p}\tau} \qquad Y = \bar{Y} e^{\tilde{p}\tau} \qquad (3-7)$$

where

$$\tilde{p} = \frac{a}{\omega_o} + i\gamma \quad , \quad \gamma = \frac{\omega}{\omega_o}$$

Substituting (3-7) into (3-5), solving for Y, substituting for Y in (3-4), and rearranging gives a cubic equation in p

$$A\tilde{p}^3 + B\tilde{p}^2 + C\tilde{p} + D = 0 \qquad (3-8)$$

where

$$
\begin{aligned}
A &= \nu - 2B_2 \\
B &= \nu g_0 \bar{u} + 2\zeta\nu\gamma_\alpha - 2B_2 g_0 \bar{u} - 2B_1 \bar{u} \\
C &= 2\bar{u}\zeta\gamma_\alpha\nu g_0 + 2\gamma_\alpha^2\nu - 2(B_1 g_0 + B_0 + G_1)\bar{u}^2 \\
D &= \nu\bar{u}g_0\gamma_\alpha^2 - 2B_0 g_0 \bar{u}^3
\end{aligned}
\qquad (3\text{-}9)
$$

The cubic equation is solved for the roots $\tilde{p} = a_1/\omega_\theta \pm i\gamma$, and a_2/ω_θ. Flutter occurs when $\tilde{p} = \pm i\gamma$ and $a_2 \leq 0$. The roots of this equation are shown by the dashed line in figure 7. Only the upper half-plane is shown. The plot shows the roots associated with increasing values of reduced velocity $\bar{u}$, for a structural damping ratio $\zeta = 0$, and frequency ratio $\gamma_\alpha = 1$. Using data for NASA Test Rotor 12, the value of the inertia ratio $\nu = 86.2$, for the elastic axes of the blades at their midchords. The addition of an augmented state produces a pole with a high decay rate. This pole stays on the negative real axis as the reduced velocity is increased, and is not plotted.

As can be seen in figure 7, the isolated airfoil does not flutter for this set of parameters. At a reduced speed of zero the free vibration response is obtained. Since there is no structural damping, the free vibration is an undamped sinusoidal vibration. As the reduced velocity, $\bar{u}$, is increased, the exponential decay rate (the magnitude of which is given by the real part of the eigenvalue) of the motion increases due to aerodynamic damping only. Finally, as the frequency (the imaginary part of the eigenvalue) drops to zero, the airfoil becomes overdamped and no

vibratory response is possible. Note that the root locus is shown only up to $\bar{u} = 4$, at which speed the response is still a damped vibration. After the root locus touches the real axis, it moves in the direction of the positive real axis. The point of divergence is reached when the root is at the origin. Increasing the reduced velocity further brings the root into the unstable right half-plane.

3.2 Tuned Cascade

For a tuned cascade the equation of motion for any blade is identical to the equation of motion for any other blade. Here we look at the case of a tuned cascade, where by definition no structural coupling of the blades is allowed. This is also the case of blades on a rotor with a massive, rigid disk. The equation for each blade can be written

$$I_{\alpha_j} \ddot{\alpha}_j + 2\zeta_j \omega_{\alpha_j} I_{\alpha_j} \dot{\alpha}_j + \omega_{\alpha_j}^2 I_{\alpha_j} \alpha_j = m_j + m_j^D \tag{3-10}$$

By substituting for the aerodynamic moment as obtained in the previous chapter (2-36), and dividing by $\pi \rho b^4 \omega_\alpha^2$, one can obtain the nondimensional equations of motion:

$$\nu_j^2 \ddot{\alpha}_j + 2\zeta_j \gamma_{jj} \nu_j \dot{\alpha}_j + \nu_j \gamma_{\alpha_j}^2 \alpha_j = \underset{\sim}{P}\left\{ 2\underset{\sim}{B}_2 \ddot{\underset{\sim}{q}} + 2\bar{u}\underset{\sim}{B}_1 \dot{\underset{\sim}{q}} + 2\bar{u}^2 \underset{\sim}{B}_0 \underset{\sim}{q} + 2\bar{u}^2 \underset{\sim}{G}_1 \underset{\sim}{Y} \right\} + m_j^{D*} \qquad (3\text{-}11)$$

$$\dot{\underset{\sim}{Y}} + \bar{u}\underset{\sim}{g}_0 \underset{\sim}{Y} = \dot{\underset{\sim}{q}} \qquad (3\text{-}12)$$

where the nondimensional disturbance moment acting on the blade is,

$$m_j^{D*} = m_j^D / \pi \rho b^4 \omega_0^2$$

and the matrices are defined by (2-38). Next, express the blade rotations on the right hand side of (3-11) in terms of multiblade coordinates of mode r as,

$$\alpha_j = \underset{\sim}{P}\,\underset{\sim}{q} \qquad (2\text{-}29)$$

Premultiplying by $\underset{\sim}{P}^T$ yields,

$$\underset{\sim}{P}^T \nu_j \underset{\sim}{P}\, \underset{\sim}{\ddot{q}} + \underset{\sim}{P}^T 2\zeta_j \gamma_{\alpha_j} \nu_j \underset{\sim}{P}\, \underset{\sim}{\dot{q}} + \underset{\sim}{P}^T \nu_j \gamma_{\alpha_j}^2 \underset{\sim}{P}\, \underset{\sim}{q} =$$

$$= \underset{\sim}{P}^T \underset{\sim}{P} \{ 2 \underset{\sim}{B}_2 \underset{\sim}{\ddot{q}} + 2\bar{u} \underset{\sim}{B}_1 \underset{\sim}{\dot{q}} + 2\bar{u}^2 \underset{\sim}{B}_0 \underset{\sim}{q}$$

$$+ 2\bar{u}^2 \underset{\sim}{G}_1 \underset{\sim}{Y} \} + \underset{\sim}{P}^T m_j^{D^*} \qquad (3\text{-}13)$$

$$\dot{\underset{\sim}{Y}} + \bar{u} \underset{\sim}{g}_0 \underset{\sim}{Y} = \underset{\sim}{\dot{q}} \qquad (3\text{-}14)$$

Rearranging yields,

$$\underset{\sim}{M}\, \underset{\sim}{\ddot{q}} + \underset{\sim}{C}\, \underset{\sim}{\dot{q}} + \underset{\sim}{K}\, \underset{\sim}{q} + \underset{\sim}{G}\, \underset{\sim}{Y} = \underset{\sim}{P}^T m_j^{D^*} \qquad (3\text{-}15)$$

$$\dot{\underset{\sim}{Y}} + \underset{\sim}{H}\, \underset{\sim}{Y} = \underset{\sim}{\dot{q}} \qquad (3\text{-}16)$$

where

$$\underset{\sim}{M} = \underset{\sim}{P}^T \nu_j \underset{\sim}{P} - 2\underset{\sim}{P}^T \underset{\sim}{P}\ \underset{\sim}{B}_2$$

$$\underset{\sim}{C} = \underset{\sim}{P}^T 2\zeta_j \gamma_j \nu_j \underset{\sim}{P} - 2\bar{u}\underset{\sim}{P}^T \underset{\sim}{P}\ \underset{\sim}{B}_1$$

$$\underset{\sim}{K} = \underset{\sim}{P}^T \nu_j \gamma_j^2 \underset{\sim}{P} - 2\bar{u}^2 \underset{\sim}{P}^T \underset{\sim}{P}\ \underset{\sim}{B}_0 \qquad (3\text{-}17)$$

$$\underset{\sim}{G} = -2\bar{u}^2 \underset{\sim}{P}^T \underset{\sim}{P}\ \underset{\sim}{G}_1$$

$$\underset{\sim}{H} = \bar{u}\underset{\sim}{g}_0$$

This set of two second order equations (3-15), and two first order augmented equations (3-16) can be cast into six first order equations of motion for the tuned cascade as follows,

$$\underset{\sim}{A}\ \dot{\underset{\sim}{X}} - \underset{\sim}{B}\ \underset{\sim}{X} = \underset{\sim}{F} \qquad (3\text{-}18)$$

where

$$\underset{\sim}{A} = \begin{bmatrix} \underset{\sim}{I} & \underset{\sim}{0} & \underset{\sim}{0} \\ \underset{\sim}{0} & \underset{\sim}{M} & \underset{\sim}{0} \\ \underset{\sim}{0} & \underset{\sim}{0} & \underset{\sim}{I} \end{bmatrix} \qquad \underset{\sim}{X} = \begin{Bmatrix} q_{b_{cr}} \\ q_{b_{sr}} \\ \dot{q}_{b_{cr}} \\ \dot{q}_{b_{sr}} \\ Y_{cr} \\ Y_{sr} \end{Bmatrix} \qquad \underset{\sim}{F} = \begin{Bmatrix} \underset{\sim}{0} \\ \underset{\sim}{P}^T m_j D^* \\ \underset{\sim}{0} \end{Bmatrix}$$

$$\underset{\sim}{B} = \begin{bmatrix} \underset{\sim}{0} & \underset{\sim}{I} & \underset{\sim}{0} \\ -\underset{\sim}{K} & -\underset{\sim}{C} & -\underset{\sim}{G} \\ \underset{\sim}{0} & \underset{\sim}{I} & -\underset{\sim}{H} \end{bmatrix} \qquad (3\text{-}19)$$

To look at the flutter problem, let $\underset{\sim}{F} = \underset{\sim}{0}$ and assume solutions of the form

$$\underset{\sim}{X} = \overline{\underset{\sim}{X}}\, e^{\tilde{p}\tau} \qquad (3\text{-}20)$$

which give, upon substitution into (3-18) and rearranging, the standard eigenvalue problem

$$\tilde{p}\, \overline{\underset{\sim}{X}} = \underset{\sim}{A}^{-1}\, \underset{\sim}{B}\, \overline{\underset{\sim}{X}} \qquad (3\text{-}21)$$

The real and imaginary part of the eigenvalues $\tilde{p} = a/\omega_b \pm i\gamma$ are plotted in figure 7 for the case of a nine-bladed cascade. Flutter occurs when the real part of the eigenvalue, a/ω_b, is zero, corresponding to a solution of the form,

$$\underset{\sim}{X} = \overline{\underset{\sim}{X}} e^{i\gamma\tau}$$

This is an undamped sinusoidal motion that characterizes flutter. If the frequency ratio, γ, drops to zero before the exponential damping rate, a/ω_c, the phenomenon of divergence is observed, as the damping rate crosses the imaginary axis. The solution in that case grows exponentially,

$$\underset{\sim}{X} = \overline{\underset{\sim}{X}} e^{\frac{a}{\omega_c}\tau} \qquad a > 0$$

The system shown in figure 7 is a nine-bladed rotor with a stagger angle ξ = 45 degrees, gap-to-chord ratio of 1, zero structural damping, an inertia ratio ν = 86.2, and the elastic axis at midchord, η = 0.5. The plot shows the eigenvalues associated with each interblade phase angle mode. For each interblade phase angle there are two roots, one corresponding to a forward traveling wave, the other corresponding to a backward traveling wave. The three modes that flutter are forward traveling waves. There will be more about the flutter modes in a following section. For a tuned cascade with nine blades and a stagger angle of 45 degrees, the flutter reduced speeds associated with an interblade phase angle mode are shown in figure 7. These were verified by comparing with the sinusoidal solution results using Whitehead coefficients directly. See Appendix B. A comparison of the structural damping required for flutter, and the actual damping for a given reduced velocity are shown in figure 8. The difference between the sinusoidal

solution curve and the curve $\zeta_A = 0$ is proportional to the amount of structural damping required to obtain flutter. The curve obtained by solutions of the form $\underset{\sim}{\bar{X}} e^{\bar{p}\tau}$ shows the decay rate associated with vibration in that mode for a given reduced velocity. Since there is no structural damping, the decay rate indicates the level of aerodynamic damping present. The value of reduced frequency $k = \omega b/u$ at which $\zeta_A = 0$ is the flutter reduced frequency. The two dampings, although essentially different in origin, are approximately equal. For the important region below the flutter point the two values are hardly distinguishable.

3.3 Mistuned Cascade

Mistuning refers to small differences between the natural frequencies, stiffnesses, and inertias of the blades of a cascade. Since it is easiest to measure blade frequencies in an actual rotor, the undamped natural frequencies of the blades are the quantities to be mistuned. For any blade j the natural frequency is defined as,

$$\omega_{\alpha j} = \sqrt{k_{\alpha j}/I_{\alpha j}} \qquad (3\text{-}22)$$

where $k_{\alpha j}$ refers to the torsional spring stiffness of the blade and $I_{\alpha j}$ is the moment of inertia of the blade about the elastic axis. A reference

frequency is defined as the average natural frequency of the blades as follows,

$$\omega_o = \frac{1}{N} \sum_j \omega_{\alpha j} \qquad (3\text{-}23)$$

If one blade is to have a 5% higher frequency than the remaining blades, the frequency of the blades must be given by,

$$\omega_o = \frac{1}{N}\left[1 \cdot \omega_{high} + (N-1)\,\omega_{low}\right]$$

$$\omega_{high} / \omega_{low} = 1.05$$

or, solving the above to give the blade frequencies,

$$\omega_{high} = \frac{1.05\,N}{N+.05}\,\omega_o \qquad \omega_{low} = \frac{N}{N+.05}\,\omega_o$$

Which yields, for a nine-bladed rotor, N = 9, with one blade at a 5% higher frequency than the remaining eight,

$$\omega_{high} = 1.044\,\omega_o \qquad \omega_{low} = 0.994\,\omega_o$$

To achieve these frequencies one must mistune the blade stiffnesses and/or the blade inertias. If frequency is to be mistuned by varying the inertia alone, then the stiffness is constant and (3-22) can be used to solve for the inertias

$$\frac{I_{high}}{I_o} = \left(\frac{\omega_o}{\omega_{high}}\right)^2 \qquad \frac{I_{low}}{I_o} = \left(\frac{\omega_o}{\omega_{low}}\right)^2 \qquad (3\text{-}24)$$

This means that the average inertia is not equal to the reference inertia,

$$\frac{I_{AVE}}{I_o} = \frac{1}{N}\left[\left(\frac{\omega_o}{\omega_{high}}\right)^2 + (N-1)\left(\frac{\omega_o}{\omega_{low}}\right)^2\right]$$

For a nine-bladed cascade with one blade of 5% higher frequency than the remaining blades, the difference between the reference inertia and the average inertia is slight, $I_{AVE}/I_o = 1.0016$

For alternately mistuned blades, the difference between adjacent blades is set to, say, 5%. To find the high and low frequency for an average (reference) frequency of 1,

$$\omega_o = \frac{1}{N}\left(\frac{N+1}{2}\omega_{high} + \frac{N-1}{2}\omega_{low}\right)$$

$$\omega_{high}/\omega_{low} = 1.05 \qquad (3\text{-}25)$$

or, solving for the frequencies,

$$\omega_{high} = \frac{2.1\ N\ \omega_o}{2.05\ N + .05} \qquad \omega_{low} = \frac{2N\omega_o}{2.05\ N + .05}$$

For N = 9 with 5% "alternate" mistuning,

$$\omega_{high} = 1.022\ \omega_o \qquad \omega_{low} = 0.973\ \omega_o$$

The corresponding average inertia, $I_{Avg} = 1.0013\ I_o$

For a mistuned cascade the equation of motion of each blade is as for the tuned cascade (3-10). To express the motion of each blade of a mistuned cascade, the modal coordinates are summed as follows,

$$\underset{\sim}{\alpha} = \underset{\sim}{P}\,\underset{\sim}{q} \qquad (3\text{-}26)$$

This allows for N different blade amplitudes and N different blade phase angles. The moment acting on a mistuned cascade (3-15), (3-16), was developed in the previous chapter. By substituting for the blade amplitudes and moment into (3-10), and rearranging as was done for the tuned cascade, similar equations of motion are defined as follows,

$$\underset{\sim}{M}\,\ddot{\underset{\sim}{q}} + \underset{\sim}{C}\,\dot{\underset{\sim}{q}} + \underset{\sim}{K}\,\underset{\sim}{q} + \underset{\sim}{G}\,\underset{\sim}{Y} = \underset{\sim}{P}^{T}\,\underset{\sim}{m}^{D^*} \qquad (3\text{-}27)$$

$$\dot{\underset{\sim}{Y}} + \underset{\sim}{H}\,\underset{\sim}{Y} = \dot{\underset{\sim}{q}} \qquad (3\text{-}28)$$

For a mistuned cascade with N blades, there are N second order equations of motion (3-27), and N corresponding augmented equations (3-28). The

new, N-by-N matrices have been defined as follows,

$$\underset{\sim}{M} = \underset{\sim}{P}^T \left[\nu_j \right] \underset{\sim}{P} - 2 \underset{\sim}{P}^T \underset{\sim}{P} \underset{\sim}{B}_2$$

$$\underset{\sim}{C} = \underset{\sim}{P}^T \left[2 \varsigma_j \gamma_{\alpha_j} \nu_j \right] \underset{\sim}{P} - 2\bar{u} \underset{\sim}{P}^T \underset{\sim}{P} \underset{\sim}{B}_1$$

$$\underset{\sim}{K} = \underset{\sim}{P}^T \left[\nu_j \gamma_{\alpha_j}^2 \right] \underset{\sim}{P} - 2\bar{u}^2 \underset{\sim}{P}^T \underset{\sim}{P} \underset{\sim}{B}_0 \qquad (3\text{-}29)$$

$$\underset{\sim}{G} = -2\bar{u}^2 \underset{\sim}{P}^T \underset{\sim}{P} \underset{\sim}{G}_1$$

$$\underset{\sim}{H} = \bar{u} \underset{\sim}{g}_0$$

All the matrices needed above are defined by (2-42). By making use of the orthoganality of the standing wave modes, one obtains,

$$\sum_{j=0}^{N-1} \cos^2 j\beta_r = \sum_{j=0}^{N-1} \sin^2 j\beta_r = N/2$$

$$\sum_{j=0}^{N-1} \sin j\beta \cos j\beta = 0 \qquad (3\text{-}30)$$

By applying (3-30), the matrix product $\underset{\sim}{P}^T \underset{\sim}{P}$, which appears in (3-29) can

be reduced to a very simple form,

$$\underset{\sim}{P}^T \underset{\sim}{P} = \underset{\sim}{D} \quad , \qquad \underset{\sim}{D} = \begin{bmatrix} N & & & 0 \\ & N/2 & & \\ & & N/2 & \\ 0 & & & \ddots \end{bmatrix} \tag{3-31}$$

$$\underset{\sim}{P}^{-1} = \underset{\sim}{D}^{-1} \underset{\sim}{P}^T$$

where the first entry is N because it represents the sum

$$\sum_{j=0}^{N-1} \cos^2 j \cdot 0 = N$$

Casting (3-27) and (3-28) into first order form yields

$$\underset{\sim}{A}\dot{\underset{\sim}{X}} - \underset{\sim}{B}\underset{\sim}{X} = \underset{\sim}{F} \tag{3-32}$$

where the matrices of the 3N order system have been defined as,

$$\underset{\sim}{A} = \begin{bmatrix} \underset{\sim}{I} & \underset{\sim}{0} & \underset{\sim}{0} \\ \underset{\sim}{0} & \underset{\sim}{M} & \underset{\sim}{0} \\ \underset{\sim}{0} & \underset{\sim}{0} & \underset{\sim}{I} \end{bmatrix} \qquad \underset{\sim}{B} = \begin{bmatrix} \underset{\sim}{0} & \underset{\sim}{I} & \underset{\sim}{0} \\ -\underset{\sim}{K} & -\underset{\sim}{C} & -\underset{\sim}{G} \\ \underset{\sim}{0} & \underset{\sim}{I} & -\underset{\sim}{H} \end{bmatrix} \tag{3-33}$$

$$\underset{\sim}{X} = \begin{Bmatrix} \underset{\sim}{q} \\ \underset{\sim}{\dot{q}} \\ \underset{\sim}{b} \\ \underset{\sim}{Y} \end{Bmatrix} \qquad \underset{\sim}{F} = \begin{Bmatrix} \underset{\sim}{0} \\ \underset{\sim}{P}^T \mathfrak{m}^* \\ \underset{\sim}{0} \end{Bmatrix}$$

A flutter mode will now consist of a linear combination of all interblade phase angle modes. Setting the disturbance vector $\underset{\sim}{F} = \underset{\sim}{0}$, the 6-by-6 standard eigenvalue problem (3-21), now becomes a 3N-by-3N eigenvalue problem:

$$\tilde{p}\, \underset{\sim}{\bar{X}} = \underset{\sim}{A}^{-1} \underset{\sim}{B}\, \underset{\sim}{\bar{X}} \tag{3-34}$$

Because of the form of the 3N-by-3N matrix $\underset{\sim}{A}$, only the N-by-N matrix $\underset{\sim}{M}$ must be inverted to set up the eigenvalue problem.

A computer program was written to set up and solve the eigenvalue problem for the tuned (3-21), or mistuned (3-34) cascade. See Appendix C. The root locus associated with the system with one blade of a nine-bladed rotor being mistuned 5% in frequency by varying the mass is shown in

figure 9. Each of the root loci of the mistuned system approach the root loci of the tuned system for sufficiently large values of reduced velocity, $\bar{u}$. The relationship between reduced frequency, k, and reduced velocity is,

$$k = \frac{\omega b}{u} = \frac{\omega}{\omega_0} \frac{\omega_0 b}{u} = \frac{\gamma}{\bar{u}} \qquad (3-35)$$

All roots on the plot with a value of $\bar{u}$ greater than about 1 are within the range of the original approximation to the unsteady airloads, $k = 0$ to $k = 1$. Note the effect on the flutter speed. For the case of one blade mistuned 5%, the flutter reduced speed increased 19%. The flutter reduced frequency decreased by 18%. The magnitude of this effect decreases with an increasing number of blades. The one mistuned blade becomes a smaller part of the system and localized behavior is observed. To show that this is the case, a similar five-bladed cascade gained 33% in flutter reduced speed, and lost 26% in flutter reduced frequency over the tuned case. For a realistic number of blades, one can expect that the flutter speed will not be increased greatly.

The eigenvalues associated with the alternately mistuned system are shown in figure 10. The eigenvalues are plotted in the complex plane, for increasing values of reduced velocity, $\bar{u}$. Again, for high values of reduced velocity the individual mistuned root loci approach the tuned root loci. A measure of the effectiveness of this type of mistuning is the 61% increase in flutter reduced velocity corresponding to a 40% decrease in the flutter reduced frequency.

The effect on the eigenvalues of mistuning one blade at a given reduced speed is shown in figure 11. At this value of reduced speed two of the tuned eigenvalues are in the unstable right half-plane. Mistuning just one blade shifts all of the eigenvalues. There is now one high frequency eigenvalue, and the remaining eigenvalues have shifted towards each other. This shifting together is beneficial in that the unstable eigenvalues have been made more stable. The shifting has also resulted in less damping for the most stable eigenvalues, a problem which can have a adverse effect on the forced response of the system, as will be seen in the next chapter. See reference [8].

"Alternate" mistuning has a much greater effect on the eigenvalues (See figure 11). Now there is a high frequency group and a low frequency group of eigenvalues. All the eigenvalues of the mistuned system are in the stable left half-plane. Again, the least stable eigenvalues are made more stable, but the most stable eigenvalues are made less stable. The effect that the level of alternate mistuning has on the flutter reduced speed is shown in figure 12. Starting with a tuned rotor (alternate mistuning of 0%), the level of mistuning was increased gradually to 10%. There is a significant effect on flutter speed, as was shown in [8]. The example is a nine-bladed rotor, with a stagger angle of 45 degrees, gap-to-chord ratio of 1.0, no structural damping, and with the elastic axis of the blades at the midchord.

3.4 Flutter Vibration Modes

The information in the preceding sections was obtained entirely from the eigenvalues of tuned and mistuned cascades. To study the flutter vibration modes of the blades, it is necessary to examine the eigenvectors associated with the eigenvalue of the form $\tilde{p} = \pm i\gamma$. Solutions at the flutter point are of the form

$$\underset{\sim}{q} = \underset{\sim}{\bar{q}}\, e^{i\gamma\tau} \tag{3-36}$$

where $\underset{\sim}{\bar{q}}$ is the complex eigenvector denoting the motion of the modal coordinates at the flutter point. To examine the motion of the blades use (2-39) to obtain,

$$\underset{\sim}{\alpha} = \underset{\sim}{P}\,\underset{\sim}{\bar{q}}\, e^{i\gamma\tau} = \underset{\sim}{\bar{\alpha}}\, e^{i\gamma\tau} \tag{3-37}$$

where $\underset{\sim}{\bar{\alpha}}$ is the eigenvector of complex amplitudes of the blades. Motion of the type (3-37) can also be represented in terms of amplitude and phase as follows,

$$\underset{\sim}{\alpha} = \left\{ \begin{array}{l} |\bar{\alpha}|_j e^{i(\gamma\tau + \phi_j)} \\ \vdots \end{array} \right\} \tag{3-38}$$

where the amplitude $|\alpha|$ and phase ϕ of each blade are given by

$$|\bar{\alpha}|_j = \sqrt{\bar{\alpha}_{R_j} + \bar{\alpha}_{I_j}} \qquad (3\text{-}39)$$

$$\phi_j = \tan^{-1}\left[\frac{\bar{\alpha}_{I_j}}{\bar{\alpha}_{R_j}}\right]$$

To examine the actual motion of each blade, take the real part of (3-38) to obtain,

$$\left\{\begin{matrix} \alpha_j(t) \\ \vdots \end{matrix}\right\} = \left\{\begin{matrix} |\bar{\alpha}|_j \cos(\gamma\tau + \phi_j) \\ \vdots \end{matrix}\right\} \qquad (3\text{-}40)$$

If adjacent blades have a different phase, then the blade with a larger value of phase is the blade that leads the motion. Figure 13 shows the amplitude and phase of each blade, for a tuned cascade, and the amplitude and phase for the two types of mistuning discussed in this chapter. For the tuned cascade all the blades have the same amplitude and the same interblade phase angle. Plotted as straight lines are the phases each blade would have with respect to blade zero for flutter in pure $\beta_r = 40$ degrees and $\beta_r = 80$ degrees interblade phase angle traveling wave modes. The actual tuned cascade fluttered in a pure $\beta_r = 40$ degrees forward traveling wave mode, in the same direction as the rotation of the rotor. To an observer on the disk, the traveling wave speed is ω/r, where ω is the frequency of vibration. To an observer away from the disk, the

wave would appear to be traveling with a speed $(\Omega+\omega/r)$, greater than the speed of rotation, Ω.

It can be seen in figure 13 that mistuning one blade creates a "dead spot" in the area of the mistuned blade. The mistuned blade and the blades immediately after it (those numbered higher) do not participate in the flutter mode as much as those farther along. The blade immediately before the mistuned blade vibrates with the greatest amplitude. It is interesting to note that the dominant interblade phase angle of the flutter motion is now 80 degrees, whereas the flutter interblade phase angle of the tuned cascade was 40 degrees. This can be seen in figure 9 where it appears that the root locus associated primarily with the $\beta_r = 80$ degrees interblade phase angle mode is the first to go unstable. A similar case was examined in which the one mistuned blade had a 5% lower frequency than the remaining blades. There was no significant change in flutter speed between the two mistuned systems, and the mistuned blade created a dead spot just as the mistuning with one high frequency blade had.

In the alternately mistuned cascade, the high frequency blades vibrate with the greatest amplitude. Pairs of blades vibrate in phase, with the low frequency blades lagging slightly behind the high frequency blades. The dominant interblade phase angle is the same as for the tuned cascade, namely, 40 degrees. The results are similar to those of reference [8].

The amplitudes of the complex modal eigenvectors give an indication

of the amounts of each standing wave mode present in the flutter vibration. Table 8 shows the amounts of each mode present in the flutter mode for the tuned and two mistuned cases studied. Again, the tuned and alternately mistuned flutter modes vibrate predominantly with an interblade phase angle of 40 degrees (one nodal diameter traveling wave), while the interblade phase angle for the mistuning of a single blade is predominantly 80 degrees (two nodal diameter traveling wave).

4. Application to Forced Response

4.1 Engine Order Excitation

Consider the case of a typical section of a single blade of the obstructed rotor shown in figure 14. Due to the obstruction, the blade is subjected to a sinusoidal variation in velocity of $n = 2$ cycles per revolution, where n is sometimes refered to as the engine order of the excitation. The velocity at which the blade approaches the sinusoidal gusts is ΩR, where R is the radius from the center of the rotor to the section of the blade under consideration, and Ω is the speed of rotation of the rotor, in radians/sec. For a stagger angle $\xi = 45$ degrees, $\Omega R = U_{Axial}$. See figure 1.

In order to assume quasi-steady conditions, the cyclic velocity variations must be slow enough to allow the moment acting on the blade to reach most of its steady-state value. If, instead of a sinusoidal variation in velocity there is a step change in velocity causing a step change in angle of attack, the moment acting on the blade about the midchord can be written

$$M = 2\pi\rho U^2 b^2 \alpha_0 \left[\frac{1}{2}\psi(s)\right] \qquad (4-1)$$

where $\psi(s)$ is the Küssner gust function, and $s=Ut/b$ is the distance the blade travels in semichords. See [10], for example. The Küssner function is shown in figure 15. The blade must travel about 20 semichords for the

moment acting on the airfoil to reach most of its steady-state value. If this unsteady effect is ignored, the error in the moment produced by a step change in velocity (angle of attack) will be negligible at the end of 20 semichords of travel.

Now, if the sinusoidal gusts are broken up into step changes in velocity, and the airfoil is allowed to travel 20 semichords after each step change, the quasi-steady moment and the unsteady moment will be approximately equal. Ignoring the time lag between the moment and the velocity will not introduce significant errors. See figure 15. For nearly sinusoidal velocity variations, the error between the unsteady and quasi-steady moments will be less than that for the step changes considered above. For accuracy, any blade should travel 20 semichords for each half-cycle of velocity variation,

$$(\text{velocity}) \times (\text{time per half-cycle}) \geq 20\, b$$

$$\Omega R \times \frac{\pi}{\Omega n} \geq 20\, b \qquad (4\text{-}2)$$

$$\frac{R}{b} \geq \frac{20}{\pi} n$$

For the quasi-steady assumption to be valid, the ratio of the radius of the rotor to the semichord of a blade must be greater than a number which is proportional to the engine order of the disturbance. For the typical

section model used here, the reference radius is at the three-quarters span of the blade. Using data for the NASA Test Rotor 12, R/b is approximately 11. Using (4-2) the minimum acceptable R/b is 6.4 for a one engine order excitation, and 12.7 for an $n = 2$ engine order. The work that follows makes use of the quasi-steady assumption, necessarily limiting itself to low engine order excitations, examples of which are inlet distortion or the presence of struts or supports. Whitehead [2] has a provision for the unsteady effect of sinusoidal upstream disturbances, but they are not used in this work. To study the effect of higher engine order disturbances, the corresponding Whitehead coefficients would have to be included.

To incorporate an engine order forcing into the equations of motion already developed, assume that the nondimensional moment acting on blade j due to inlet velocity distortion can be expressed as,

$$m_j^{D^*}(t) = f_{cn} \cos n\bar{\theta}_j + f_{sn} \sin n\bar{\theta}_j \qquad (4-3)$$

See [1]. Here, n represents the engine order and $\bar{\theta}_j$ represents the position of blade j with respect to axes fixed in space, as shown in figure 14. The position of blade j with respect to fixed axes can be represented in terms of the rotation rate and an angle that gives the position of the blades in the rotating frame as follows,

$$\bar{\theta}_j = \theta_j - \Omega t \qquad (4-4)$$

where $\theta_j = j2\pi/N$, is the position of blade j with respect to an axis system fixed to the disk. Substituting (4-4) into (4-3), making the trigonometric expansion, and rearranging yields the force on blade j due to engine order n,

$$m_j^{D^*} = [f_{cn} \cos n\Omega t - f_{sn} \sin n\Omega t] \cos n\theta_j + [f_{cn} \sin n\Omega t + f_{sn} \cos n\Omega t] \sin n\theta_j \qquad (4\text{-}5)$$

Writing the force on each blade in matrix form yields

$$\underset{\sim}{m}^{D^*} = \underset{\sim}{T} \begin{Bmatrix} f_{cn} \cos n\Omega t - f_{sn} \sin n\Omega t \\ f_{cn} \sin n\Omega t + f_{sn} \cos n\Omega t \end{Bmatrix} \qquad (4\text{-}6)$$

where

$$\underset{Nx2}{\underset{\sim}{T}} = \begin{bmatrix} \cos n\frac{2\pi}{N}0 & \sin n\frac{2\pi}{N}0 \\ \cos n\frac{2\pi}{N}1 & \sin n\frac{2\pi}{N}1 \\ \vdots & \vdots \end{bmatrix} \qquad (4\text{-}7)$$

Equation (4-6) can be further reduced by making use of the fact that

$$\begin{Bmatrix} f_{cn}\cos n\Omega t - f_{sn}\sin n\Omega t \\ f_{cn}\sin n\Omega t + f_{sn}\cos n\Omega t \end{Bmatrix} = Re\left[\begin{Bmatrix} \bar{f}_n \\ -i\bar{f}_n \end{Bmatrix} e^{in\Omega t} \right] \tag{4-8}$$

where

$$\bar{f}_n = f_{cn} + i f_{sn}$$

Now the forcing on the blades due to an engine order disturbance can be written in matrix form as,

$$\underset{\sim}{m}^{D*} = \underset{\sim}{T} \begin{Bmatrix} 1 \\ -i \end{Bmatrix} \bar{f}_n e^{in\Omega t} \tag{4-9}$$

Substituting (4-9) into (3-27) gives an equation of motion for sinusoidal forcing as follows,

$$\underset{\sim}{M1}\,\underset{\sim}{\ddot{q}_b} + \underset{\sim}{C}\,\underset{\sim}{\dot{q}_b} + \underset{\sim}{K}\,\underset{\sim}{q_b} + \underset{\sim}{G}\,\underset{\sim}{Y} = \underset{\sim}{P}^T\underset{\sim}{T} \begin{Bmatrix} 1 \\ -i \end{Bmatrix} \bar{f}_n e^{in\frac{\Omega}{\omega_0}\tau}$$

$$\underset{\sim}{\dot{Y}} + \underset{\sim}{H}\,\underset{\sim}{Y} = \underset{\sim}{\dot{q}_b} \tag{4-10}$$

where the matrices $\underset{\sim}{M}$, $\underset{\sim}{C}$, $\underset{\sim}{K}$, $\underset{\sim}{G}$, $\underset{\sim}{H}$, , and $\underset{\sim}{Y}$ have been defined in (3-29) and (2-42). Since the problem is linear, solutions for different

engine orders can be superposed. It is only necessary to solve for a single engine order response at a time. Later, constructing the response to any engine order forcing pattern is a matter of superposing the responses to the different engine orders.

Next, examine the form of the matrix product $\underset{\sim}{P}^T\underset{\sim}{T}$. For engine orders n up to the maximum structural mode (here, (N-1)/2), the trigonometric relations (3-30) can be used to obtain

$$\underset{\sim}{P}^T \underset{\sim}{m}^{D^*} = \underset{\sim}{P}^T \underset{\sim}{T} \begin{Bmatrix} 1 \\ -i \end{Bmatrix} \bar{f}_n e^{i n \frac{\Omega}{\omega_0} \tau} = \begin{Bmatrix} N\ \delta_{0n}\ \bar{f}_0 \\ N/2\ \delta_{1n}\ \bar{f}_1 e^{i \frac{\Omega}{\omega_0} \tau} \\ -iN/2\ \delta_{1n}\ \bar{f}_1 e^{i \frac{\Omega}{\omega_0} \tau} \\ N/2\ \delta_{2n}\ \bar{f}_2 e^{i \frac{2\Omega}{\omega_0} \tau} \\ -iN/2\ \delta_{2n}\ \bar{f}_2 e^{i \frac{2\Omega}{\omega_0} \tau} \\ \vdots \\ N/2\ \delta_{\frac{N-1}{2}n}\ \bar{f}_{\frac{N-1}{2}} e^{i \frac{N-1}{2} \frac{\Omega}{\omega_0} \tau} \\ -iN/2\ \delta_{\frac{N-1}{2}n}\ \bar{f}_{\frac{N-1}{2}} e^{i \frac{N-1}{2} \frac{\Omega}{\omega_0} \tau} \end{Bmatrix} \qquad (4\text{-}11)$$

$$0 \le n \le \frac{N-1}{2} \qquad \delta_{rn} = \begin{cases} 0 & n \neq r \\ 1 & n = r \end{cases}$$

where δ_{rn} is the Kronecker delta, and n is the engine order chosen. So, in a tuned rotor, forcing in engine order n will excite only the n = r structural modes for harmonics r less than N/2. In a mistuned rotor, the cross-coupling of the structural modes generally leads to an excitation of all structural modes, even though a single engine order is being forced. In reality, engine orders higher than the number of structural modes used often are of interest. In these cases the relations (3-30) can no longer be applied. Use instead the following to determine $\underset{\sim}{P}^T\underset{\sim}{T}$,

$$\begin{aligned}
\sin n\theta_j \sin r\theta_j &= \tfrac{1}{2}\cos(n-r)\theta_j - \tfrac{1}{2}\cos(n+r)\theta_j \\
\sin n\theta_j \cos r\theta_j &= \tfrac{1}{2}\sin(n-r)\theta_j + \tfrac{1}{2}\sin(n+r)\theta_j \\
\cos n\theta_j \sin r\theta_j &= -\tfrac{1}{2}\sin(n-r)\theta_j + \tfrac{1}{2}\sin(n+r)\theta_j \\
\cos n\theta_j \cos r\theta_j &= \tfrac{1}{2}\cos(n-r)\theta_j + \tfrac{1}{2}\cos(n+r)\theta_j
\end{aligned} \qquad (4-12)$$

$$\sum_{j=0}^{N-1} \sin m\theta_j = 0$$

$$\sum_{j=0}^{N-1} \cos m\theta_j = \begin{cases} N & \text{for } m = N, 2N, 3N\cdots \\ 0 & \text{for } m \neq N, 2N, 3N\cdots \end{cases}$$

See [12]. Now it can be seen that the r = 0 structural mode is excited not only by the n = 0 engine order but also the n = N, 2N, 3N, etc. engine orders. Whenever the sum or difference of the engine order and the

structural mode number equals a multiple of the number of blades, there will be an excitation of that structural mode by that engine order. As an example, the engine orders and the structural modes of vibration they will excite in a tuned rotor are listed in Table 9.

To find the response of the blades to engine order excitations, start with the mistuned cascade equations of motion (3-32), where the disturbance moment for the engine order chosen has been defined above,

$$\underset{\sim}{A}\,\underset{\sim}{\overset{\circ}{X}} - \underset{\sim}{B}\,\underset{\sim}{X} = \underset{\sim}{F} = \left\{ \begin{matrix} \underset{\sim}{0} \\ \underset{\sim}{P}^{T}\,\underset{\sim}{T}\left\{ \begin{matrix} 1 \\ -i \end{matrix} \right\} \bar{f}_n \\ \underset{\sim}{0} \end{matrix} \right\} e^{i n \frac{\Omega}{\omega_0} \tau} \qquad (3\text{-}32)$$

The steady-state solution to forcing that has a time variation of the form $e^{i n \frac{\Omega}{\omega_0} \tau}$ can be expressed as,

$$\underset{\sim}{X} = \underset{\sim}{\bar{X}}\, e^{i n \frac{\Omega}{\omega_0} \tau} \qquad (4\text{-}13)$$

Substituting into (3-32) and solving for $\underset{\sim}{\bar{X}}$ yields,

$$\underset{\sim}{\bar{X}} = \left[i n \frac{\Omega}{\omega_0} \underset{\sim}{A} - \underset{\sim}{B} \right]^{-1} \left\{ \begin{matrix} \underset{\sim}{0} \\ \underset{\sim}{P}^{T}\,\underset{\sim}{T}\left\{ \begin{matrix} 1 \\ -i \end{matrix} \right\} \bar{f}_n \\ \underset{\sim}{0} \end{matrix} \right\} \qquad (4\text{-}14)$$

Since $\underset{\sim}{X} = [\underset{\sim}{q}_b \quad \dot{\underset{\sim}{q}}_b \quad \underset{\sim}{Y}]^T$, the torsional response of the blades, $\underset{\sim}{\alpha}$, can be obtained by extracting the modal eigenvector $\bar{q}$ from $\bar{\underset{\sim}{X}}$, and using (3-26) to obtain,

$$\underset{\sim}{\alpha} = \underset{\sim}{P}\,\underset{\sim}{q}_b \qquad (3\text{-}26)$$

For a tuned rotor, $\underset{\sim}{A}$, $\underset{\sim}{B}$, $\underset{\sim}{F}$, and $\underset{\sim}{X}$ are as in (3-19), where m^{b*} is given by (4-5). A computer program was written to set up and solve the forced response problem associated with tuned and mistuned cascades. See Appendix C. Shown in figure 16 is the frequency response of the blades of a tuned rotor to an $n = 1$ engine order excitation. It is typical of the response of a single degree of freedom system.

A comparison can be made of the damping obtained by solving the flutter problem in transient form with the damping ratio obtained from the half-power points of the response curve. The relationships required are

$$\frac{a}{\omega_0} = \zeta \frac{\omega_n}{\omega_0} \quad , \quad \left(\frac{\Delta\omega}{\omega_0}\right)_{\text{half-power}} \cong 2\zeta \frac{\omega_n}{\omega_0} \qquad (4\text{-}15)$$

where a/ω_0 is the real part of the eigenvalue associated with interblade phase angle mode being forced. In this case the backward traveling wave is being forced. The damping ratio using the flutter data is $\zeta_A = 0.0079$ for the backward traveling wave mode. See figure 7. From the half-power points of the response curve, the damping ratio $\zeta_A = 0.0086$. Remember that there is no structural damping, so these numbers represent levels of aerodynamic damping.

Also plotted in figure 16 are the responses of the rotor mistuned by letting blade zero have a 5% higher frequency than the remaining blades. Now the n = 1 engine order excitation forces all the interblade phase angle modes, resulting in different levels of response for each blade. For clarity only the responses of the mistuned blade and the blades adjacent to it are shown in the amplitude plot. The forced response of adjacent blades is similar to the response of a two degree of freedom system. See, for example, [13]. The 40 degree interblade phase angle representing the backward traveling wave of the forcing function is apparent in the phase plot. At resonances the mistuned blade, blade 0, is vibrating in phase with the adjacent blade, blade 8. Instead of lagging the motion of blade 8 as in the tuned case, the motion of blade 0 leads the motion of blade 8, for frequencies between their respective resonance frequencies. Far away from resonances the tuned and mistuned systems show essentially the same response.

The forced response of the mistuned system is worse than the response of the tuned system. To explain this, examine the shifting of the eigenvalues of the two systems, shown in figure 17. The damping ratio associated with the mode being forced decreases when the rotor is mistuned, hence the worsening of the forced response for this particular case. Although the structural mode being forced is not a pure $\beta_r = 40$ degrees mode (because of mistuning), that mode will still have the largest response, as will be shown for the case of the alternately mistuned cascade. For forcing frequencies away from resonance, the phase between adjacent blades is -40 degrees, showing that the forcing is of the form of

a backward traveling wave, which is to be expected.

The frequency response for the "alternately" mistuned rotor is shown in figures 18 and 19. Again, the mistuned response is worse for the mistuned cascade than for the tuned cascade. The eigenvalue of the mistuned system associated most closely with the type of forcing has been shifted to the right due to mistuning, resulting in lower levels of damping for that mode. (See figure 17.) Note that at resonances, pairs of high and low frequency blades vibrate in phase, while between resonances, the high frequency blade leads the low frequency blade in the motion. Far below resonance, the motion of all blades is in phase with the engine order forcing.

The modal response of the tuned and mistuned systems is shown in figures 20-22. Only the amplitudes are shown. To reconstruct the blade amplitudes from the modal amplitudes, information about the relative phasing of the blades is required. For the tuned system, the only modal response is in the mode that is being forced, as was stated earlier. For the mistuned cascade, all modes are excited, the largest response still being in the mode being forced. Note that the mode associated with the engine order forcing has a smaller mistuned response.

4.2 Transient Response

The flutter and forced response of cascades can be examined using either traveling wave analysis or standing wave analysis. However, the

important problem of the transient response of cascades can not be examined using traveling wave analysis. One way to examine the transient behavior of cascades is by expressing the motion of the blades and corresponding airloads in terms of standing wave modes.

By casting the cascade airloads into a general form, (2-40) and (2-42), the transient response of the cascade can be calculated. The response of a tuned cascade to an impulsive motion of blade zero is shown in figure 23. These results were obtained by a computer program developed by the Joint Computer Facility, at M.I.T. The program DYSYS (Dynamic System Simulation) uses a fourth order Runge-Kutta integration in time. Blade zero underwent an impulsive motion and the subsequent "ringing down" of the rotor was observed. Only the envelope of the responses is shown in the lower half of figure 23. Remember that the only coupling between the blades is through the aerodynamics.

With this standing wave analysis, the response of a cascade to impacts can be examined. Current transient dynamic analyses do not allow for aerodynamic loads to influence the motion of the blades. The technique described in this work could be applied to study the effect of aerodynamic loads on the transient response of rotors.

5. Miscellaneous Applications

5.1 Flexible Disk Rotors

The present analysis dealt with a rotor whose blades were mounted on a rigid disk. In many rotors, the blades would be mounted on a flexible disk so that structural coupling between the blades would be present. To analyze these flexible disk rotors, one generally obtains the vibration modes of the coupled blade-disk system by a Rayleigh-Ritz or a finite element method, and then one expresses the torsion angle α at, say, the 80% blade span section in terms of a superposition of k normal coordinates $\underset{\sim}{\xi}(t)$ as,

$$\underset{\sim}{\alpha} = \underset{\sim}{\Phi}\,\underset{\sim}{\xi} \qquad (5\text{-}1)$$

In the above, $\underset{\sim}{\Phi}$ is an N x k matrix relating the torsion angle α at each of the N blades for each of the k vibration modes assumed in the analysis. For tuned rotors, the vibration modes generally occur in pairs for each nodal diameter r, corresponding to the $\cos j\beta_r$ and $\sin j\beta_r$ modes, used earlier for the rigid disk, (2-22), (2-35). The standing wave analysis then expresses the rotor equations of motion in the uncoupled normal form as,

$$\underset{\sim}{M}\,\ddot{\underset{\sim}{\xi}} + 2\underset{\sim}{\zeta_k}\,\underset{\sim}{\omega_k}\,\underset{\sim}{M}\,\dot{\underset{\sim}{\xi}} + \underset{\sim}{M}\,\underset{\sim}{\omega_k^2}\,\underset{\sim}{\xi} = \underset{\sim}{\Pi} \qquad (5\text{-}2)$$

where the generalized forces $\underset{\sim}{\Pi} = \underset{\sim}{\Phi}^T\,\underset{\sim}{m}$. To express the aerodynamic moment $\underset{\sim}{m}$ of (2-40) and (2-41) and the subsequent generalized forces $\underset{\sim}{\Pi}$ in terms of the normal coordinates $\underset{\sim}{\xi}$, one notes from (2-39) and (5-1) that,

$$\underset{\sim}{\alpha} = \underset{\sim}{P}\,\underset{\sim}{q} = \underset{\sim}{\Phi}\,\underset{\sim}{\xi} \qquad (5\text{-}3)$$

Multiplying this by the inverse of $\underset{\sim}{P}$ as given by (3-31) gives,

$$\underset{\sim}{q} = \underset{\sim}{P}^{-1}\underset{\sim}{\Phi}\underset{\sim}{\xi} = \underset{\sim}{D}^{-1}\underset{\sim}{P}^{T}\underset{\sim}{\Phi}\underset{\sim}{\xi} \qquad (5\text{-}4)$$

which can be substituted into $\underset{\sim}{m}$ and then into $\underset{\sim}{\Pi}$ to obtain the generalized force,

$$\underset{\sim}{\Pi} = 2\pi\rho U^2 b^2 \left\{ \underset{\sim}{E}_2 \frac{b^2}{U^2}\ddot{\underset{\sim}{\xi}} + \underset{\sim}{E}_1 \frac{b}{U}\dot{\underset{\sim}{\xi}} + \underset{\sim}{E}_0 \underset{\sim}{\xi} + \underset{\sim}{J}_1 \underset{\sim}{Y} \right\} \qquad (5\text{-}5)$$

$$\frac{b}{U}\dot{\underset{\sim}{Y}} + \underset{\sim}{q}_0 \underset{\sim}{Y} = \underset{\sim}{J}_2 \frac{b}{U}\dot{\underset{\sim}{\xi}} \qquad (5\text{-}6)$$

where,

$$\underset{\sim}{E}_2 = \underset{\sim}{\Phi}^T \underset{\sim}{P}\,\underset{\sim}{B}_2\,\underset{\sim}{D}^{-1}\underset{\sim}{P}^T\underset{\sim}{\Phi}\,, \qquad \underset{\sim}{J}_1 = \underset{\sim}{\Phi}^T\underset{\sim}{P}\,\underset{\sim}{G}$$

$$\underset{\sim}{E}_1 = \underset{\sim}{\Phi}^T \underset{\sim}{P}\,\underset{\sim}{B}_1\,\underset{\sim}{D}^{-1}\underset{\sim}{P}^T\underset{\sim}{\Phi}\,, \qquad \underset{\sim}{J}_2 = \underset{\sim}{D}^{-1}\underset{\sim}{P}^T\underset{\sim}{\Phi}$$

$$\underset{\sim}{E}_0 = \underset{\sim}{\Phi}^T \underset{\sim}{P}\,\underset{\sim}{B}_0\,\underset{\sim}{D}^{-1}\underset{\sim}{P}^T\underset{\sim}{\Phi} \qquad (5\text{-}7)$$

while $\underset{\sim}{B}_2\ \underset{\sim}{B}_1\ \underset{\sim}{B}_0\ \underset{\sim}{G}_1\ \underset{\sim}{q}_0\ \underset{\sim}{Y}$ are as defined (2-42). Equations (5-5) and (5-6) can be readily incorporated into the flutter and forced vibration of tuned and mistuned flexible bladed-disk rotors, (5-1) and (5-2).

5.2 Aerodynamic Influence Coefficients

For interest, it is sometimes useful to express the transient cascade aerodynamic influence coefficients, that is, how the motion of blade j influences the forces on another blade i in the cascade. This is readily done by inverting (2-39) to give

$$\underset{\sim}{q} = \underset{\sim}{D}^{-1} \underset{\sim}{P}^{T} \underset{\sim}{\alpha} \qquad (5\text{-}8)$$

then placing the above into the aerodynamic forces m of (2-40) and (2-41) to give,

$$\underset{\sim}{m} = 2\pi\rho U^2 b^2 \left\{ \underset{\sim}{E}_2 \frac{b^2}{U^2} \ddot{\underset{\sim}{\alpha}} + \underset{\sim}{E}_1 \frac{b}{U} \dot{\underset{\sim}{\alpha}} + \underset{\sim}{E}_0 \underset{\sim}{\alpha} + \underset{\sim}{J}_1 \underset{\sim}{Y} \right\} \qquad (5\text{-}9)$$

$$\frac{b}{U} \dot{\underset{\sim}{Y}} + \underset{\sim}{g}_0 \underset{\sim}{Y} = \underset{\sim}{J}_2 \frac{b}{U} \dot{\underset{\sim}{\alpha}} \qquad (5\text{-}10)$$

where the matrices $\underset{\sim}{E}_2$, $\underset{\sim}{E}_1$, $\underset{\sim}{E}_0$, $\underset{\sim}{J}_1$, $\underset{\sim}{J}_2$ are defined in (5-7), but without the $\underset{\sim}{\Phi}$ or $\underset{\sim}{\Phi}^T$ matrices present. Allowing only motion of the j^{th} blade α_j and setting all other blade motions equal to zero, gives the forces on the i^{th} blade as,

$$m_i = 2\pi\rho U^2 b^2 \left\{ (E_2)_{ij} \frac{b^2}{U^2} \ddot{\alpha}_j + (E_1)_{ij} \frac{b}{U} \dot{\alpha}_j + (E_0)_{ij} \alpha_j + \underset{\sim}{J}_1 \underset{\sim}{Y} \right\} \qquad (5\text{-}11)$$

$$\frac{b}{U} \dot{\underset{\sim}{Y}} + \underset{\sim}{g}_0 \underset{\sim}{Y} = \underset{\sim}{J}_2 \frac{b}{U} \dot{\alpha}_j \qquad (5\text{-}12)$$

where $\underset{\sim}{Y}$ still represents a column matrix, while $\underset{\sim}{J}_1$ now represents the i^{th} row of the previous square matrix $\underset{\sim}{J}_1$, and $\underset{\sim}{J}_2$ the j^{th} column of the previous square matrix J_2. The above cascade aerodynamic influence coefficients are valid provided the number of blades N is large enough for cascade influences to die out.

The influence coefficients representation given by (5-11) and (5-12) can be written in more familiar form by solving for the augmented state variables $\underset{\sim}{Y}$ from (5-12) and placing into (5-11) to obtain,

$$m_i = 2\pi\rho U^2 b^2 \left\{ (E_2)_{ij} \frac{b^2}{U^2} \ddot{\alpha}_j + (E_1)_{ij} \frac{b}{U} \dot{\alpha}_j + (E_0)_{ij} \alpha_j + \sum_{k=0}^{N-1} (J_1)_{ik} (J_2)_{kj} \int_0^t e^{-(g_0)_k \frac{b}{U}(t-t')} \dot{\alpha}_j(t')\, dt' \right\} \tag{5-13}$$

The convolution integrals above represent a form of aerodynamic "lag" effect, as discussed previously, see Equation (2-17).

Cascade aerodynamic influence coefficients were determined numerically for the $N = 9$, $s/c = 1$, $\xi = 45^\circ$, $\eta = .5$ case considered previously in most of the torsional flutter and forced response calculations. Table 10 gives values of the basic $\underset{\sim}{P}$ matrix defined in (2-39) and (2-42) for a nine bladed rotor, N = 9. Table 11 shows the transient Whitehead coefficients used for all the torsional flutter analyses here, that is, type D, N = 9, S/C = 1, $\xi = 45^0$, and $\eta = .5$ cases. These values were interpolated from the general Table 2, for pitching about the midchord ($\eta = .5$) and N = 9. Finally, Table 12 gives the aerodynamic influence coefficients for the moment on blade i due to the motion of blade j = 0. For this case, (5-13) can be expressed as,

$$m_i = 2\pi\rho U^2 b^2 \left\{ (E_2)_{i0} \frac{b^2}{U^2} \ddot{\alpha}_0 + (E_1)_{i0} \frac{b}{U} \dot{\alpha}_0 + (E_0)_{i0} \alpha_0 + \sum_{m=1}^{4} (H_m)_{i0} \int_0^t e^{-(g_0)_m \frac{b}{U}(t-t')} \dot{\alpha}_0(t')\, dt' \right\} \tag{5-14}$$

Because of the cyclic symmetry of the $\underset{\sim}{E}_i$ matrices, it can easily be shown that the m_1 due to α_0 is the same as m_2 due to α_1, m_3 due to α_2, m_0

due to α_8, etc. Hence, the coefficients given in Table 12 can be used to assess the forces on any blade due to the motion of any other blade. For comparison, the isolated blade (Theodorsen) forces are also given in Table 12. These, of course, can only express the forces on a blade due to the motion of the same blade.

6. Conclusions

The present report has given a unified standing wave approach to the flutter and forced response of turbine engine rotors. Both tuned and mistuned rotors can be readily accomodated.

The traditional traveling wave cascade airforces have been recast into standing wave, arbitrary motion form, by making use of Padé approximants. Some standing wave coefficients are given for Whitehead's 2-dimensional incompressible cascade theory.

Flutter analyses were conducted using standard constant coefficient, linear systems techniques. The analyses give true damping decay rates rather than damping margins. Typical examples for tuned and mistuned rotors are given.

The forced response of the rotor to periodic engine order excitation of all the blades, and to the transient impulsive excitation of a single blade is obtained using the same aerodynamic damping as for the flutter cases. Typical examples for tuned and mistuned rotors are given.

Extensions of the procedure here is indicated for the case of flexible disk rotors, where structural as well as aerodynamic coupling exists between the blades. Also, the aerodynamic influence coefficients for the effect of one blade's motion on the forces produced at another blade is given.

The standing wave analysis methods given here can be extended to other flow regimes [3], [4], [5], by similar fitting of the sinusoidal

traveling wave coefficients. Also, they can be extended to flexible disk rotors as indicated previously in Chapter 5. These standing wave methods may prove to be more versatile for dealing with certain applications, such as coupling flutter with forced response and dynamic shaft problems, transient impulses on the rotor, low engine order excitation, bearing motions, and mistuning effects in rotors.

References

[1] Dugundji, J., "Flutter Analysis of a Tuned Rotor with Rigid and Flexible Disks," GT&PDL Report No. 146, M.I.T., Cambridge, MA, July 1979.

[2] Whitehead, D. S., "Force and Moment Coefficients for Vibrating Airfoils in Cascade," R&M No. 3254, British Aeronautical Research Council, London, February 1960.

[3] Smith, S. N., "Discrete Frequency Sound Generation in Axial Flow Turbomachinery," R&M No. 3709, British Aeronautical Research Council, London, 1973.

[4] Adamczyk, J. J., and Goldstein, M. E., "Unsteady Flow in a Supersonic Cascade with Subsonic Leading Edge Locus," AIAA Journal, Vol. 16, No. 12, December 1978.

[5] Whitehead, D. S., and Grant, R. J., "Force and Moment Coefficients for High Deflection Cascades," University of Cambridge, CUED/A-Turbo/TR 98, May 1980.

[6] Edwards, J. W., Ashley, H., and Breakwell, J. V., "Unsteady Aerodynamic Modeling for Arbitrary Motions," AIAA Journal, Vol. 17, No. 4, April 1979.

[7] Srinivasan, A. V., "Influence of Mistuning on Blade Torsional Flutter," NASA CR-165137, August 1980.

[8] Kaza, K. R. V. and Kielb, R. E., "Effects of Mistuning on Bending-Torsion Flutter and Response of a Cascade in Incompressible Flow," AIAA/ASME/ASCE/AHS 22nd Structures, Structural Dynamics and Materials Conference, April 9-10, 1981, Atlanta, Georgia.

[9] Vepa, R., "On the Use of Pade Approximants to Represent Unsteady Aerodynamic Loads for Arbitrary Small Motions of Wings," AIAA Paper 76-17, 1976.

[10] Bisplinghoff, R. L., Ashley, H. and Halfman, R. L., Aeroelasticity, Addison-Wesley Publishing Co., Cambridge, MA, 1955.

[11] Rock, S. M., and DeBra, D. B., "Prediction and Experimental Verification of Transient Airfoil Motion," J. Aircraft, Vol. 19, No. 6, June 1982.

[12] Dugundji, J. and Wendall, J. H., "General Review of the MOSTAS Computer Code for Wind Turbines," DOE/NASA/3303-1, NASA CR-165835, ASRL TR 197-1, M.I.T., June 1981.

[13] Den Hartog, J. P., Mechanical Vibrations, McGraw-Hill Book Co., Inc., New York, 1947.

[14] "Numerical Analysis User's Guide," Application Program Series AP-3, Revision 2. Information Processing Services, M.I.T., November 1982.

[15] "EISPACK at IPS," Application Program Series AP-4, Revision 2. Information Processing Services, M.I.T., October 1982.

Appendix A. Fitting Aerodynamic Coefficients

The first step in the fitting process is to express the traveling wave aerodynamic forces in the form

$$\ell = 2\pi\rho U^2 b\left[A_A \frac{\bar{h}}{b} + A_B \bar{\alpha}\right] e^{i(\omega t + j\beta_r)} \qquad (A1)$$

$$m/b = 2\pi\rho U^2 b\left[A_C \frac{\bar{h}}{b} + A_D \bar{\alpha}\right] e^{i(\omega t + j\beta_r)} \qquad (A2)$$

where the nondimensional complex coefficients A_A, A_B, A_C, A_D, are functions of reduced frequency k, interblade phase angle β_r, and other geometric and flight parameters. The relations between these coefficients and the tabulated data of Whitehead are given by (2-27). Traveling waves with interblade phase angles β_r between 0 degrees and 180 degrees are refered to as forward traveling waves (in the direction of rotation), and those with interblade phase angles β_r between 180 degrees and 360 degrees are referred to as backward traveling waves. Backward traveling waves have an interblade phase angle of $-\beta_r$ or $(360 - \beta_r)$. In this way the coefficients defined by (2-10) can be generated. A_R^+ refers to the real part of a traveling wave aerodynamic force or moment which has the form

$$f = (A_R^+ + i A_I^+)\alpha_o e^{i(\omega t + j\beta_r)} \qquad (A3)$$

A_R^- refers to the real part of a traveling wave aerodynamic force or moment which has the form

$$f = (A_R^- + i A_I^-)\alpha_o e^{i(\omega t - j\beta_r)} \qquad (A4)$$

Once $\bar{A}_R$, $\bar{A}_I$, $\bar{\bar{A}}_R$, and $\bar{\bar{A}}_I$, are formed, (2-19) can be used to solve for the standing wave coefficients B_2, B_1, B_0, etc. Since Whitehead has tabulated values of the traveling wave coefficients only for k = 0, k = .1, k = .25, k = .5, and k = 1, the coefficients $\bar{A}_R$, $\bar{A}_I$, $\bar{\bar{A}}_R$, and $\bar{\bar{A}}_I$, were fit at k = 0, k = .1, and k = 1 and the values at k = .25 and k = .5 were used to gauge the fit. This is a very simple way of determining the standing wave coefficients, and as it turns out, gives very good results. So, there are 12 equations: $\bar{A}_R(k = 0, .1, 1)$, $\bar{A}_I(k = 0, .1, 1)$, $\bar{\bar{A}}_R(k = 0, .1, 1)$, $\bar{\bar{A}}_I(k = 0, .1, 1)$, and 10 unknowns, B_2, B_1, B_0, G_1, g_c, $\tilde{B}_2$, $\tilde{B}_1$, $\tilde{B}_0$, $\tilde{G}_1$, and $\tilde{g}_c$. In order to avoid using two augmented equations (2-16) for each mode, and requiring two coefficients g_c, $\tilde{g}_c$; g_c was set to some intermediate value, and the coefficient $\tilde{g}_c$ was set to zero. Some trial-and-error was involved in picking the final value of g_c. There was a minor effect on the accuracy of the fits due to the elimination of an augmented state. The first two equations of (2-19) are solved for B_2, B_1, B_0, G_1, and g_c, at k = 0, k = .1, and k = 1. Since the second equation of (2-19) is automatically satisfied for k = 0, there are 5 equations in 5 unknowns:

$$\bar{A}_R(0) = B_0 \tag{A5}$$

$$100\left[\bar{A}_R(.1) - \bar{A}_R(0)\right] = -B_2 + \frac{G_1}{g_0^2 + .01} \tag{A6}$$

$$\left[\bar{A}_R(1) - \bar{A}_R(0)\right] = -B_2 + \frac{G_1}{g_0^2 + 1} \tag{A7}$$

$$10\,\bar{A}_I(.1) = B_1 + \frac{g_0 G_1}{g_0^2 + .01} \tag{A8}$$

$$\bar{A}_I(1) = B_1 + \frac{g_0 G_1}{g_0^2 + 1} \tag{A9}$$

Subtracting (A7) from (A6) gives

$$G_1 = \frac{100\,\bar{A}_R(.1) - 99\bar{A}_R(0) - A_R(1)}{\left(\frac{1}{g_0^2 + .01} - \frac{1}{g_0^2 + 1}\right)} \tag{A10}$$

Subtracting (A9) from (A8) gives

$$G_1 = \frac{10\,\bar{A}_I(.1) - \bar{A}_I(1)}{g_0\left(\frac{1}{g_0^2 + .01} - \frac{1}{g_0^2 + 1}\right)} \tag{A11}$$

Setting (A10) equal to (A11) and solving for g_0 gives

$$g_o = \frac{10\,\bar{A}_I(.1) - \bar{A}_I(1)}{100\,\bar{A}_R(.1) - 99\,\bar{A}_R(0) - \bar{A}_R(.1)} \qquad (A12)$$

Adding (A6) and (A7) and solving for B_2 yields

$$B_2 = -\frac{1}{2}\left\{100\bar{A}_R(.1) - 101\,\bar{A}_R(0) + \bar{A}_R(1) - G_1\left(\frac{1}{g_o^2+.01} + \frac{1}{g_o^2+1}\right)\right\} \qquad (A13)$$

Adding (A8) and (A9) and solving for B_1 yields

$$B_1 = \frac{1}{2}\left\{10\bar{A}_I(.1) + \bar{A}_I(1) - g_o G_1\left(\frac{1}{g_o^2+.01} + \frac{1}{g_o^2+1}\right)\right\} \qquad (A14)$$

The standing wave coefficients B_o, g_o, G_1, B_2, B_1, can be obtained from equations (A5), (A12), (A11), (A13), and (A14) respectively. To find the coefficients $\tilde{B}_2$, $\tilde{B}_1$, $\tilde{B}_o$, $\tilde{G}_1$, replace $\bar{A}_R$ by $-\bar{\bar{A}}_I$ and $\bar{A}_I$ by $\bar{\bar{A}}_R$ in the above equations. The coefficients for Whitehead [2] aerodynamics are shown in Tables 1 and 2 for stagger angle ξ = 0 degrees and ξ = 45 degrees, respectively.

Appendix B. Flutter Points of a Tuned Cascade

Starting with the equation of motion of any blade in a tuned cascade

$$I_{\alpha_j}\ddot{\alpha}_j + 2\zeta_j\omega_{\alpha_j}I_{\alpha_j}\dot{\alpha}_j + \omega_{\alpha_j}^2 I_{\alpha_j}\alpha_j = m_j \qquad (3\text{-}1)$$

where the moment m_j can be written in terms of the Whitehead traveling wave coeffients as,

$$m_j = 2\pi\rho U^2 b^2 \left[2(C_{M\alpha})_\eta\right]\bar{\alpha}\, e^{i(\omega t + j\beta_r)} \qquad (B1)$$

Here the coefficient $C_{M\alpha}$ is in general a function of reduced frequency, interblade phase angle, gap-to-chord ratio, stagger angle, and elastic axis location. See if there is a traveling wave flutter solution of the form

$$\alpha = \bar{\alpha}\, e^{i(\omega t + j\beta_r)} \qquad (B2)$$

Substituting (B1) and (B2) into (3-1) yields

$$-\omega^2 I_\alpha + 2\zeta\omega_\alpha i\omega + I_\alpha\omega_\alpha^2 = 2\pi\rho U^2 b^2\left[2(C_{M\alpha})_\eta\right] \qquad (B3)$$

Dividing by $\omega_0^2 I_\alpha$ and casting the equation into nondimensional form yields,

$$-\gamma^2 + i2\zeta\gamma_\alpha\gamma + \gamma_\alpha^2 = \frac{2\bar{u}^2}{\nu}\left[2(C_{m\alpha})_\eta\right] \qquad (B4)$$

Where ν, $\bar{u}$, and γ_α are defined by (3-6) and $\gamma = \omega/\omega_\alpha$. For (B2) to be the solution, the real and imaginary parts of (B4) must be true

$$\text{Re:}\quad \gamma_\alpha^2 - \gamma^2 = \frac{2\bar{u}^2}{\nu}\left[2\,\mathrm{Re}\left\{(C_{m\alpha})_\eta\right\}\right] \qquad (B5)$$

$$\text{Im:}\quad 2\zeta\gamma_\alpha\gamma = \frac{2\bar{u}^2}{\nu}\left[2\,\mathrm{Im}\left\{(C_{m\alpha})_\eta\right\}\right] \qquad (B6)$$

The real equation shows the difference between the undamped natural frequency ratio $\gamma_\alpha = \omega_\alpha/\omega_\alpha$ and the frequency ratio of vibration $\gamma = \omega/\omega_\alpha$. Since the inertia ratio ν is large for rotor blades in general, the flutter frequency is generally close to the undamped natural frequency, $\gamma \approx \gamma_\alpha$. The imaginary part of equation (B6), upon rearranging, gives the condition for instability as,

$$\zeta + \zeta_A < 0 \qquad (B7)$$

where

$$\zeta_A = -\frac{1}{\nu}\frac{\bar{u}^2}{\gamma\gamma_\alpha}\left[2\,\mathrm{Im}\left\{(C_{M\alpha})_\eta\right\}\right] \qquad (B8)$$

is the aerodynamic damping. Since $\gamma \approx \gamma_\alpha$,

$$\mathcal{S}_A = -\frac{1}{\nu k^2} \operatorname{Im}\left\{2\left(C_{M\alpha}\right)_\eta\right\}$$

Setting the structural damping $\varsigma = 0$, yields the new condition for instability,

$$\mathcal{S}_A < 0$$

See reference [1]. The values of $C_{M\alpha}$ are tabulated by Whitehead for k = 0, .1, .25, .5, and 1. The approximation to the traveling wave $C_{M\alpha}$ can be reconstructed from the standing wave coefficients as follows. For traveling wave interblade phase angles β_r = 0 degrees to β_r = 180 degrees

$$\mathcal{S}_A = \frac{-1}{\nu k^2}\left\{B_{1D}\,k - \tilde{B}_{0D} + \frac{k g_0 G_{1D} - k^2 \tilde{G}_{1D}}{k^2 + g_0^2}\right\}_\eta \qquad (B9)$$

For interblade phase angles β_r = 180 degrees to β_r = 360 degrees

$$\mathcal{S}_A = \frac{-1}{\nu k^2}\left\{B_{1D}\,k + \tilde{B}_{0D} + \frac{k g_0 G_{1D} + k^2 \tilde{G}_{1D}}{k^2 + g_0^2}\right\}_\eta \qquad (B10)$$

A comparison of exact Whitehead values of $\mathcal{S}_A$ with reconstructed values of $\mathcal{S}_A$ is shown in Table 9, for an inertia ratio ν = 86.2. The example is a nine-bladed rotor with a 45 degree stagger angle, pitching about midchord. Only the 3 least stable interblade phase angle modes are shown. Since Whitehead tabulated values of coefficients at interblade

phase angles which are multiples of 36 degrees, the Whitehead and the standing wave coefficients were linearly interpolated to find values of the coefficients at 40, 80 and 120 degrees.

These results can be compared with the eigenvalues obtained from the transient formulation. Since the tuned cascade flutter problem results in uncoupled equations, it is easy to look at the flutter of an individual mode. The uncoupled problem is third order, resulting in eigenvalues of the form $\tilde{p} = a_1/\omega_0 \pm i\gamma$ and a_2/ω_0. Since a_2 is always negative and large compared to a_1, any response associated with a_2 will be short-lived. The steady-state problem can be considered second order and the complex conjugate eigenvalues $a_1/\omega_0 \pm i\gamma$ can be represented as

$$-\zeta\omega_\alpha \pm i\omega_\alpha\sqrt{1-\zeta^2}$$

See [13], for example. For the tuned cascade, this means that the real part of the eigenvalue is equal to the amount of aerodynamic damping present,

$$-\frac{a_1}{\omega_0} = \zeta_A$$

Remember that there is no structural damping, and that for the tuned case $\omega_0 = \omega_\alpha$. Now the actual aerodynamic damping obtained from the transient decay can be compared with the structural damping required for flutter. The only point where there must be agreement is the flutter point. At the flutter point, zero structural damping is required, and the real part of

the eigenvalue is zero. Figure 8 shows the variation of the aerodynamic damping computed by both methods.

Appendix C. Standing Waves to Traveling Waves

The standing wave deflections and corresponding air forces are given by (2-22), (2-23), (2-24) and (2-25) as,

$$\alpha_j(t) = q_{cr}(t)\cos j\beta_r + q_{sr}(t)\sin j\beta_r \qquad (C-1)$$

$$\begin{aligned} m_j = 2\pi\rho U^2 b^2 \Big\{ & \Big[B_2 \frac{b^2}{U^2}\ddot{q}_{cr} + B_1 \frac{b}{U}\dot{q}_{cr} + B_0 q_{cr} + G_1 Y_{cr} \\ & - \tilde{B}_2 \frac{b^2}{U^2}\ddot{q}_{sr} - \tilde{B}_1 \frac{b}{U}\dot{q}_{sr} - \tilde{B}_0 q_{sr} - \tilde{G}_1 Y_{sr} \Big] \cos j\beta_r \\ & + \Big[B_2 \frac{b^2}{U^2}\ddot{q}_{sr} + B_1 \frac{b}{U}\dot{q}_{sr} + B_0 q_{sr} + G_1 Y_{sr} \\ & + \tilde{B}_2 \frac{b^2}{U^2}\ddot{q}_{cr} + \tilde{B}_1 \frac{b}{U}\dot{q}_{cr} + \tilde{B}_0 q_{cr} + \tilde{G}_1 Y_{cr} \Big] \sin j\beta_r \Big\} \end{aligned} \qquad (C-2)$$

$$\frac{b}{U}\dot{Y}_{cr} + g_0 Y_{cr} = \frac{b}{U}\dot{q}_{cr} \qquad (C-3)$$

$$\frac{b}{U}\dot{Y}_{sr} + g_0 Y_{sr} = \frac{b}{U}\dot{q}_{sr} \qquad (C-4)$$

To reduce to traveling wave representation, one assumes harmonic motion of the form,

$$q_{cr}(t) = \bar{\alpha}_r e^{i\omega t} \qquad (C-5)$$

$$q_{sr}(t) = i\bar{\alpha}_r e^{i\omega t}$$

This implies the two standing wave coordinates $q_{cr}(t)$ and $q_{sr}(t)$ are 90° out of phase with one another. Placing the above into (c-1) gives,

$$\begin{aligned}\alpha_j &= \bar{\alpha}_r e^{i\omega t}\cos j\beta_r + i\bar{\alpha}_r e^{i\omega t}\sin j\beta_r \\ &= \bar{\alpha}_r e^{i\omega t} e^{ij\beta_r} \\ &= \bar{\alpha}_r e^{i(\omega t + j\beta_r)}\end{aligned} \qquad (C-6)$$

This gives the traveling wave deflection indicated by (2-1).

Placing (c-5) into the augmented state equations (c-3) and (c-4), and assuming harmonic motion for Y_{cr} and Y_{sr} gives,

$$\begin{aligned}(ik + g_o)\bar{Y}_{cr} e^{i\omega t} &= ik\,\bar{\alpha}_r e^{i\omega t} \\ (ik + g_o)\bar{Y}_{sr} e^{i\omega t} &= ik\, i\bar{\alpha}_r e^{i\omega t}\end{aligned} \qquad (C-7)$$

Placing (c-5) and the Y_{cr} and Y_{sr} from (c-7) into the moment equation (c-2) gives,

$$\begin{aligned}m_j = 2\pi\rho U b^2 \Big\{ &\left[-k^2 B_2 + ikB_1 + B_o + \frac{ikG_1}{ik+g_o}\right]\bar{\alpha}_r e^{i\omega t}\cos j\beta_r \\ &- \left[-k^2\tilde{B}_2 + ik\tilde{B}_1 + \tilde{B}_o + \frac{ik\tilde{G}_1}{ik+g_o}\right] i\bar{\alpha}_r e^{i\omega t}\cos j\beta_r \\ &+ \left[-k^2 B_2 + ikB_1 + B_o + \frac{ikG_1}{ik+g_o}\right] i\bar{\alpha}_r e^{i\omega t}\sin j\beta_r \\ &+ \left[-k^2\tilde{B}_2 + ik\tilde{B}_1 + \tilde{B}_o + \frac{ik\tilde{G}_1}{ik+g_o}\right]\bar{\alpha}_r e^{i\omega t}\sin j\beta_r \Big\}\end{aligned} \qquad (C-8)$$

Comparing the above expression with the coefficients $\bar{A}_R, \bar{A}_I, \bar{\bar{A}}_R, \bar{\bar{A}}_I$ defined by (2-19), one can rewrite (c-8) as,

$$\begin{aligned} m_j = 2\pi\rho U^2 b^2 \Big\{ & (\bar{A}_R + i\bar{A}_I)\bar{\alpha}_r e^{i\omega t} \cos j\beta_r \\ & + (\bar{\bar{A}}_I - i\bar{\bar{A}}_R) i\bar{\alpha}_r e^{i\omega t} \cos j\beta_r \\ & + (\bar{A}_R + i\bar{A}_I) i\bar{\alpha}_r e^{i\omega t} \sin j\beta_r \\ & + (-\bar{\bar{A}}_I + i\bar{\bar{A}}_R)\bar{\alpha}_r e^{i\omega t} \sin j\beta_r \Big\} \end{aligned} \qquad (c-9)$$

$$= 2\pi\rho U^2 b^2 \left\{ \bar{A}_R e^{ij\beta_r} + i\bar{A}_I e^{ij\beta_r} + \bar{\bar{A}}_R e^{ij\beta_r} + i\bar{\bar{A}}_I e^{ij\beta_r} \right\} \bar{\alpha}_r e^{i\omega t}$$

$$= 2\pi\rho U^2 b^2 \left\{ (\bar{A}_R + \bar{\bar{A}}_R) + i(\bar{A}_I + \bar{\bar{A}}_I) \right\} \bar{\alpha}_r e^{i(\omega t + j\beta_r)}$$

Then, noting the definitions of $\bar{A}_R$, $\bar{A}_I$, $\bar{\bar{A}}_R$, $\bar{\bar{A}}_I$ in (2-10), the above reduces to,

$$m_j = 2\pi\rho U^2 b^2 (A_R^+ + iA_I^+) \bar{\alpha}_r e^{i(\omega t + j\beta_r)} \qquad (c-10)$$

which is the same aerodynamic force indicated by (2-2).

Similarly, if one assumes harmonic motion of the form,

$$q_{cr}(t) = \bar{\alpha}_r e^{i\omega t}$$

$$q_{sr}(t) = -i\,\bar{\alpha}_r e^{i\omega t} \qquad (C-11)$$

and goes through the same reduction, one will obtain

$$\alpha_j = \bar{\alpha}_r e^{i(\omega t - j\beta_r)} \qquad (C-12)$$

$$m_j = 2\pi\rho U^2 b^2 \left(A_R^- + iA_I^-\right) \bar{\alpha}_r e^{i(\omega t - j\beta_r)} \qquad (C-13)$$

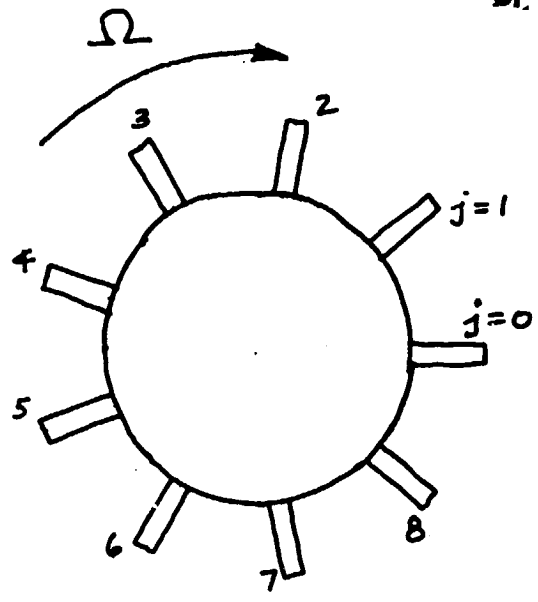

N=9

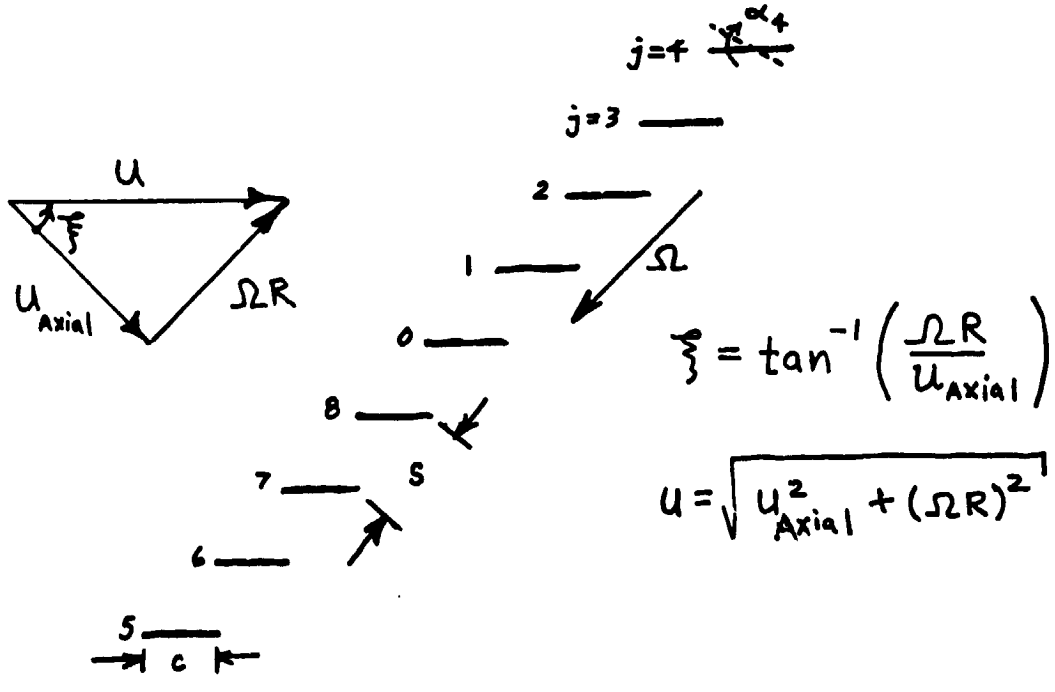

Figure 1. Rotor Geometry

C-2

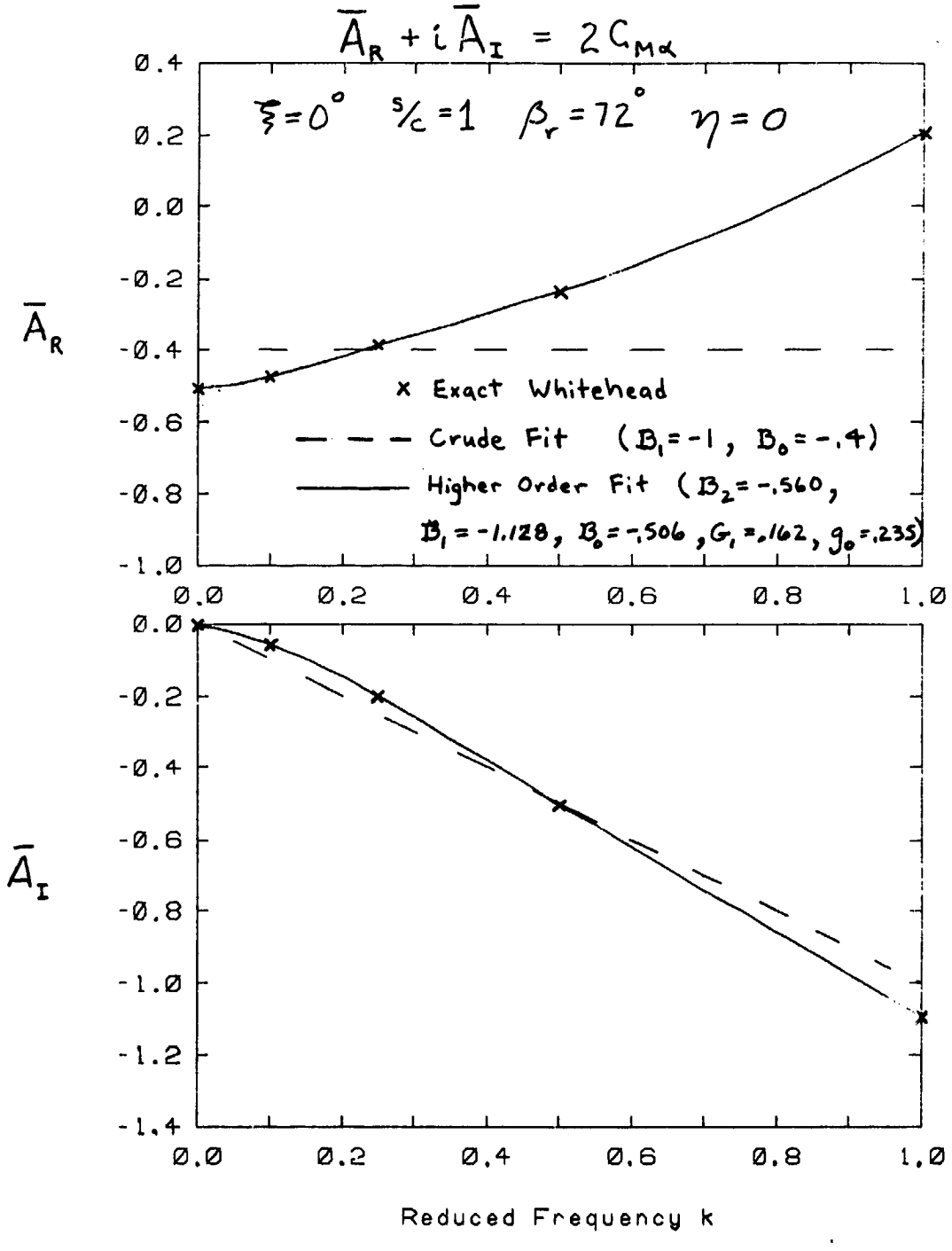

Figure 2. Fitting Whitehead Coefficients

@ LEADING EDGE

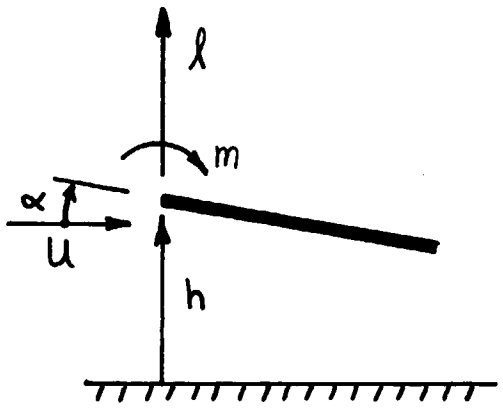

$$h_\eta = h - \eta 2b\alpha$$

$$\alpha_\eta = \alpha$$

@ η % chord

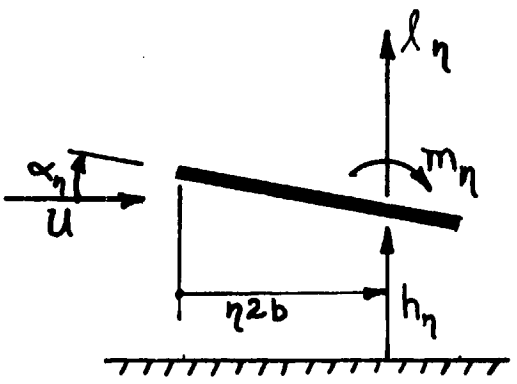

$$l_\eta = l$$

$$m_\eta = m + \eta 2b\, l$$

Figure 3. Force Notation

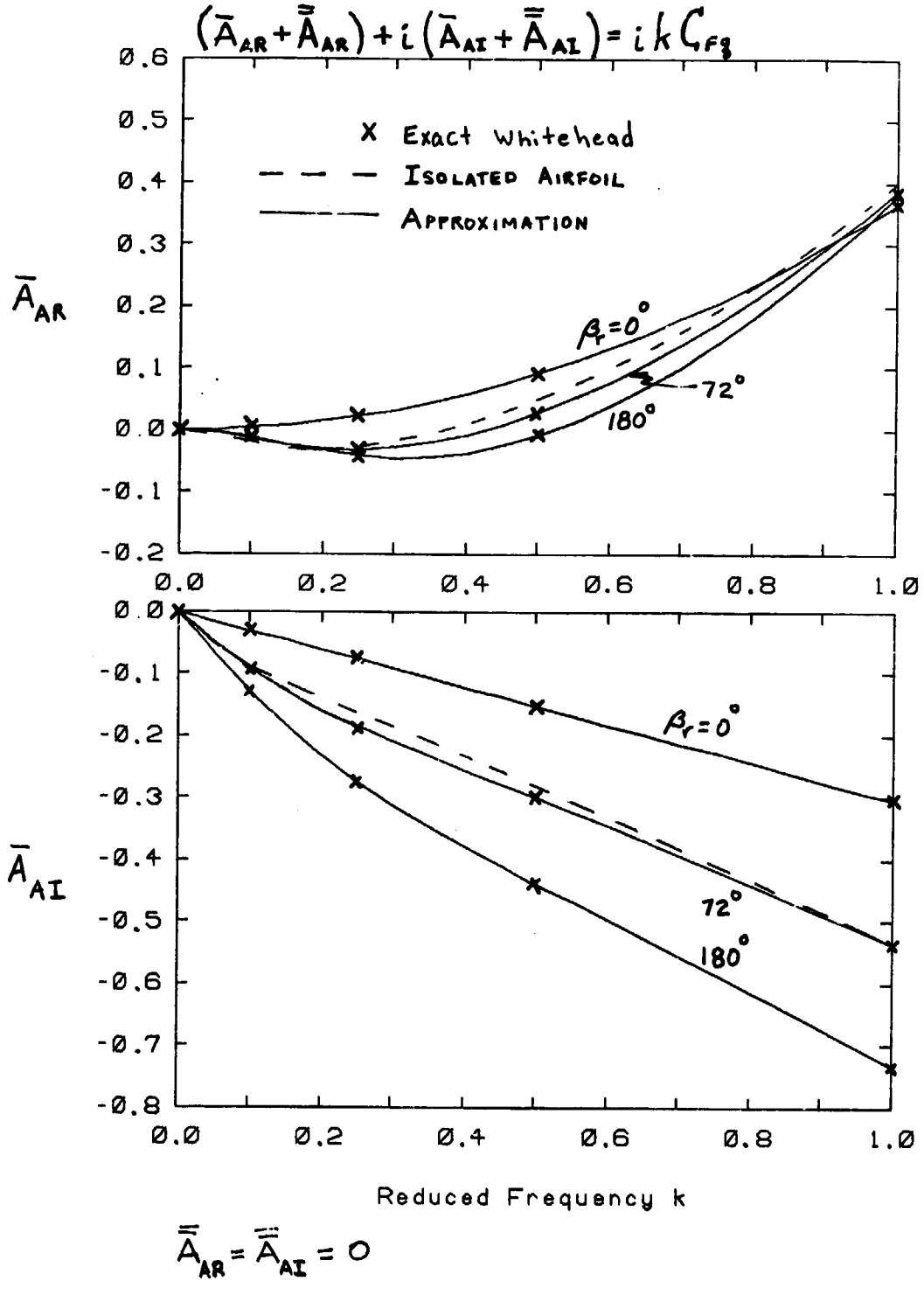

Figure 4a. Approximate Whitehead Force Coefficients

Type A_4, $\bar{\xi}$ = 0 degrees, s/c = 1, η = 0

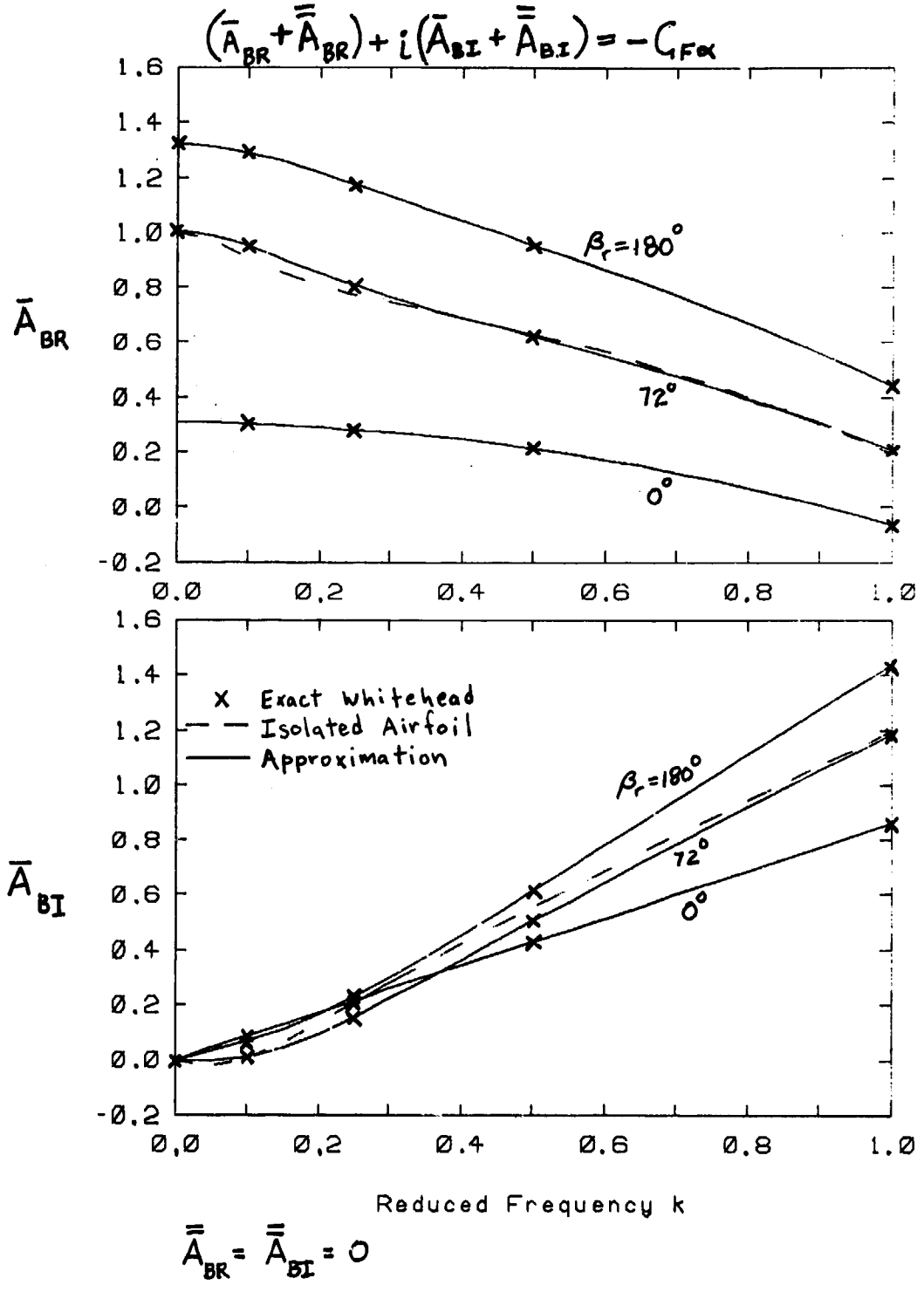

Figure 4b. Approximate Whitehead Force Coefficients

Type A_8, ξ = 0 degrees, s/c = 1, η = 0

$$\left(\bar{A}_{CR}+\bar{\bar{A}}_{CR}\right)+i\left(\bar{A}_{CI}+\bar{\bar{A}}_{CI}\right)=-2ikC_{M_\beta}$$

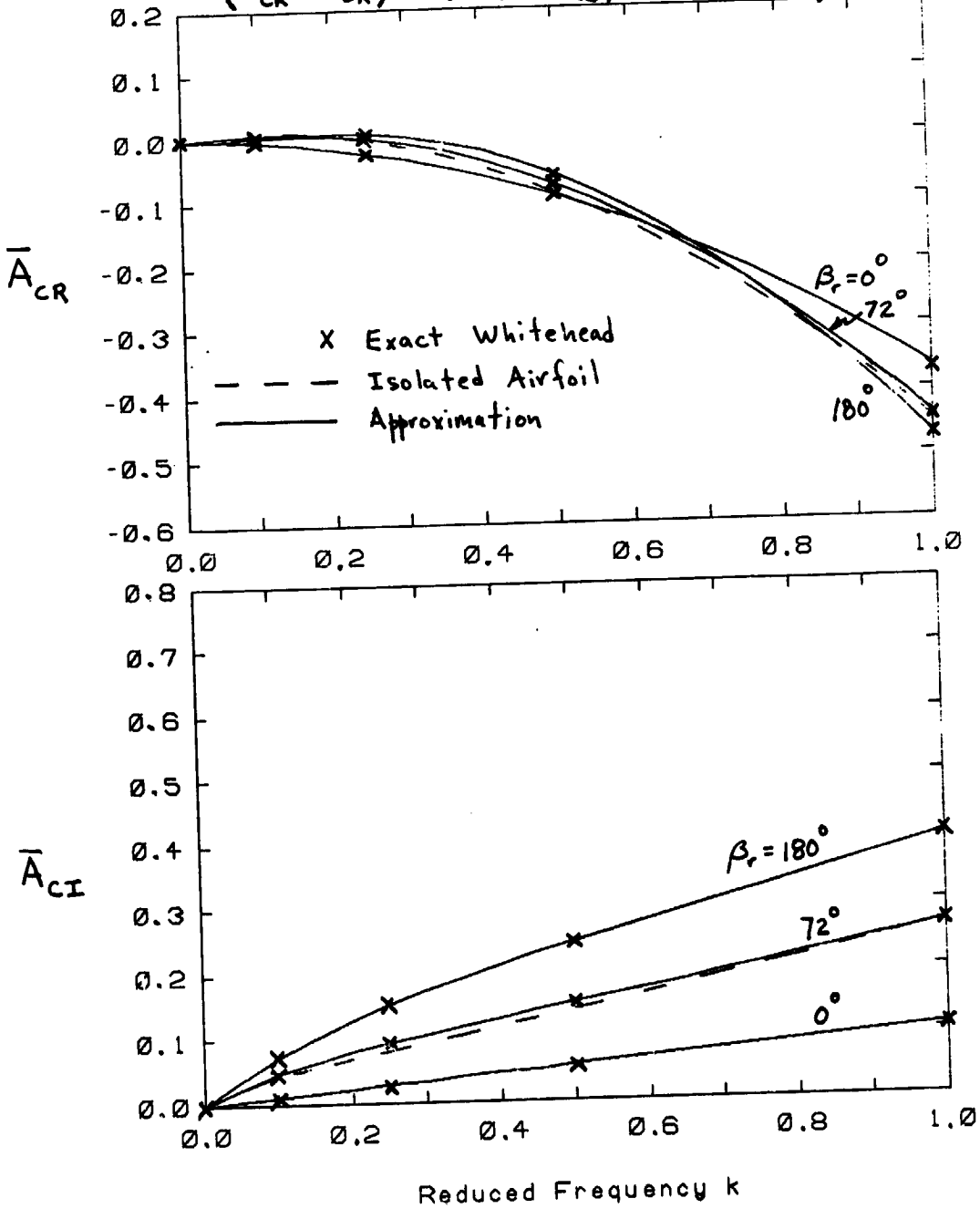

$$\bar{\bar{A}}_{CR}=\bar{\bar{A}}_{CI}=0$$

Figure 4c. Approximate Whitehead Force Coefficients

Type A_c, ζ = 0 degrees, s/c = 1, η = 0

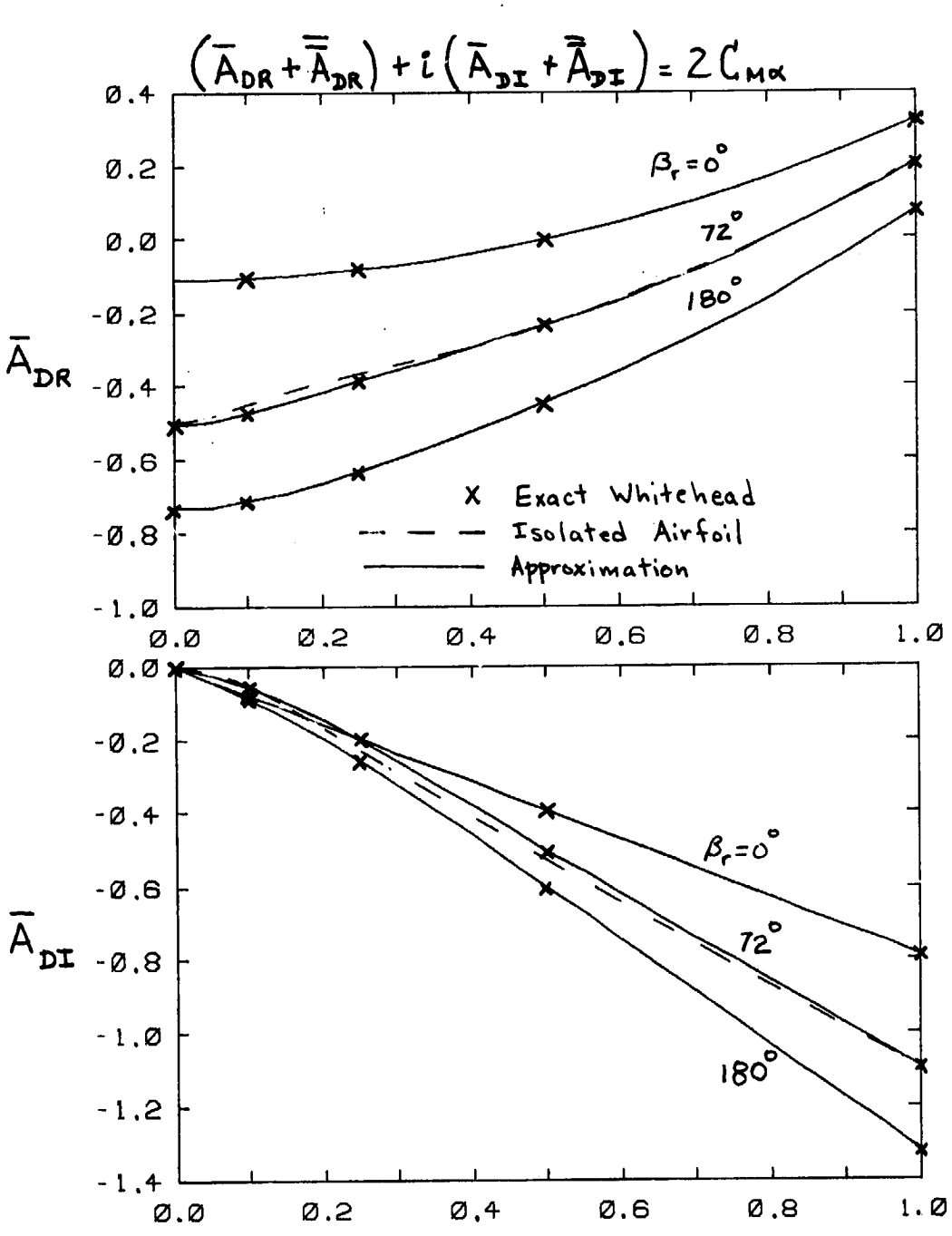

$$\bar{\bar{A}}_{DR} = \bar{\bar{A}}_{DI} = 0$$

Figure 4d. Approximate Whitehead Force Coefficients

Type A_D, ξ = 0 degrees, s/c = 1, η = 0

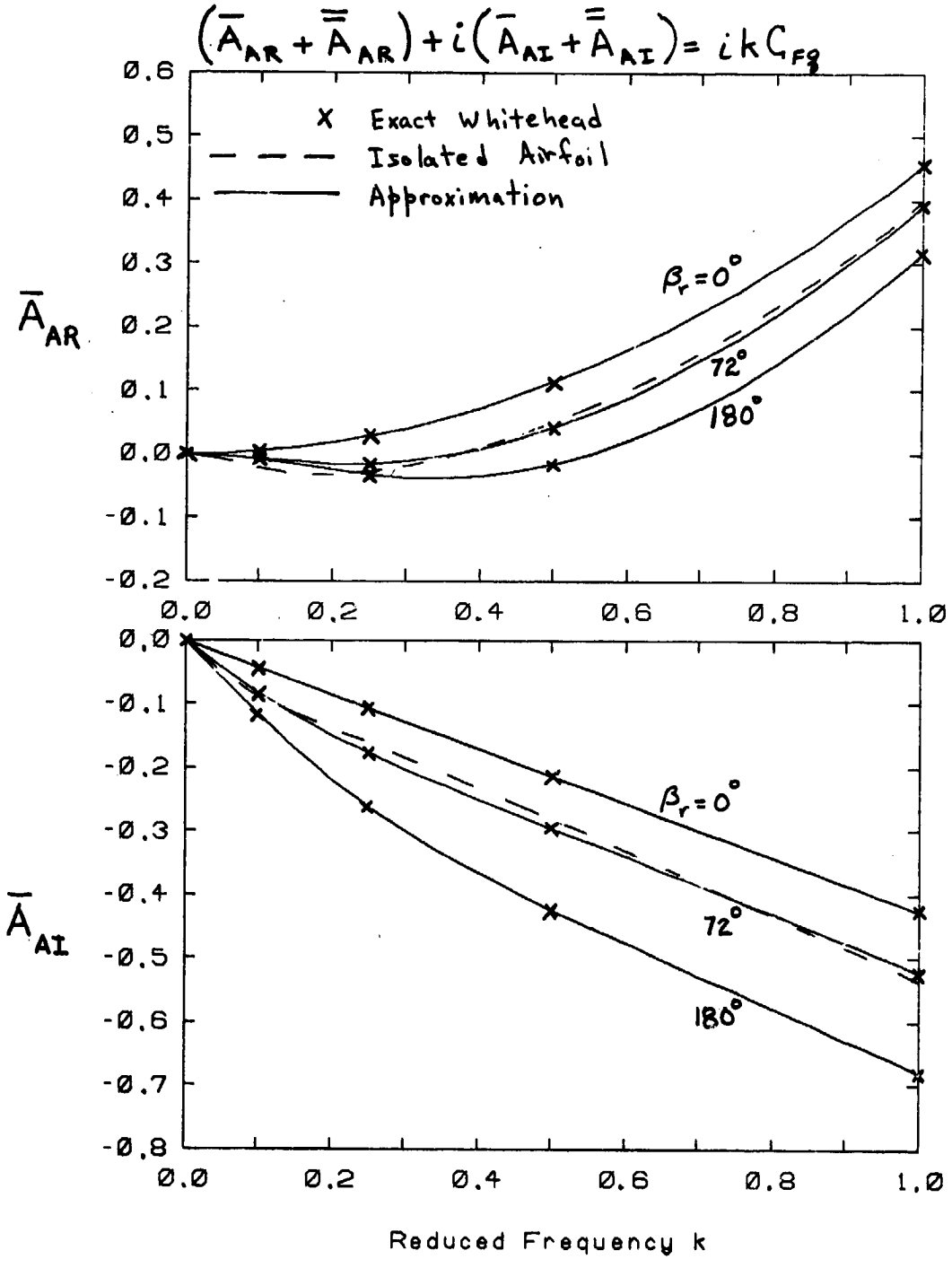

Figure 5a. Approximate Whitehead Force Coefficients

Type $\bar{A}_A$, ξ = 45 degrees, s/c = 1, η = 0

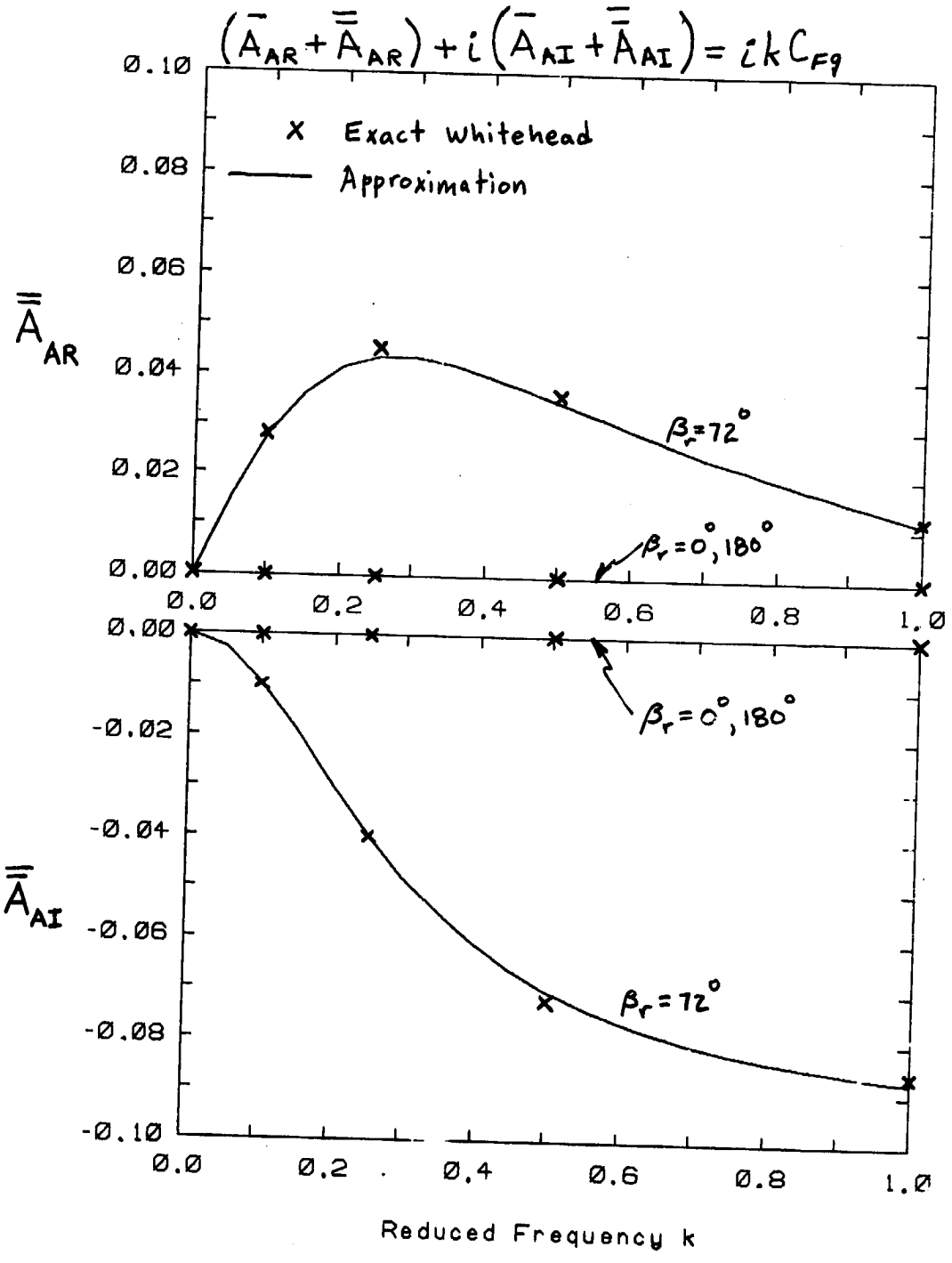

Figure 5b. Approximate Whitehead Force Coefficients Type $\bar{\bar{A}}_A$, ξ = 45 degrees, s/c = 1, η = 0

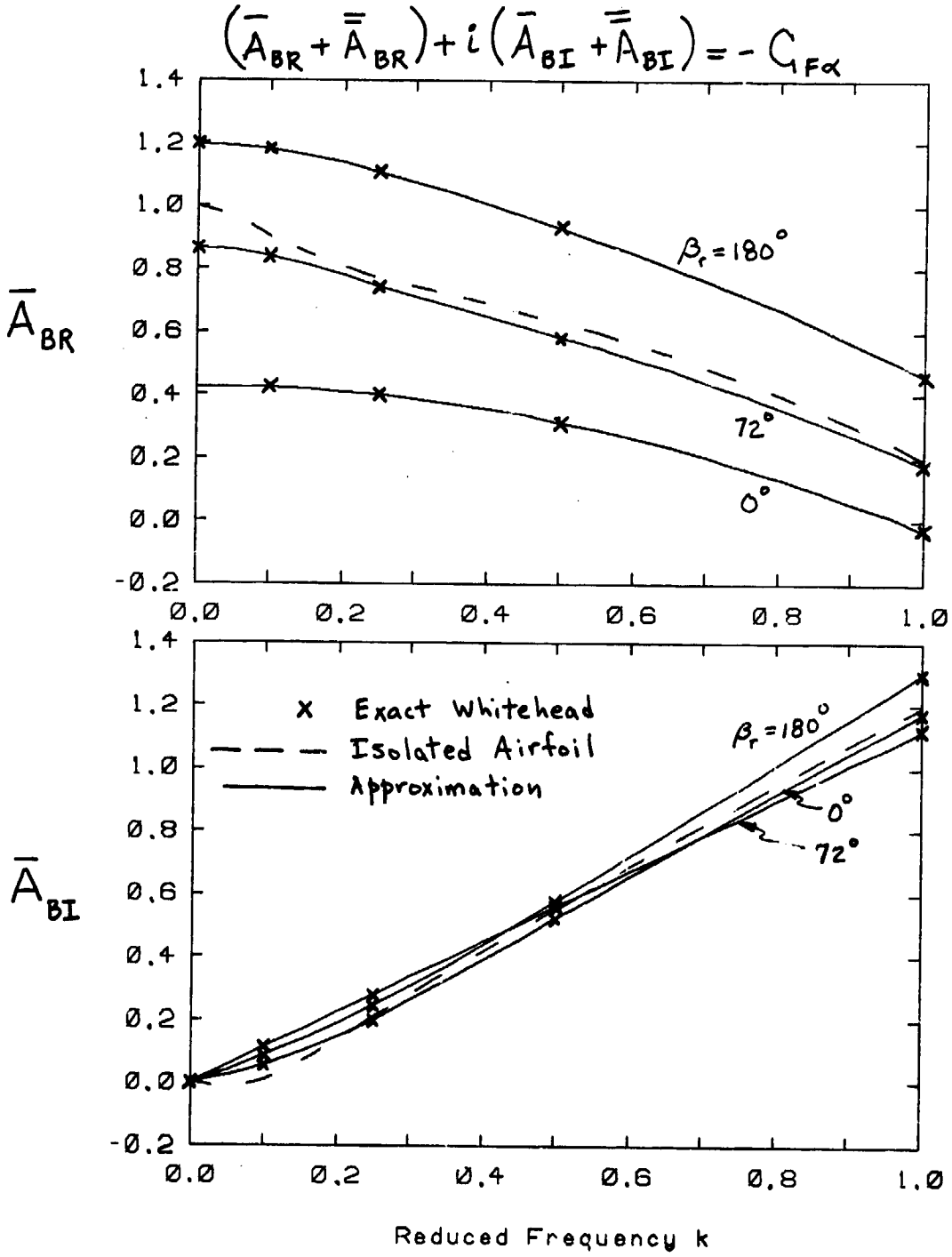

Figure 5c. Approximato Whitehead Force Coefficients

Type $\bar{A}_B$, ξ = 45 degrees, s/c = 1, η = 0

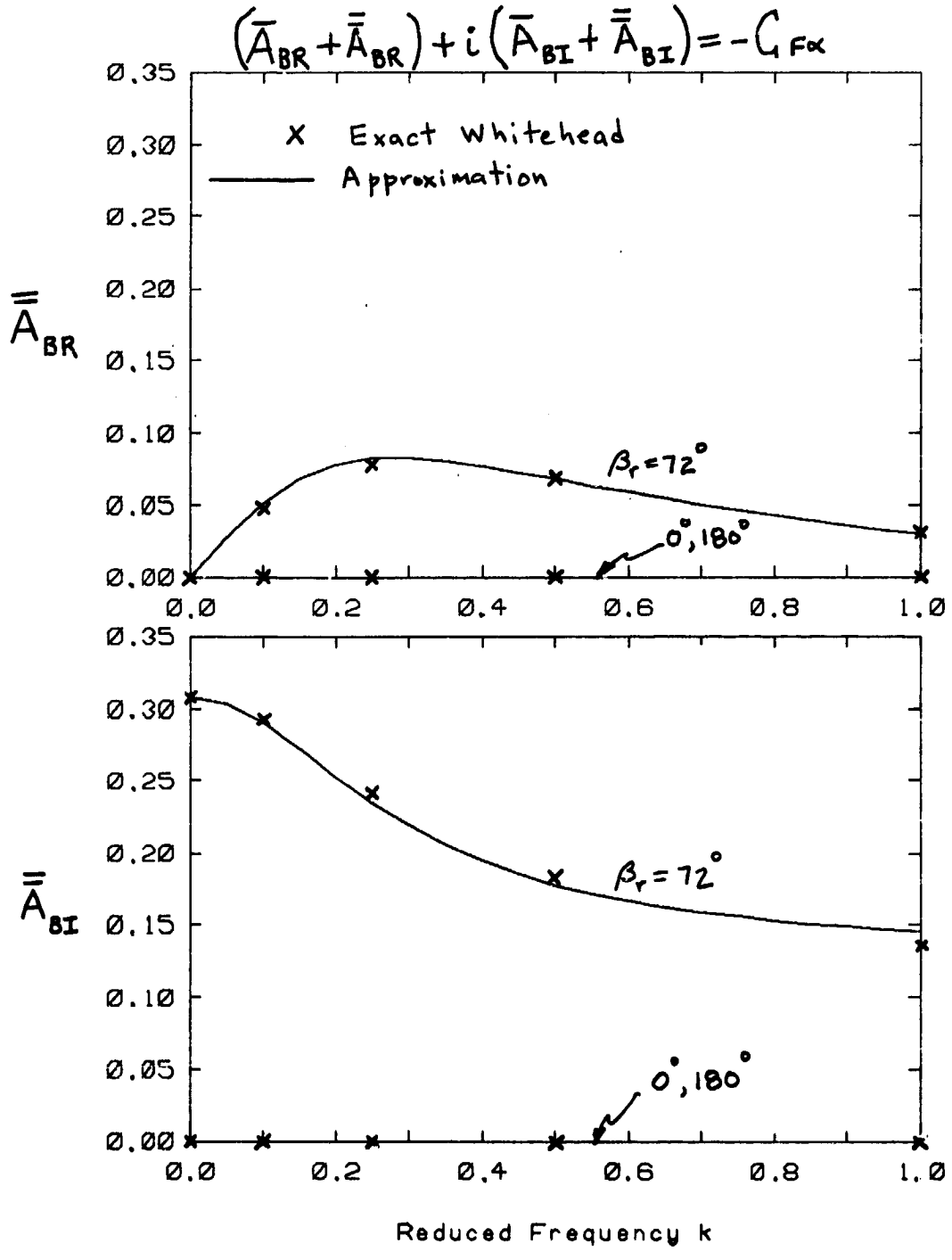

Figure 5d. Approximate Whitehead Force Coefficients

Type $\bar{\bar{A}}_B$, ξ = 45 degrees, s/c = 1, η = 0

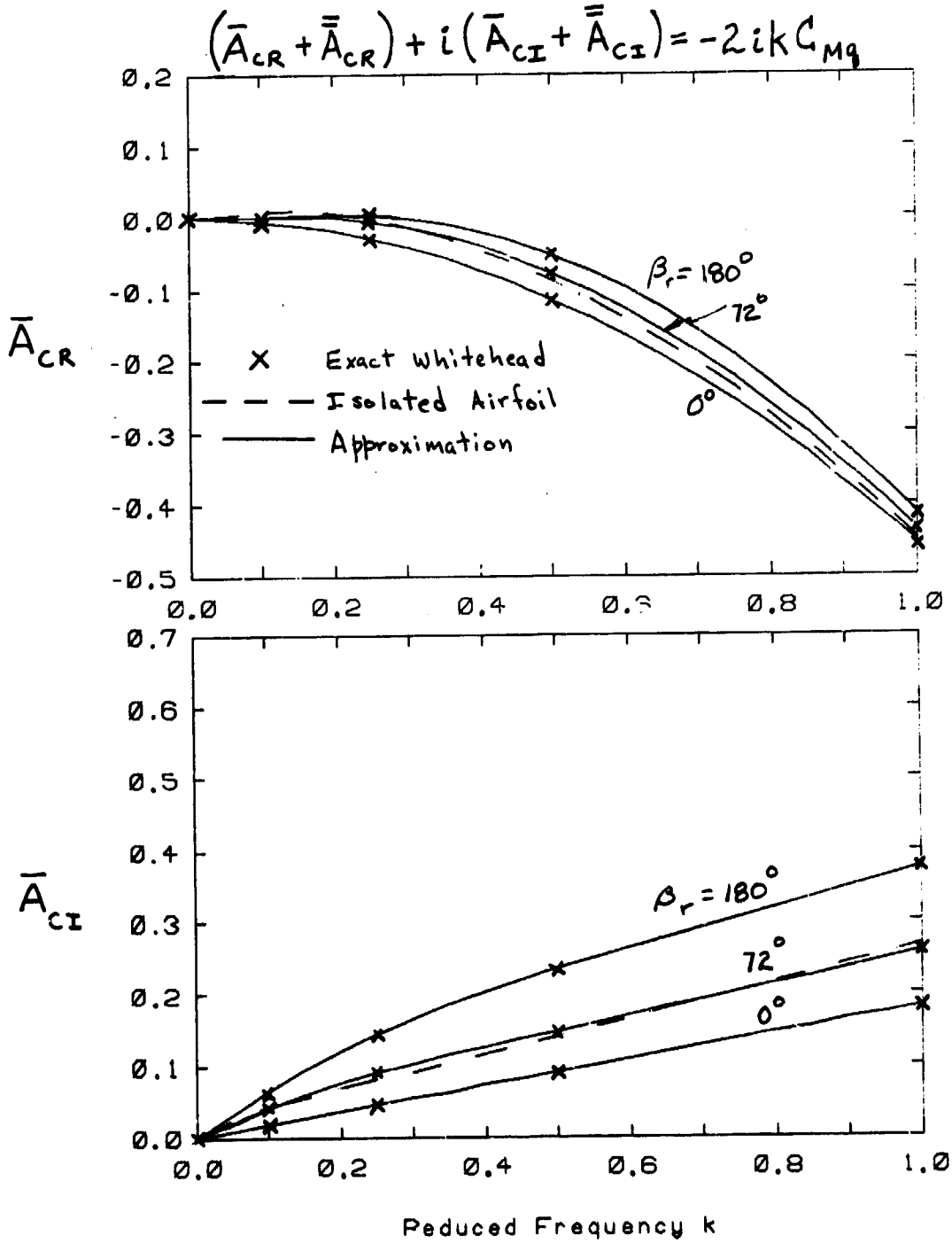

Figure 5e. Approximate Whitehead Force Coefficients

Type $\bar{A}_c$, Σ = 45 degrees, s/c = 1, η = 0

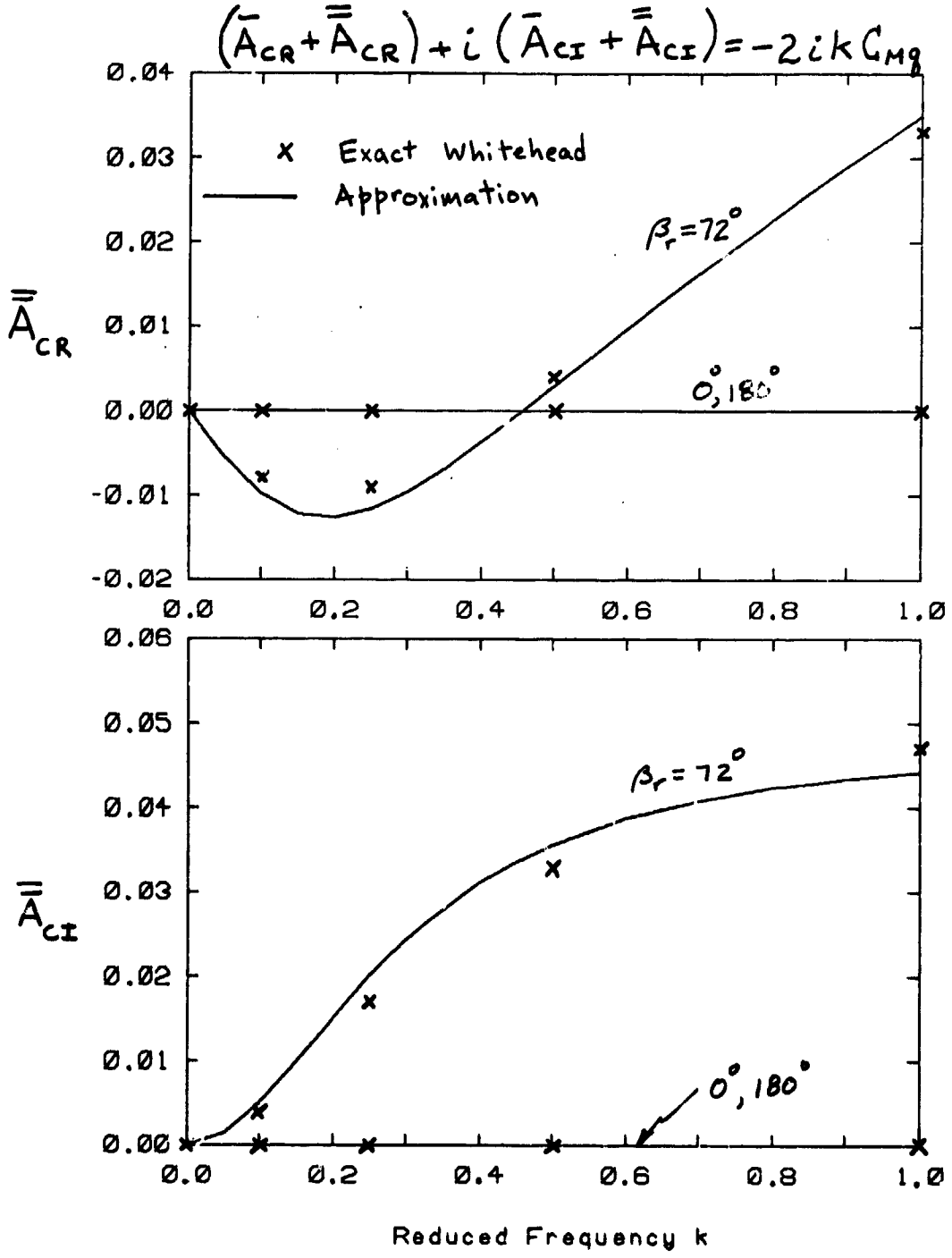

Figure 5f. Approximate Whitehead Force Coefficients

Type $\bar{\bar{A}}_C$, ξ = 45 degrees, s/c = 1, η = 0

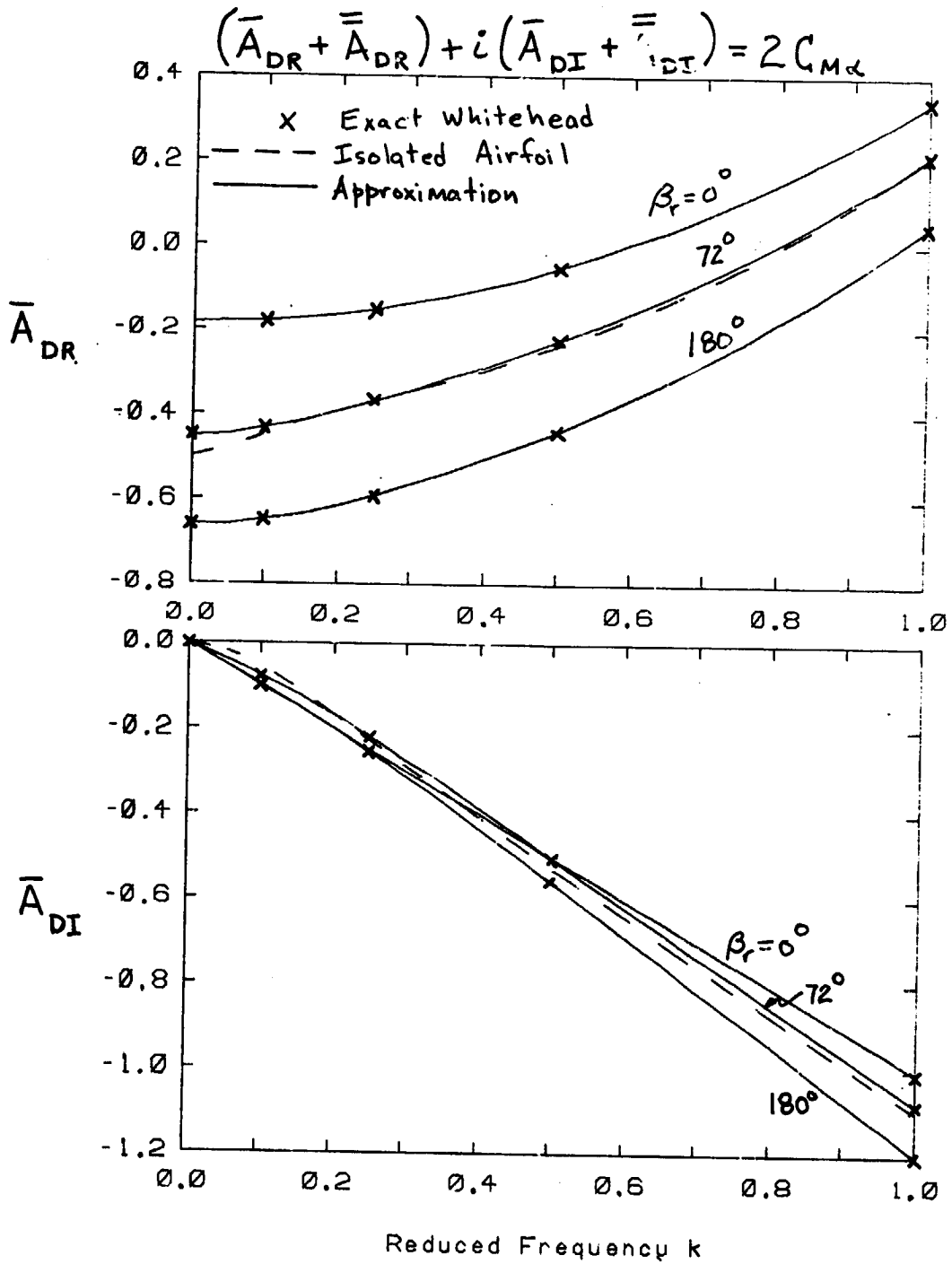

Figure 5g. Approximate Whitehead Force Coefficients

Type $\bar{A}_D$, Λ = 45 degrees, s/c = 1, η = 0

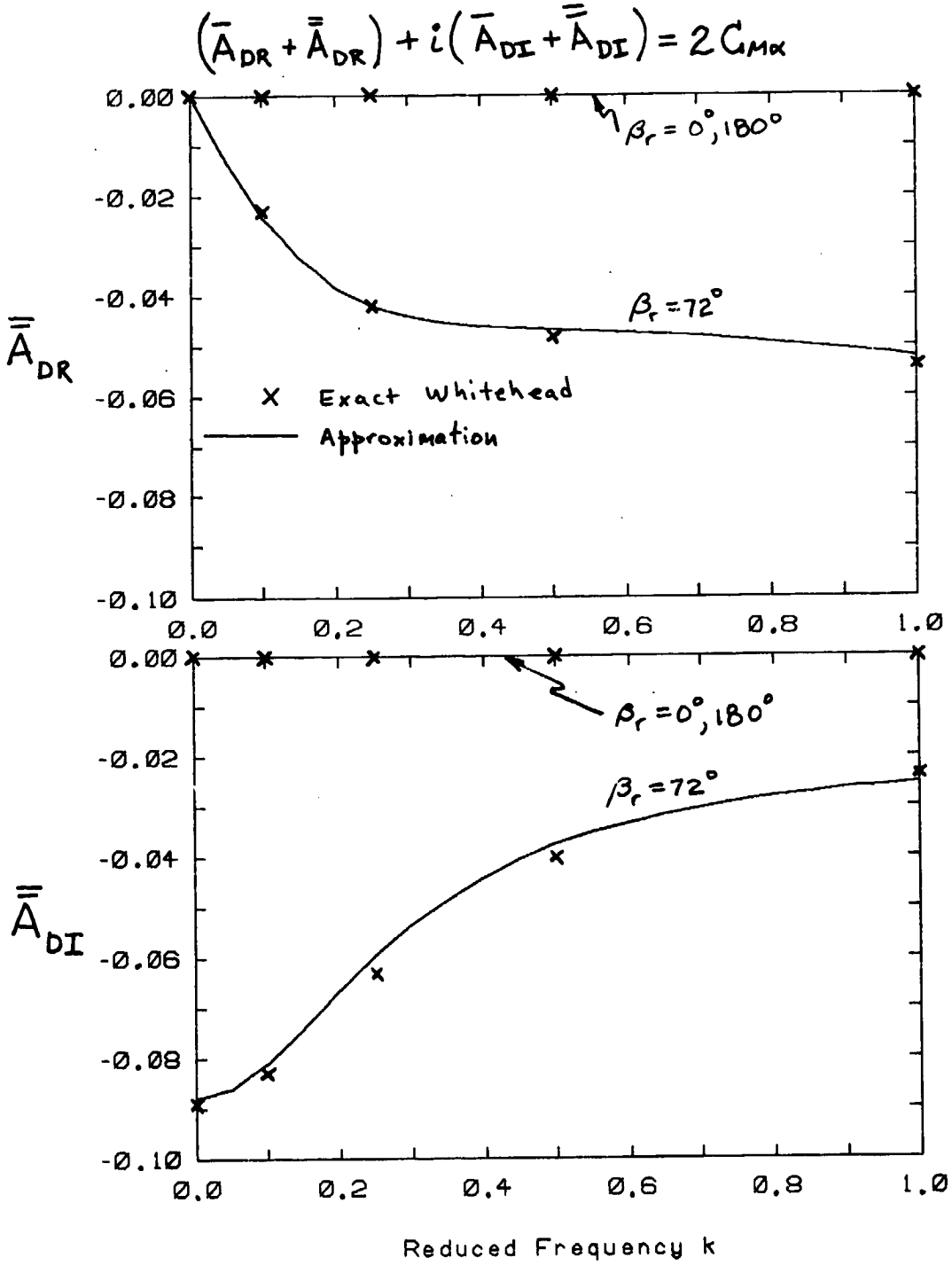

Figure 5h. Approximate Whitehead Force Coefficients

Type $\bar{\bar{A}}_D$, ξ = 45 degrees, s/c = 1, η = 0

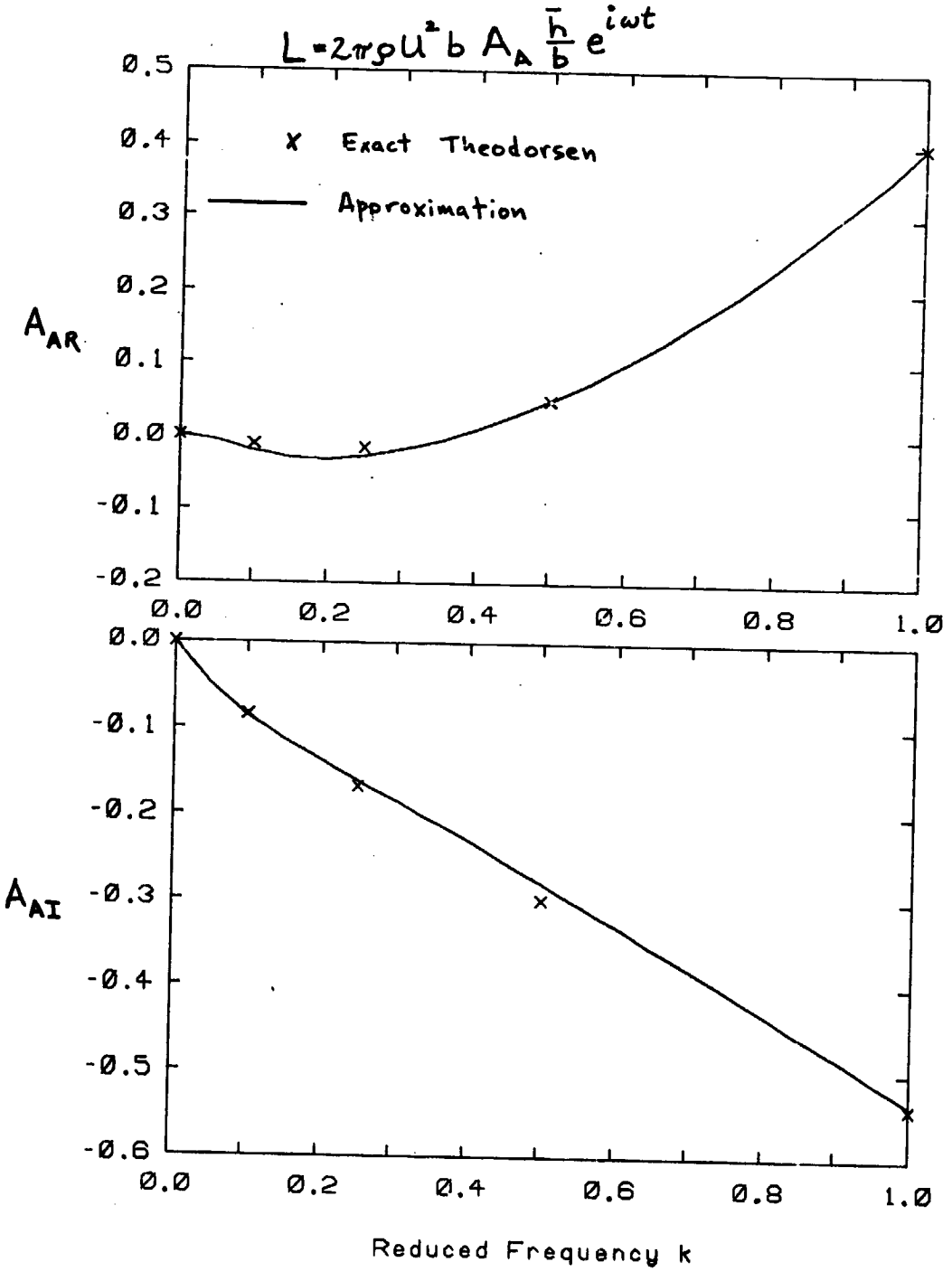

Figure 6a. Approximate Theodorsen Force Coefficients
Type A_A, $\eta = 0$

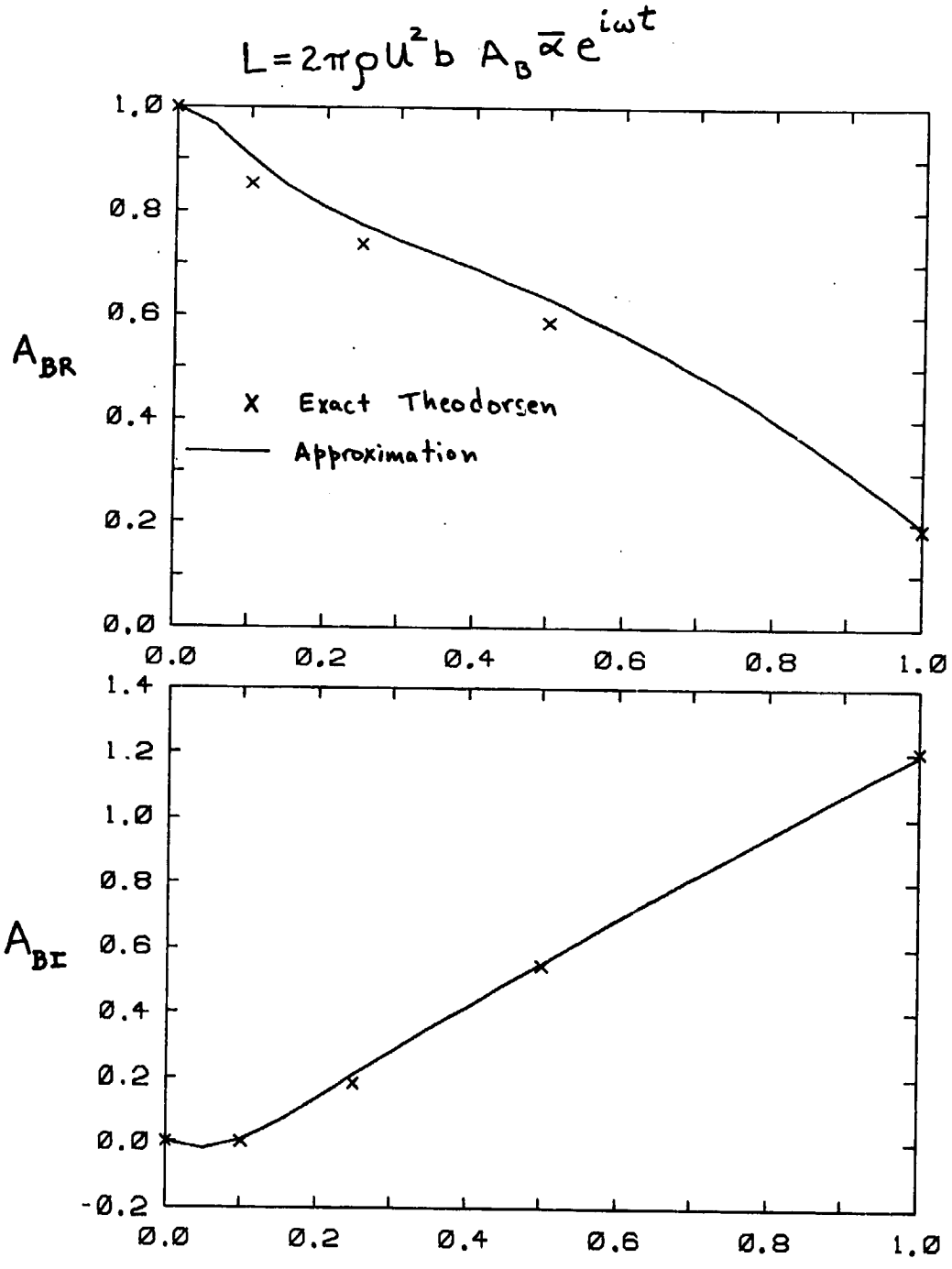

Figure 6b. Approximate Theodorsen Force Coefficients
Type A_B, $\eta = 0$

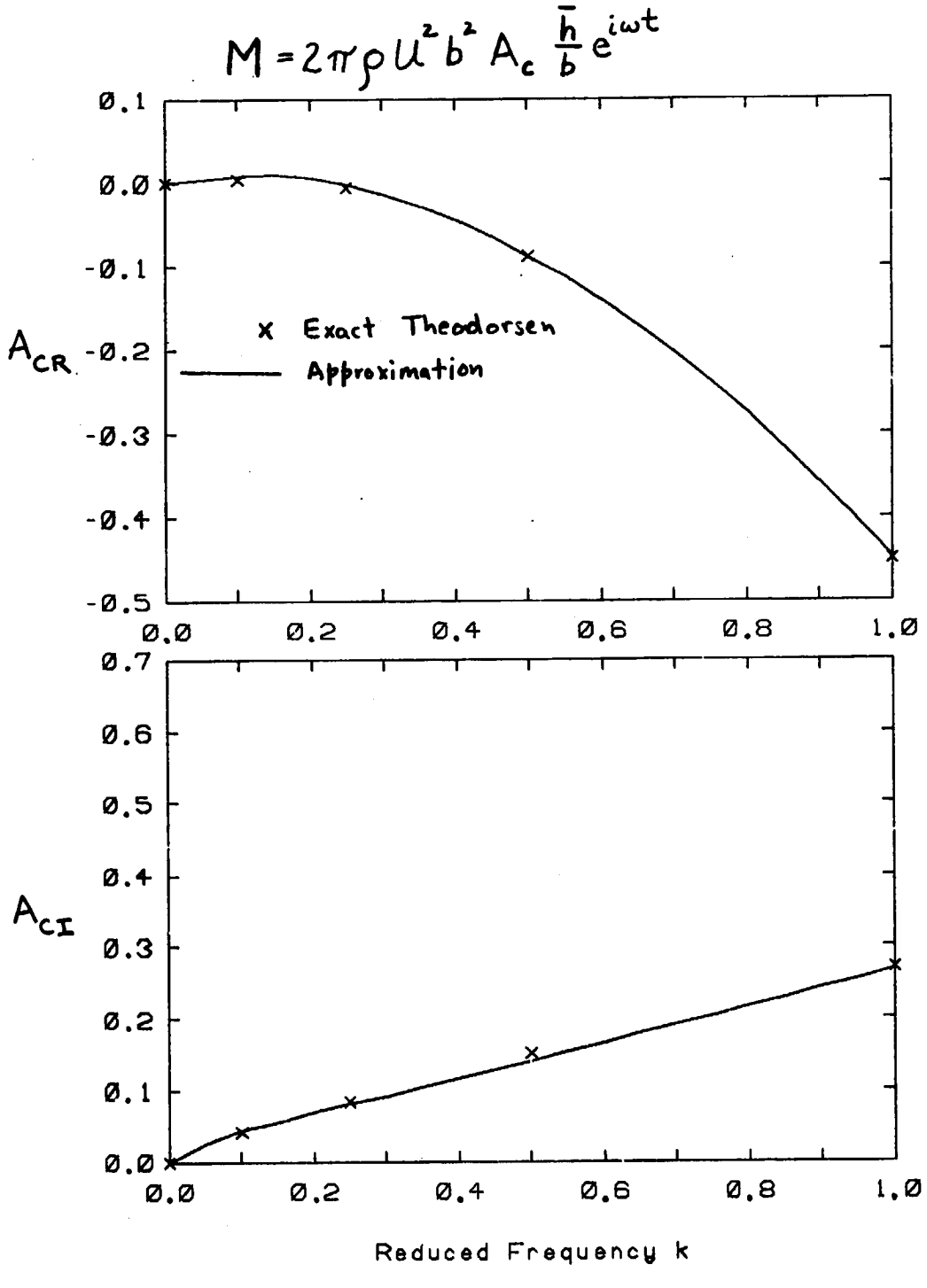

Figure 6c. Approximate Theodorsen Force Coefficients
Type A_c, $\eta = 0$

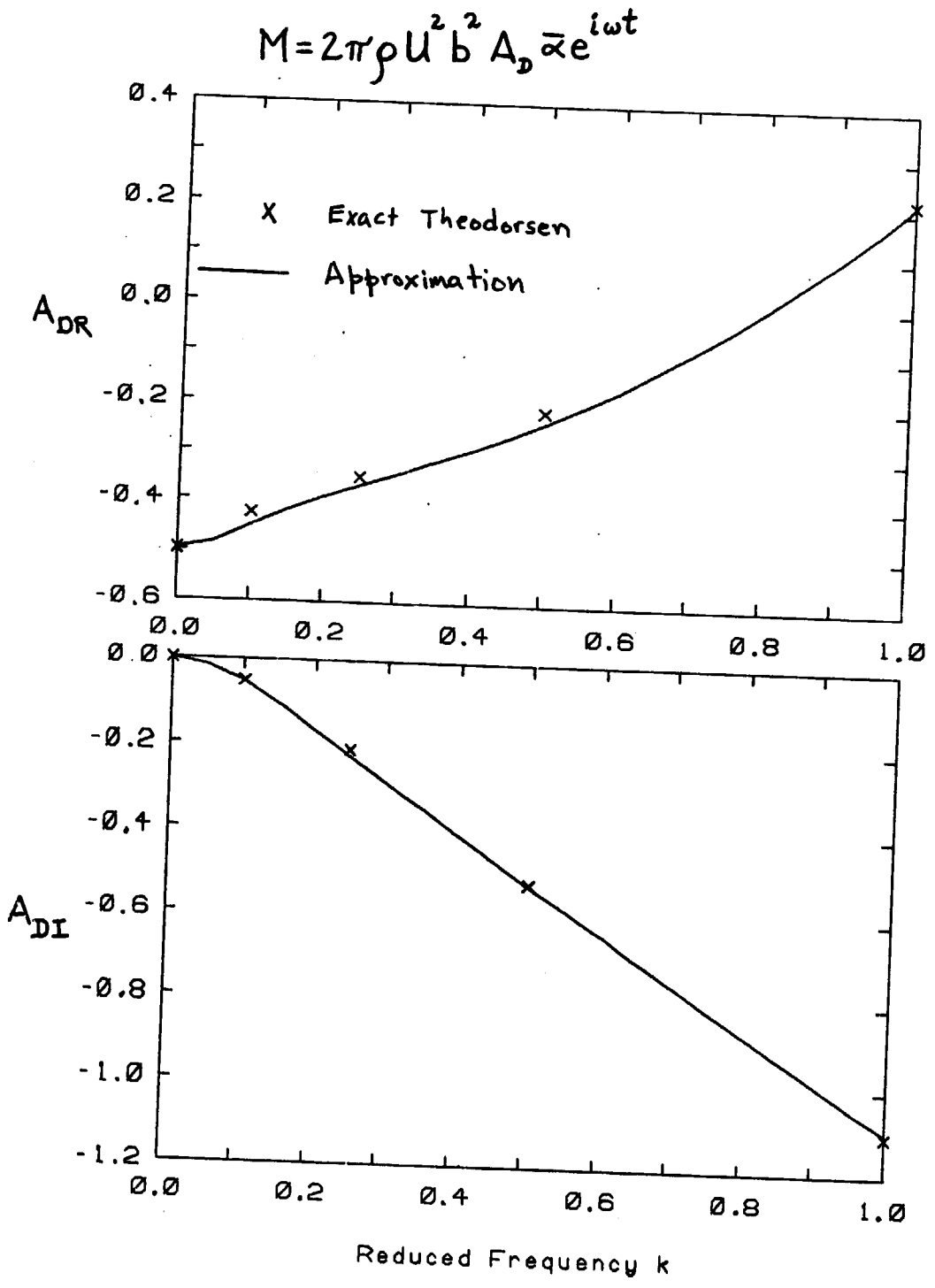

Figure 6d. Approximate Theodorsen Force Coefficients

Type A_D; $\eta = 0$

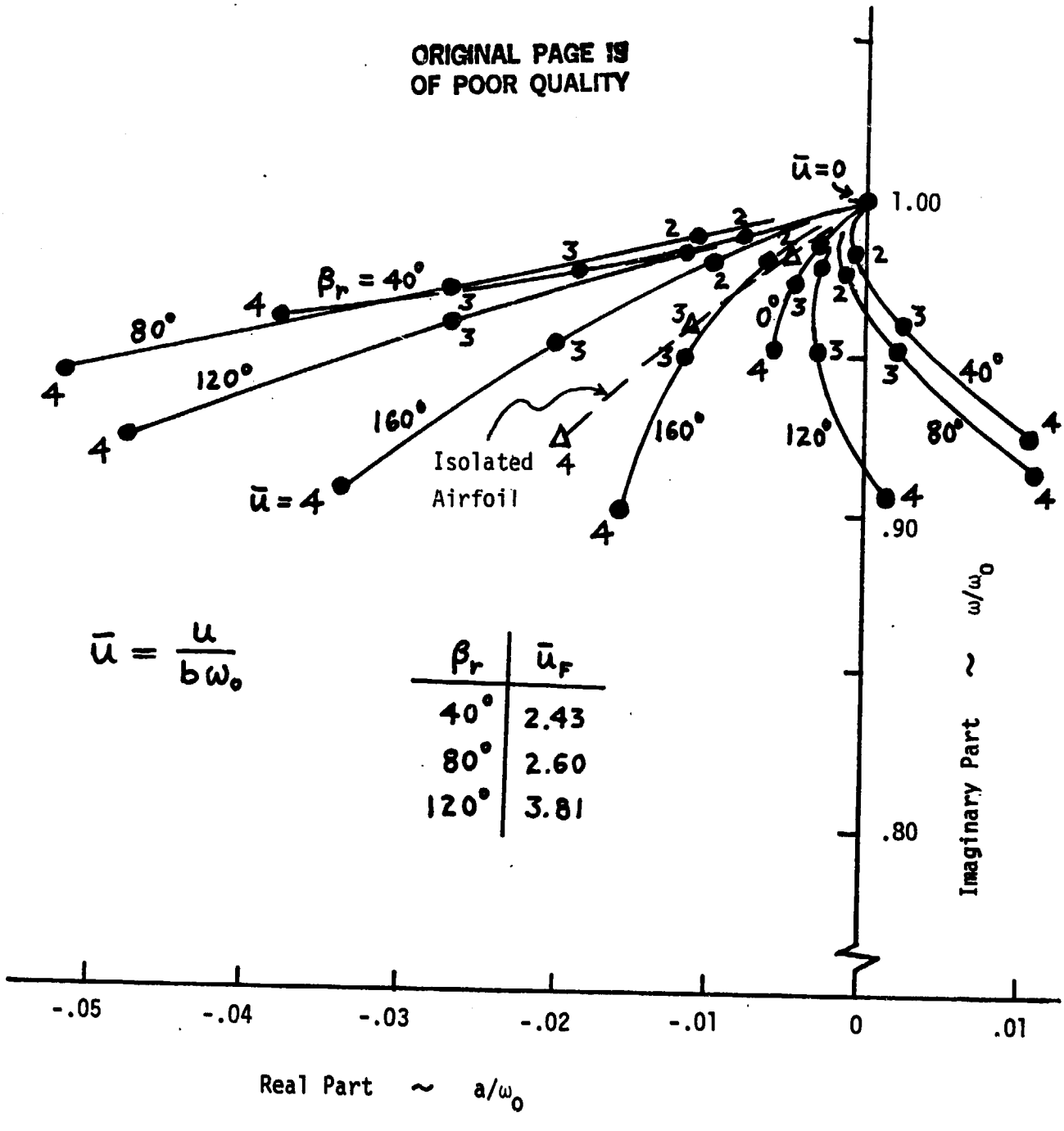

$$\bar{u} = \frac{u}{b\omega_0}$$

β_r	$\bar{u}_F$
40°	2.43
80°	2.60
120°	3.81

Figure 7. Flutter Root Locus - Isolated Airfoil and Tuned Cascade. N = 9, ξ=45 degrees, s/c = 1, η = 0.5, ν = 86.2, ζ = 0

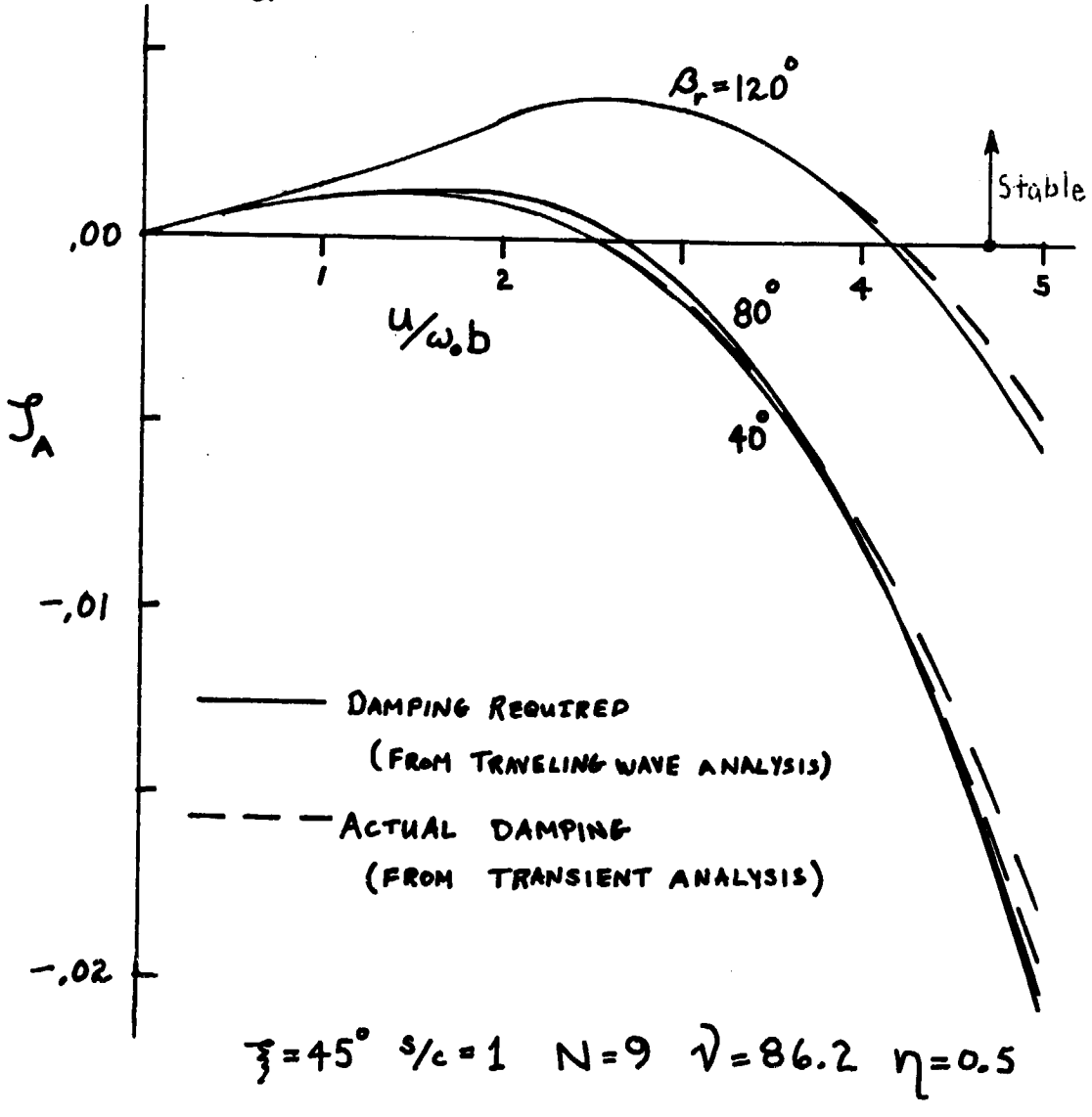

Figure 8. Comparison of the Damping Required for Flutter with the Transient Decay Rate

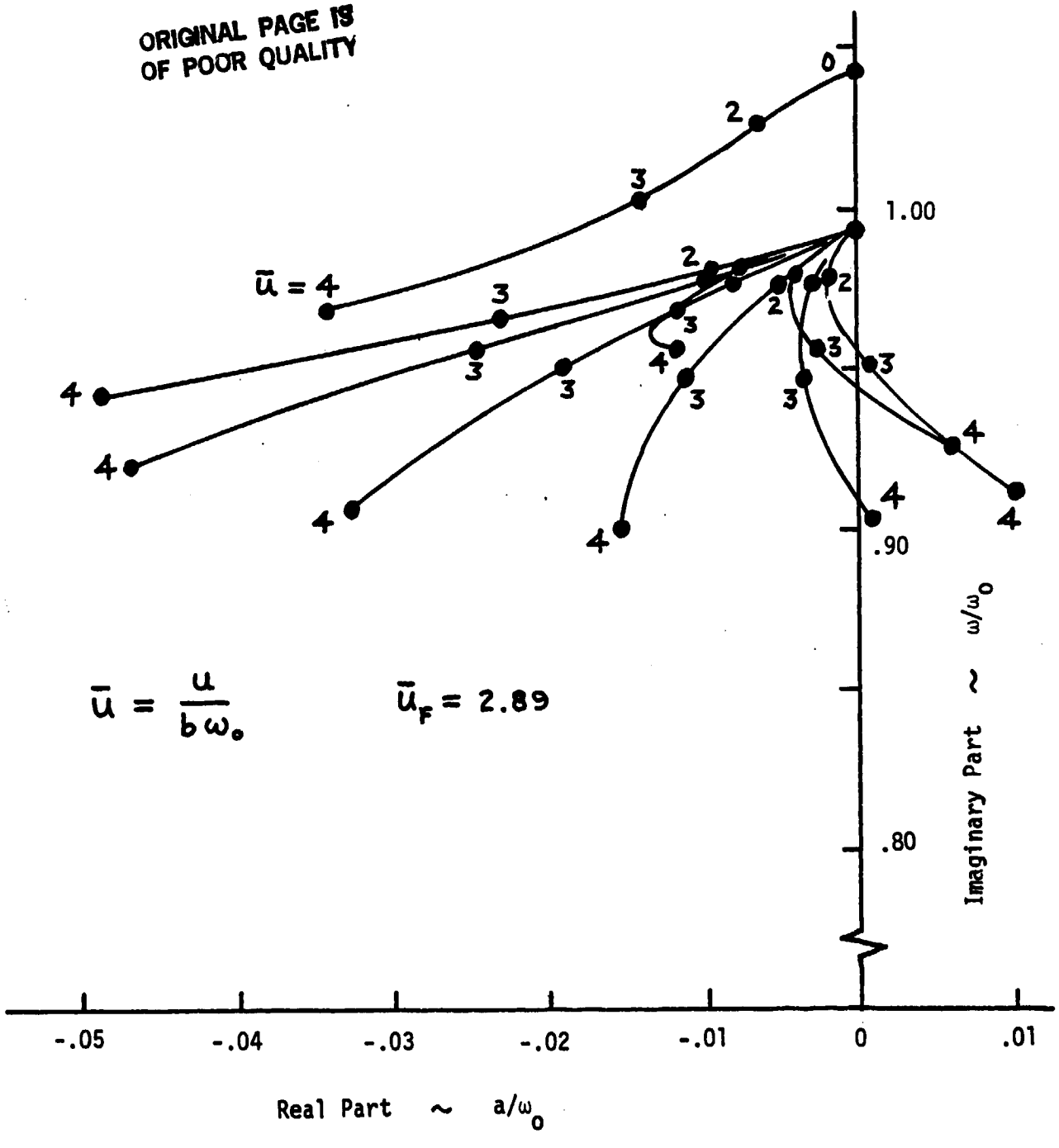

Figure 9. Flutter Root Locus - Blade "0" Mistuned 5 % in frequency. N = 9, ξ = 45 degrees, s/c = 1, η = 0.5, ν =86.2, ζ = 0

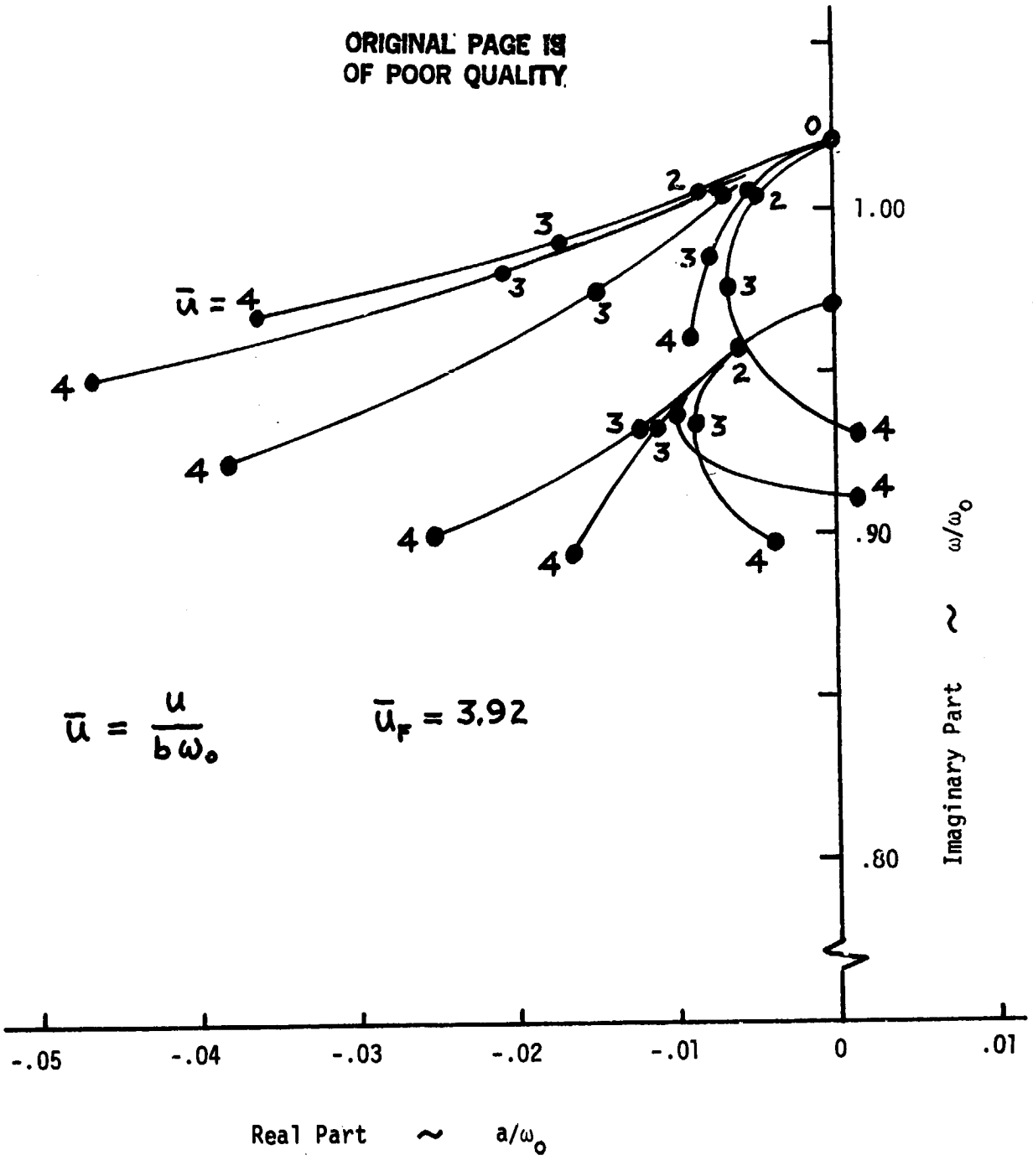

Figure 10. Flutter Root Locus - 5% Alternately Mistuned Cascade. N =9, ξ =45 degrees s/c = 1, η = 0.5, ν_o =86.2, ζ = 0

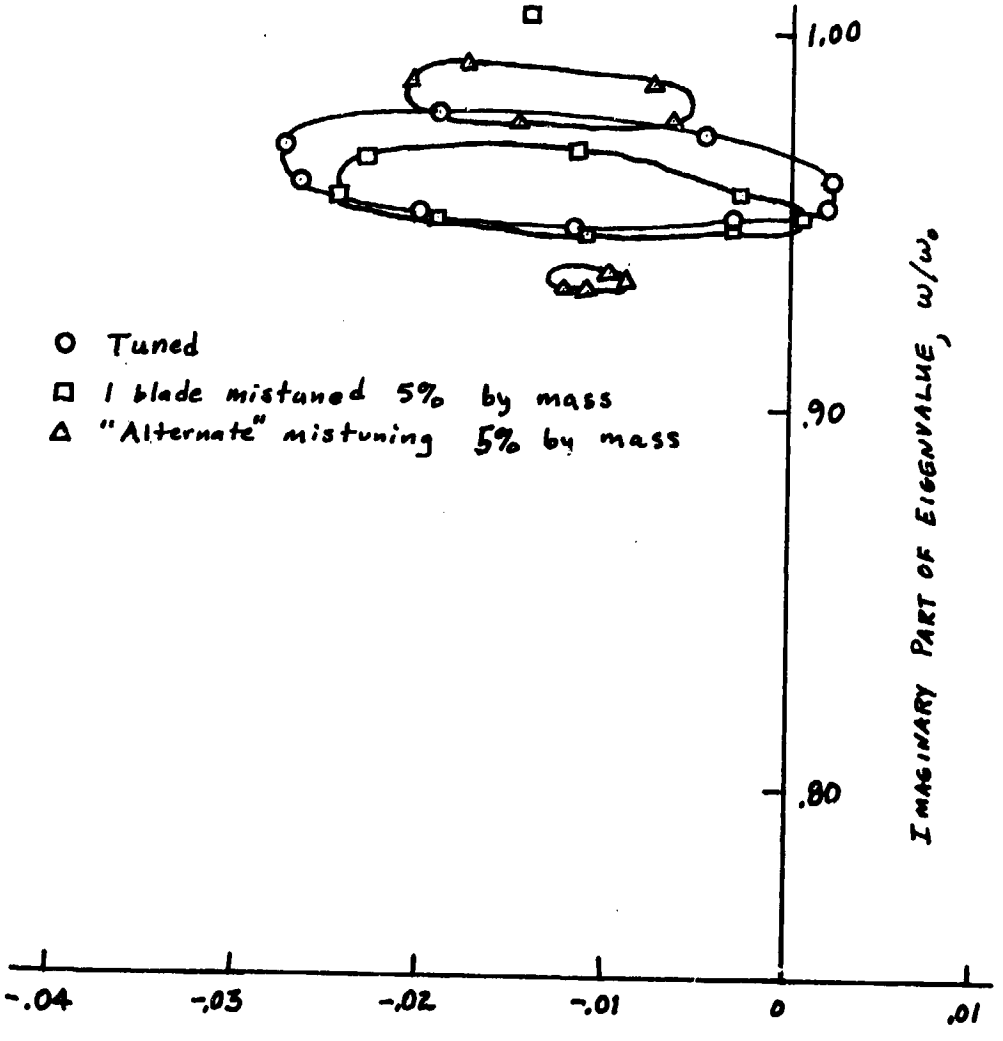

$\bar{u} = 3 \quad N = 9 \quad \beta = 45^\circ \quad s/c = 1 \quad \sigma = 0 \quad \eta = .5$

$\nu_0 = 86.2$

Figure 11. Effect of Mistuning on Eigenvalues

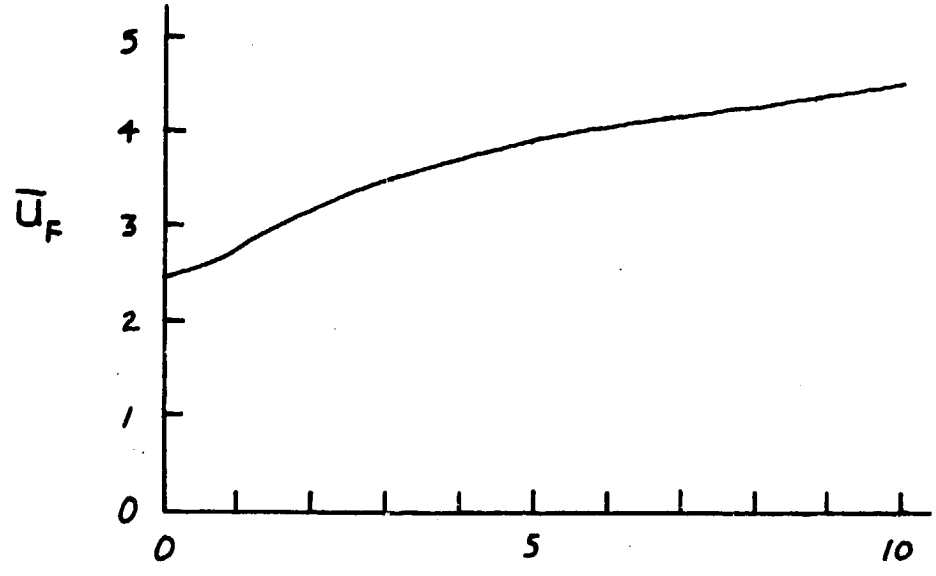

$N=9 \quad \mathfrak{F}=45^\circ \quad s/c=1 \quad \eta=0.5$

$\nu_o = 86.2 \quad \mathfrak{F}=0$

Figure 12. Effect of Alternate Mistuning on Flutter Reduced Speed

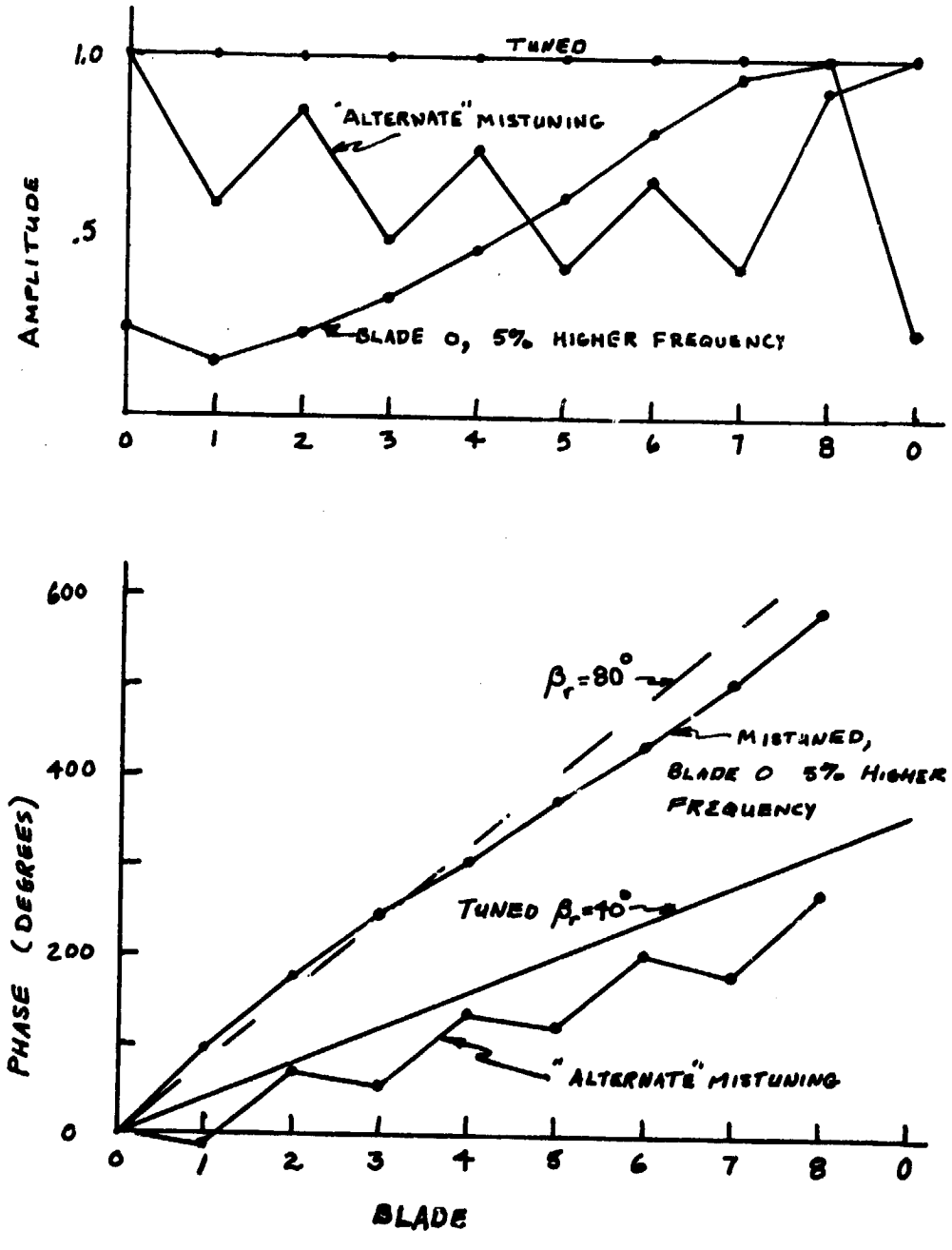

$N=9 \quad \xi=45^\circ \quad s/c=1 \quad \eta=0.5$

$\nu_0=86.2 \quad \zeta=0$

Figure 13. Flutter Vibration Modes of Tuned and Mistuned Rotors

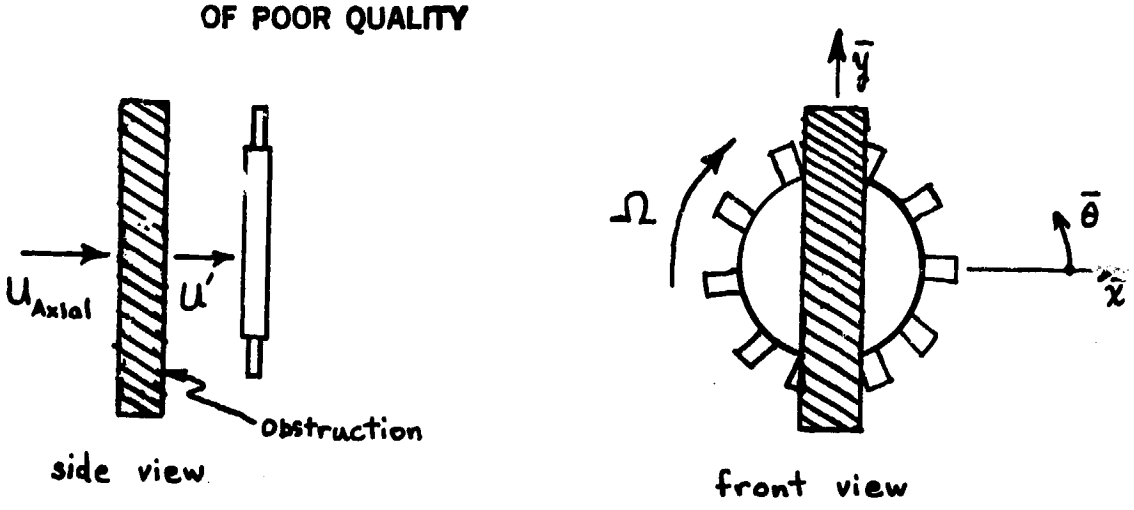

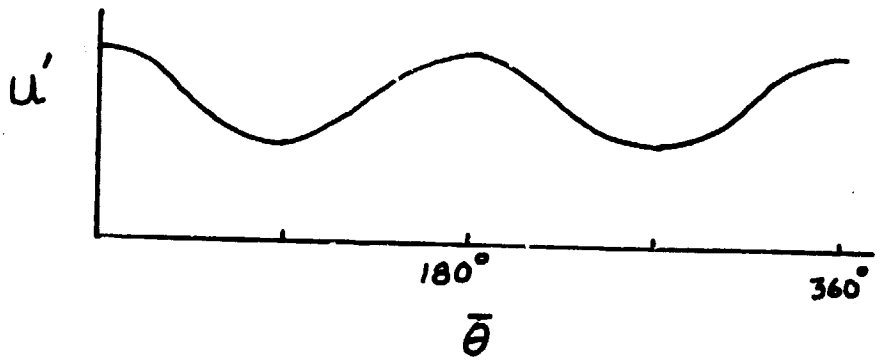

$$\theta_j = \frac{2\pi}{N} j$$

$$\bar{\theta} = \theta_j - \Omega t$$

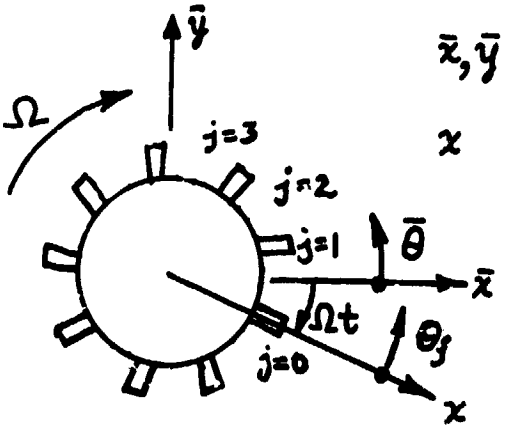

$\bar{x}, \bar{y}$ fixed in space

x fixed to rotor

Figure 14. Obstructed Rotor

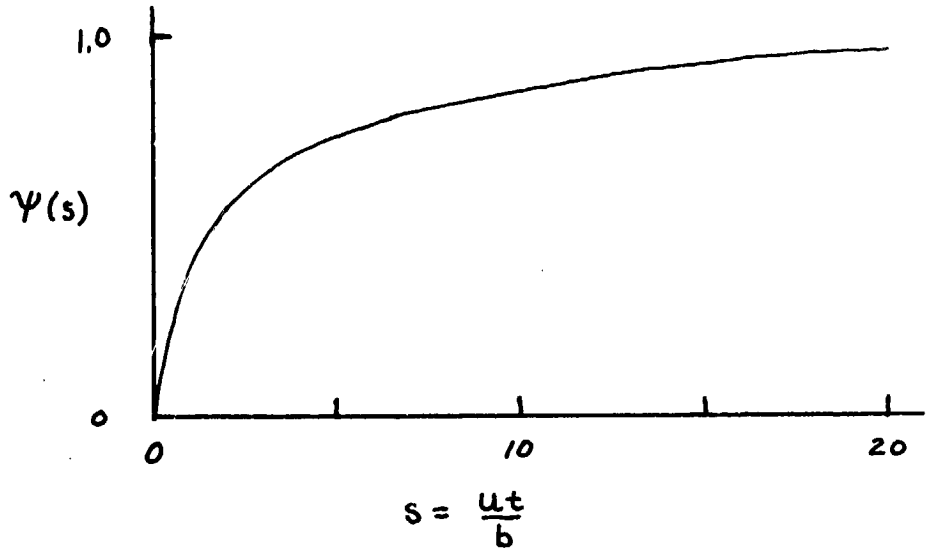

$$M = 2\pi\rho U^2 b^2 \alpha_0 \left[\tfrac{1}{2}\Psi(s)\right]$$

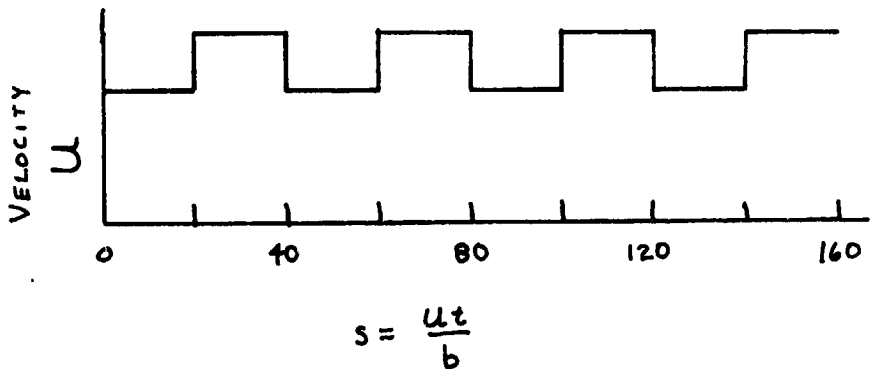

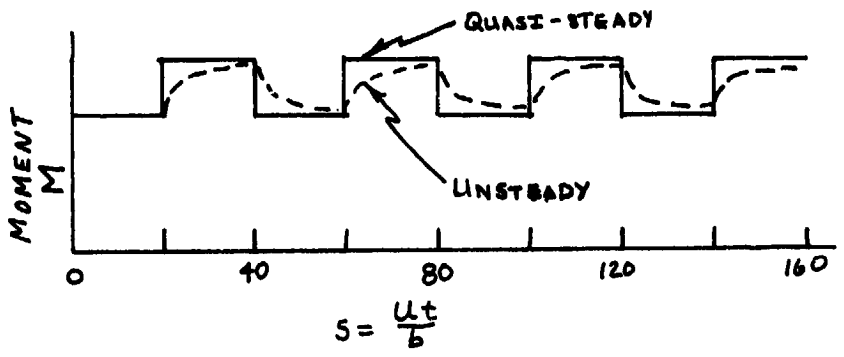

Figure 15. Küssner Function and Unsteady Moment Due to Variation of Velocity

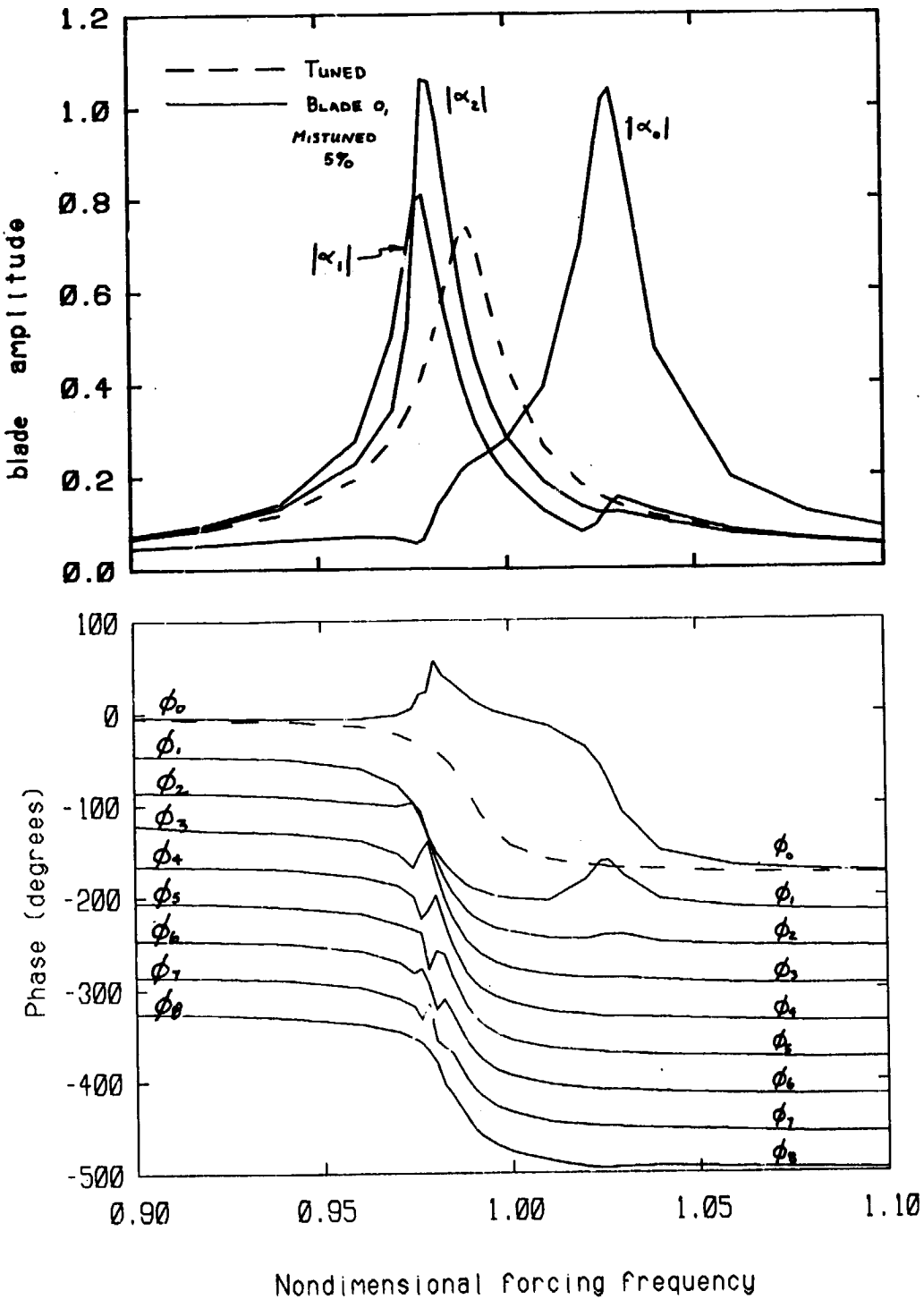

Figure 16. Frequency Response of Tuned Cascade and of Cascade with Blade "0" Mistuned 5% to a One Engine Order Excitation

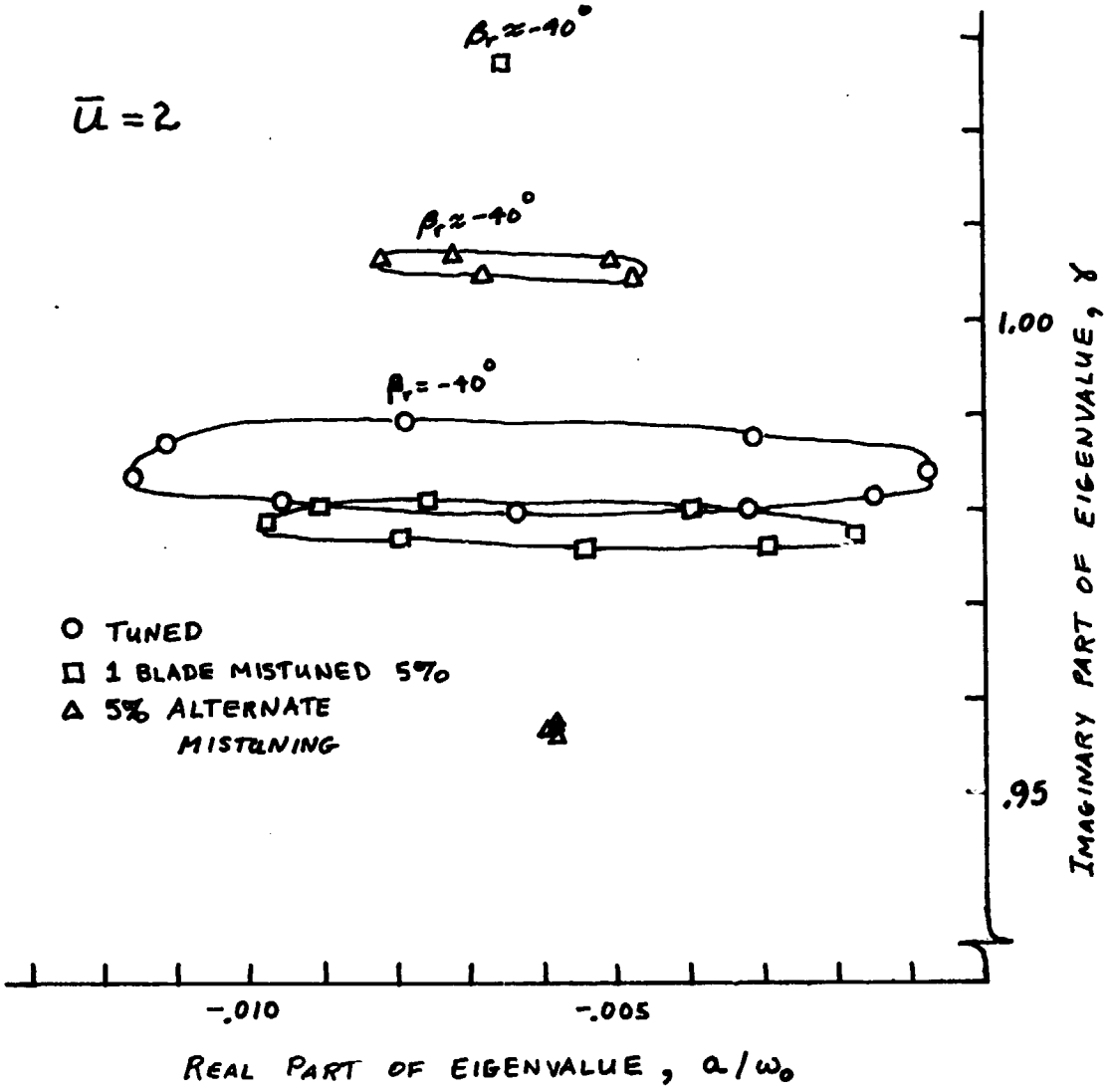

$N=9 \quad \beta = 45° \quad s/c = 1 \quad \eta = .5 \quad V_0 = 86.2 \quad \mathcal{J} = 0$

Figure 17. Effect of Mistuning on Eigenvalue Associated with Engine Order Mode being Forced

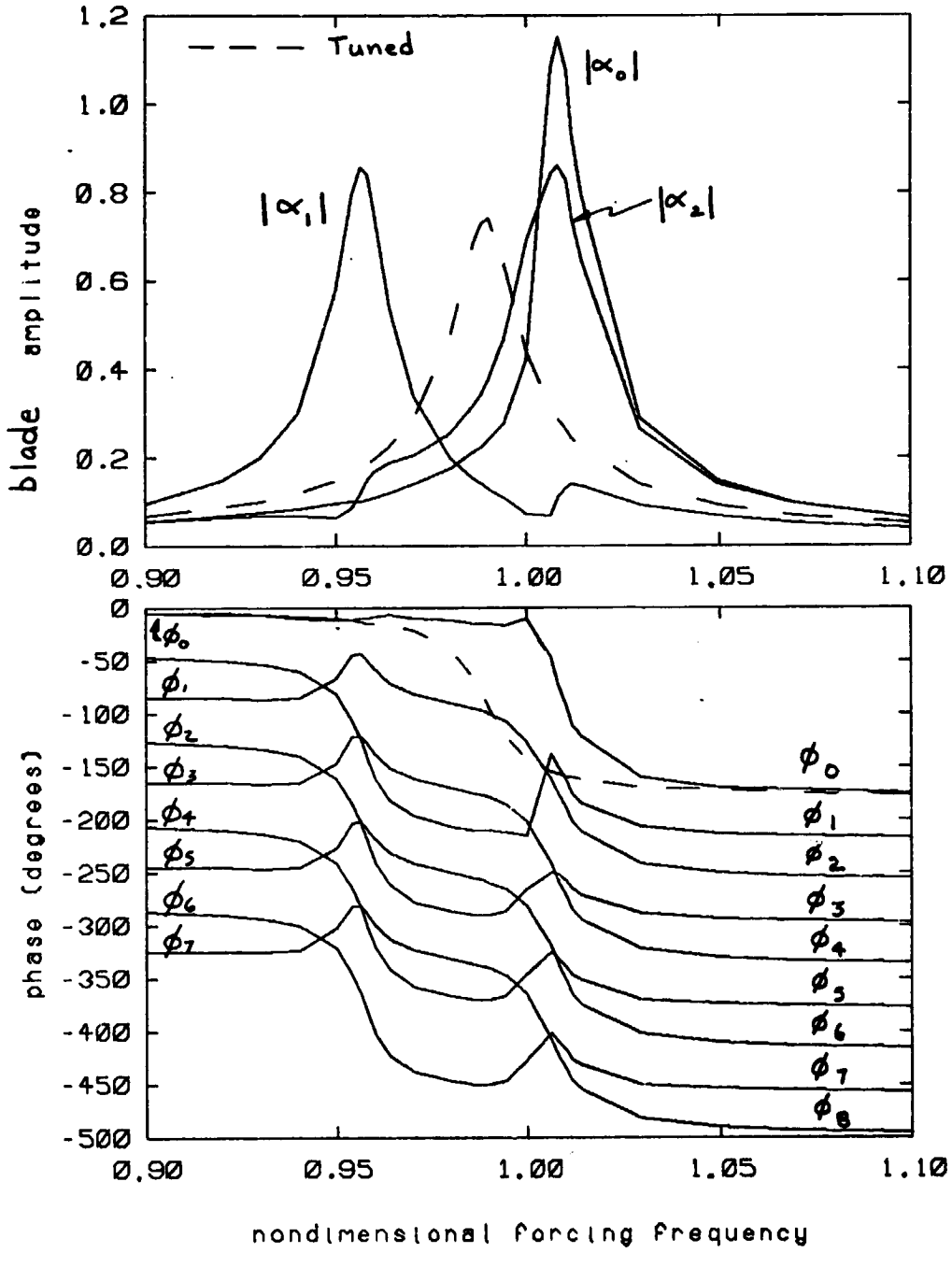

Figure 18. Frequency Response of 5% "Alternately" Mistuned Cascade

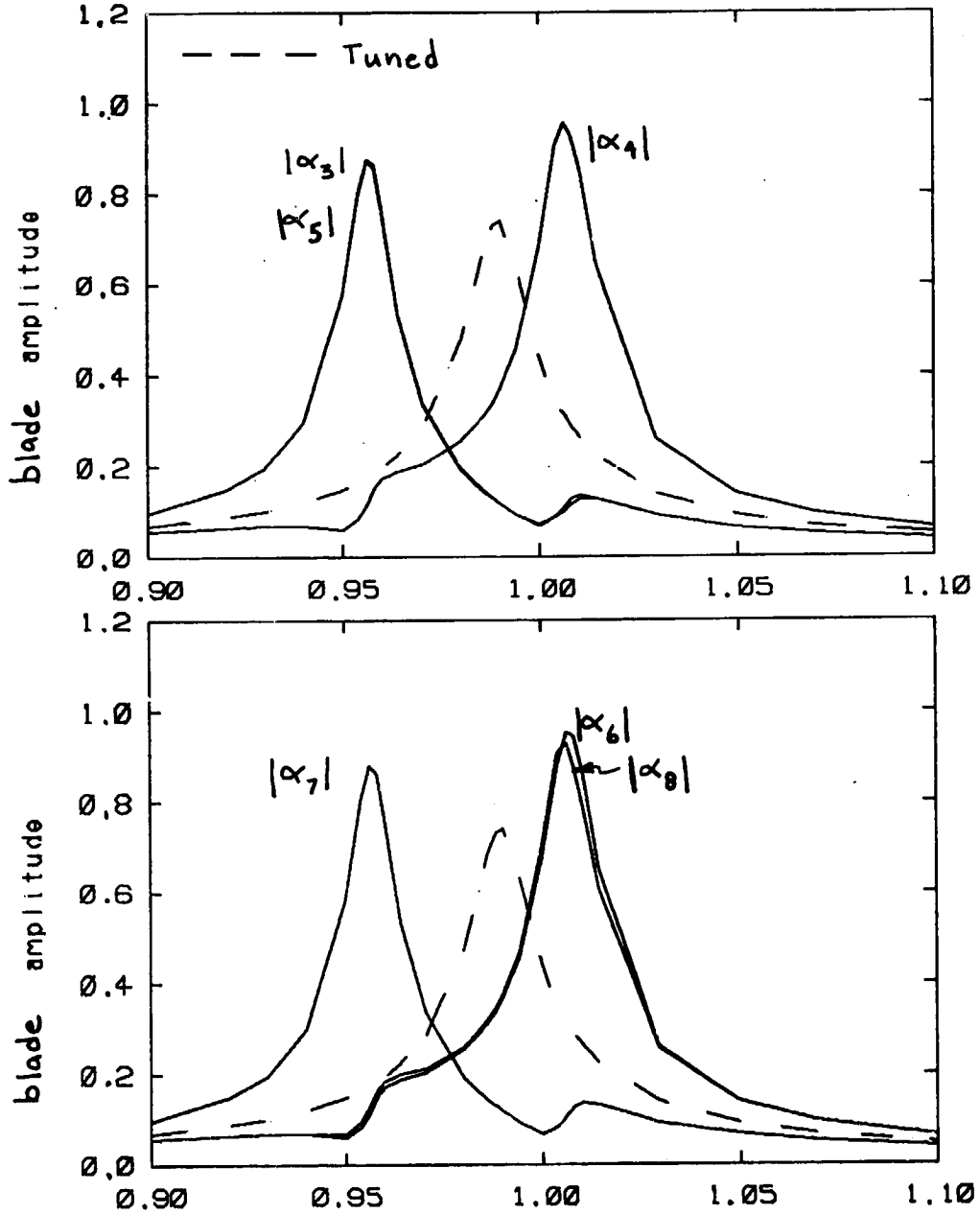

Figure 19. Frequency Response of Blade Amplitudes for 5% "Alternately" Mistuned Cascade

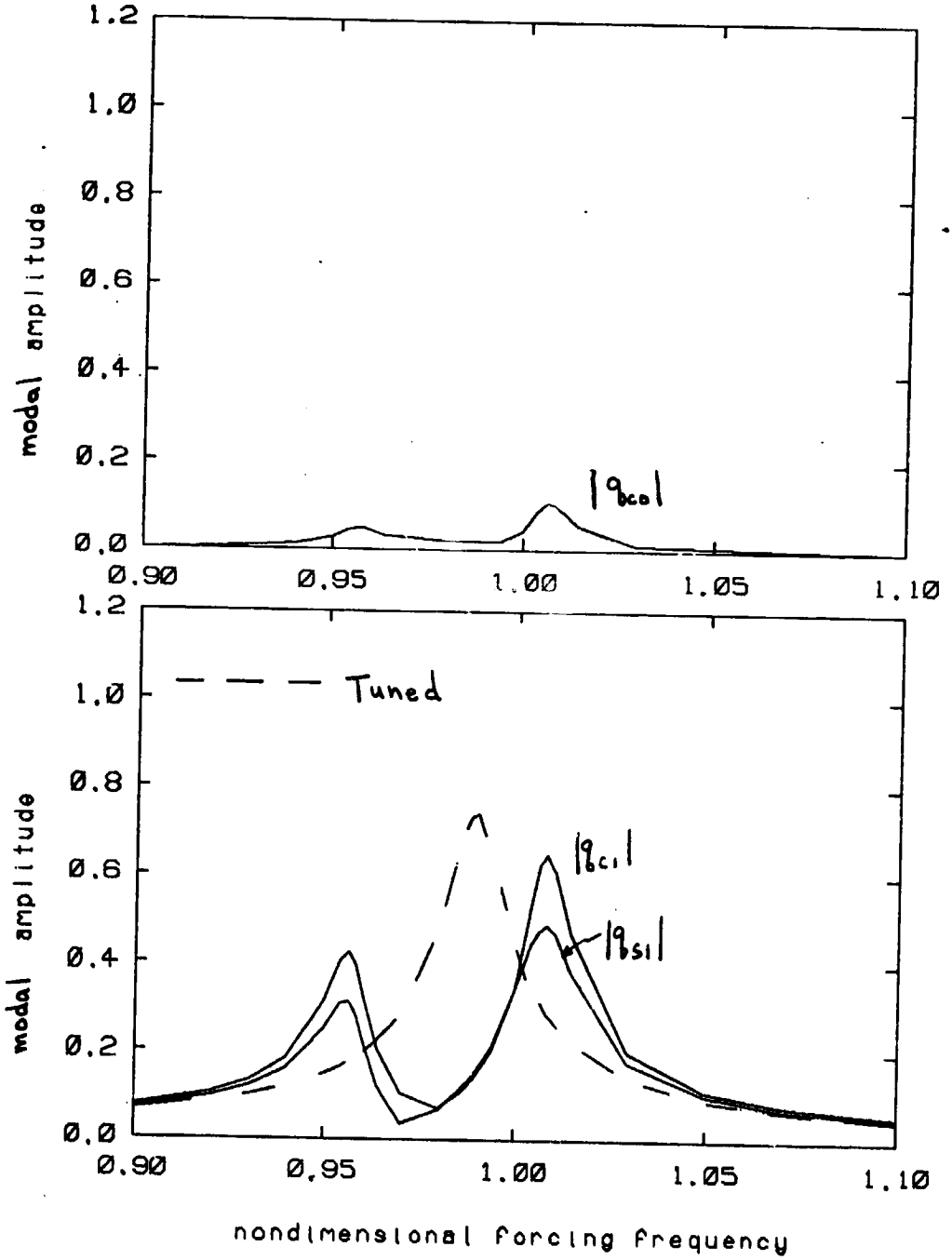

Figure 20. Frequency Response of Modal Amplitudes of an "Alternately" Mistuned Cascade to a One Engine Order Excitation

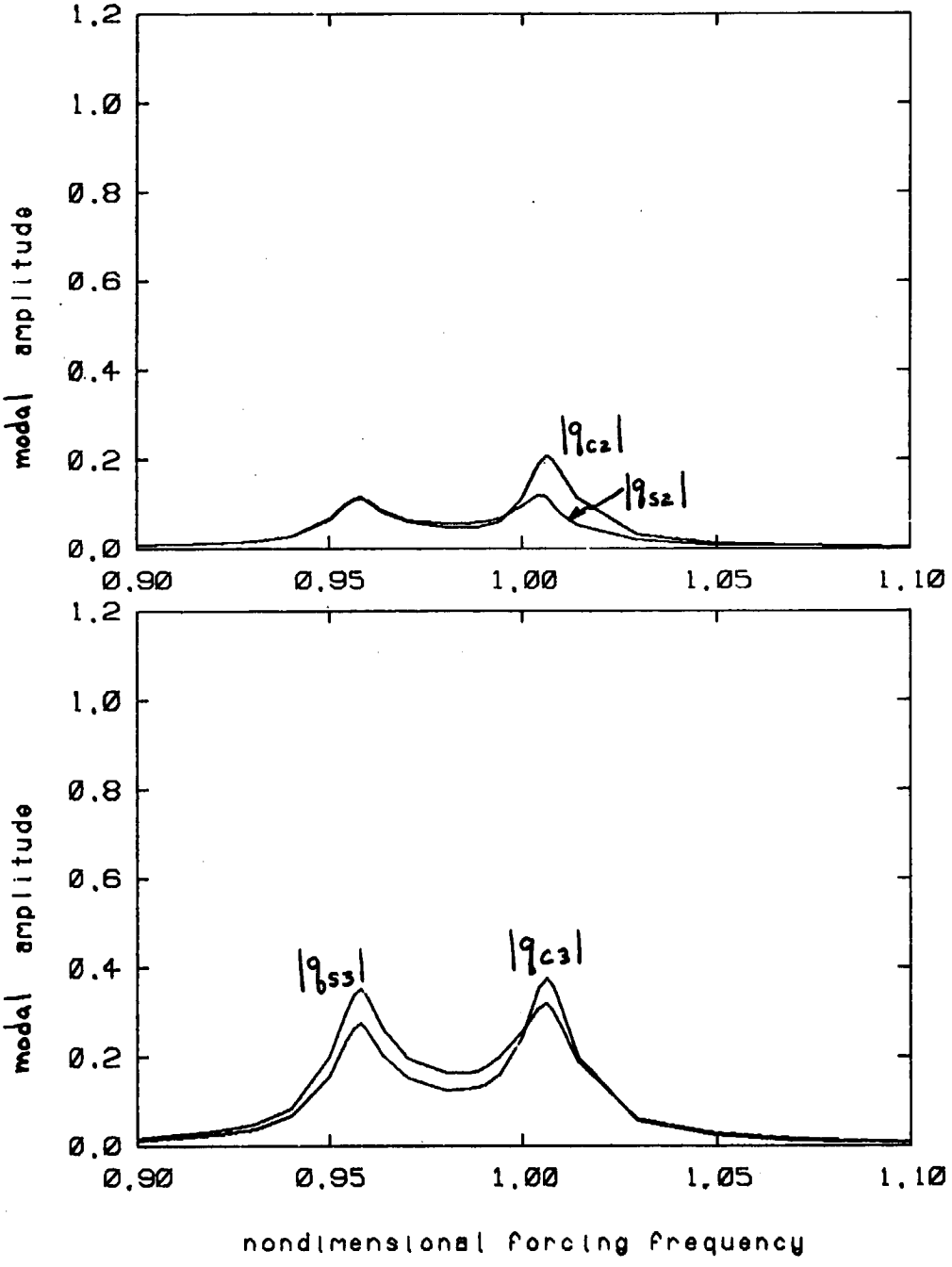

Figure 21. Frequency Response of Modal Amplitudes of an "Alternately"Mistuned Cascade to a One Engine Order Excitation

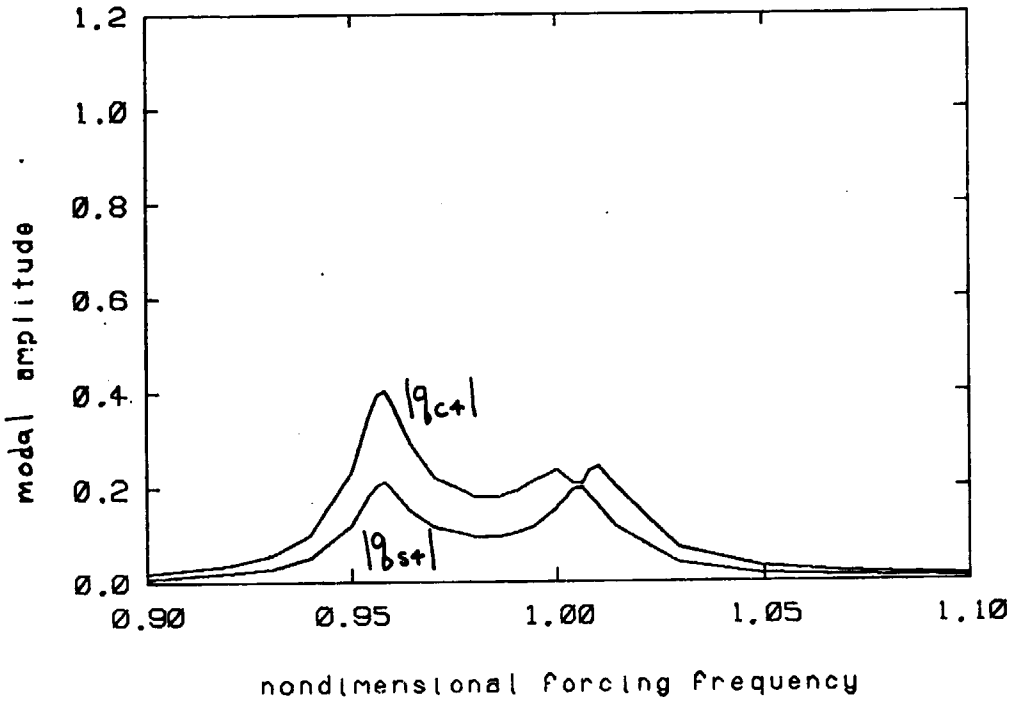

Figure 22. Frequency Response of Modal Amplitudes of an "Alternately" Mistuned Cascade to a One Engine Order Excitation

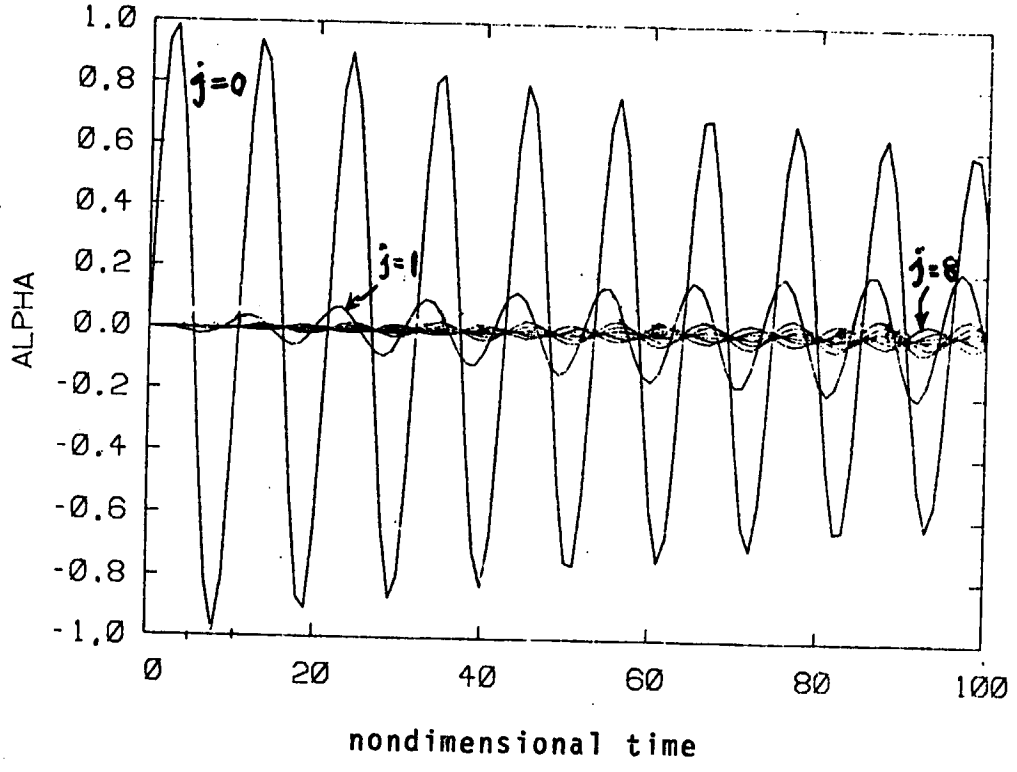

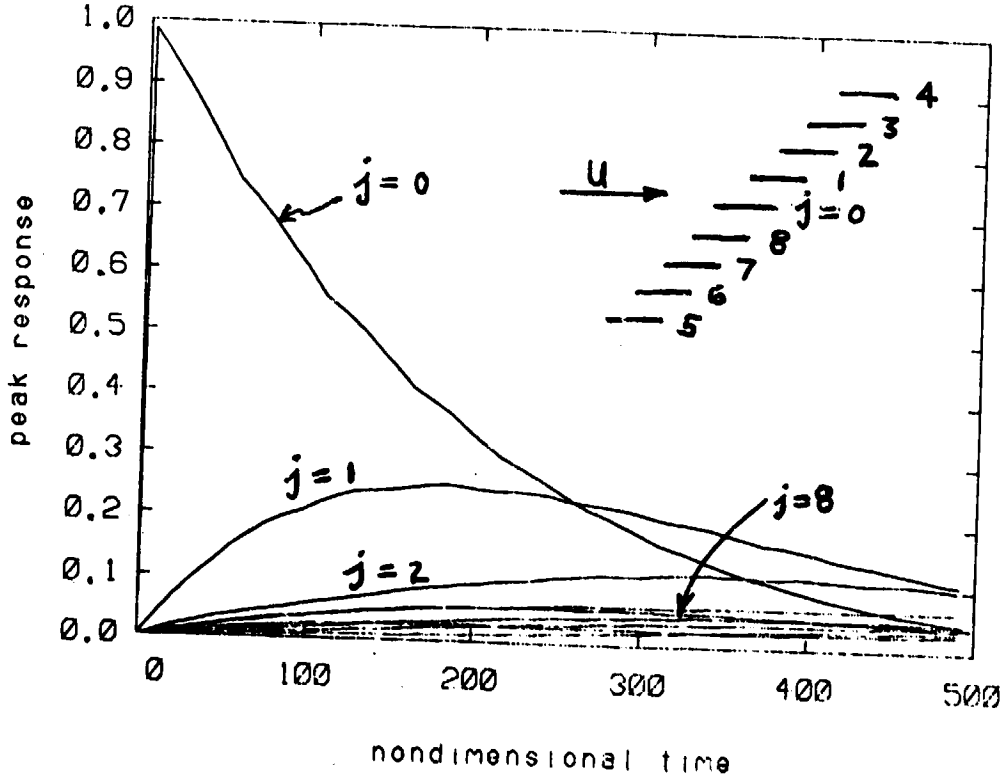

Figure 23. **Transient Response of a Tuned Cascade to Impulsive Loading of Blade "0"**

β_r	Type	B_2	B_1	B_0	G_1	g_0	$\tilde{B}_2$	$\tilde{B}_1$	$\tilde{B}_0$	$\tilde{G}_1$
0°	A	-0.366	-0.305	0.000	0.000	0.000	0.000	0.000	0.000	0.000
	B	0.366	0.860	0.305	0.000	0.000	0.000	0.000	0.000	0.000
	C	0.366	0.110	0.000	0.000	0.000	0.000	0.000	0.000	0.000
	D	-0.432	-0.788	-0.110	0.000	0.000	0.000	0.000	0.000	0.000
36°	A	-0.435	-0.410	0.000	-0.055	0.140	0.000	0.000	0.000	0.000
	B	0.435	1.068	0.800	-0.303	0.140	0.000	0.000	0.000	0.000
	C	0.435	0.184	0.000	0.025	0.140	0.000	0.000	0.000	0.000
	D	-0.498	-0.964	-0.360	0.138	0.140	0.000	0.000	0.000	0.000
72°	A	-0.496	-0.510	0.000	-0.116	0.235	0.000	0.000	0.000	0.000
	B	0.496	1.258	1.005	-0.319	0.235	0.000	0.000	0.000	0.000
	C	0.496	0.256	0.000	0.059	0.235	0.000	0.000	0.000	0.000
	D	-0.560	-1.128	-0.506	0.162	0.235	0.000	0.000	0.000	0.000
108°	A	-0.545	-0.590	0.000	-0.175	0.300	0.000	0.000	0.000	0.000
	B	0.545	1.410	1.173	-0.327	0.300	0.000	0.000	0.000	0.000
	C	0.545	0.316	0.000	0.094	0.300	0.000	0.000	0.000	0.000
	D	-0.610	-1.262	-0.628	0.174	0.300	0.000	0.000	0.000	0.000
144°	A	-0.575	-0.643	0.000	-0.214	0.335	0.000	0.000	0.000	0.000
	B	0.575	1.506	1.283	-0.328	0.335	0.000	0.000	0.000	0.000
	C	0.575	0.354	0.000	0.118	0.335	0.000	0.000	0.000	0.000
	D	-0.638	-1.348	-0.706	0.182	0.335	0.000	0.000	0.000	0.000
180°	A	-0.586	-0.661	0.000	-0.231	0.350	0.000	0.000	0.000	0.000
	B	0.586	1.540	1.321	-0.329	0.350	0.000	0.000	0.000	0.000
	C	0.586	0.366	0.000	0.129	0.350	0.000	0.000	0.000	0.000
	D	-0.648	-1.378	-0.734	0.186	0.350	0.000	0.000	0.000	0.000

Table 1. Transient Whitehead Coefficients

γ = 0 degrees, s/c = 1, η = 0

β_r	Type	B_2	B_1	B_0	G_1	g_0	$\tilde{B}_2$	$\tilde{B}_1$	$\tilde{B}_0$	$\tilde{G}_1$
0°	A	-0.455	-0.427	0.000	0.000	0.000	0.000	0.000	0.000	0.000
	B	0.455	1.119	0.427	0.000	0.000	0.000	0.000	0.000	0.000
	C	0.455	0.182	0.000	0.000	0.000	0.000	0.000	0.000	0.000
	D	-0.524	-1.008	-0.184	0.000	0.000	0.000	0.000	0.000	0.000
36°	A	-0.471	-0.445	0.000	-0.038	0.175	0.000	-0.010	0.000	0.067
	B	0.471	1.159	0.660	-0.156	0.175	0.000	-0.013	-0.370	0.275
	C	0.471	0.202	0.000	0.021	0.175	0.000	0.034	0.000	-0.034
	D	-0.534	-1.044	-0.322	0.090	0.175	0.000	-0.026	0.128	-0.116
72°	A	-0.493	-0.493	0.000	-0.110	0.295	0.000	-0.014	0.000	0.095
	B	0.493	1.236	0.867	-0.216	0.295	0.000	-0.018	-0.308	0.176
	C	0.493	0.242	0.000	0.062	0.295	0.000	0.048	0.000	-0.048
	D	-0.556	-1.112	-0.452	0.118	0.295	0.000	-0.034	0.088	-0.068
108°	A	-0.517	-0.541	0.000	-0.188	0.375	0.000	-0.014	0.000	0.089
	B	0.517	1.314	1.041	-0.234	0.375	0.000	-0.015	-0.222	0.095
	C	0.517	0.282	0.000	0.105	0.375	0.000	0.045	0.000	-0.045
	D	-0.580	-1.180	-0.562	0.128	0.375	0.000	-0.030	0.054	-0.036
144°	A	-0.536	-0.571	0.000	-0.247	0.420	0.000	-0.007	0.000	0.052
	B	0.536	1.368	1.158	-0.234	0.420	0.000	-0.008	-0.116	0.040
	C	0.536	0.312	0.000	0.136	0.420	0.000	0.025	0.000	-0.025
	D	-0.596	-1.230	-0.636	0.128	0.420	0.000	-0.018	0.026	-0.014
180°	A	-0.542	-0.582	0.000	-0.268	0.435	0.000	0.000	0.000	0.000
	B	0.542	1.387	1.198	-0.234	0.435	0.000	0.000	0.000	0.000
	C	0.542	0.322	0.000	0.148	0.435	0.000	0.000	0.000	0.000
	D	-0.602	-1.246	-0.662	0.128	0.435	0.000	0.000	0.000	0.000

Table 2. Transient Whitehead Coefficients

ζ = 45 degrees, s/c = 1, η = 0

	$\beta_r = 0^\circ$		$\beta_r = 36^\circ$	
k	$\bar{A}_A$ - exact	$\bar{A}_A$ - approx	$\bar{A}_A$ - exact	$\bar{A}_A$ - approx
.0	0.000+i0.000	0.000+i0.000	0.000+i0.000	0.000+i0.000
.1	0.004-i0.030	0.004-i0.031	-0.014-i0.067	-0.014-i0.067
.25	0.023-i0.076	0.023-i0.076	-0.014-i0.126	-0.015-i0.126
.5	0.091-i0.152	0.092-i0.153	0.059-i0.220	0.058-i0.219
1.0	0.366-i0.301	0.366-i0.305	0.381-i0.417	0.381-i0.418
	$\beta_r = 72^\circ$		$\beta_r = 108^\circ$	
k	$\bar{A}_A$ - exact	$\bar{A}_A$ - approx	$\bar{A}_A$ - exact	$\bar{A}_A$ - approx
.0	0.000+i0.000	0.000+i0.000	0.000+i0.000	0.000+i0.000
.1	-0.013-i0.093	-0.013-i0.093	-0.012-i0.111	-0.012-i0.112
.25	-0.031-i0.186	-0.031-i0.185	-0.038-i0.233	-0.038-i0.234
.5	0.029-i0.300	0.029-i0.300	0.008-i0.372	0.008-i0.372
1.0	0.385-i0.536	0.386-i0.536	0.385-i0.638	0.384-i0.638
	$\beta_r = 144^\circ$		$\beta_r = 180^\circ$	
k	$\bar{A}_A$ - exact	$\bar{A}_A$ - approx	$\bar{A}_A$ - exact	$\bar{A}_A$ - approx
.0	0.000+i0.000	0.000+i0.000	0.000+i0.000	0.000+i0.000
.1	-0.012-i0.123	-0.012-i0.123	-0.012-i0.127	-0.012-i0.127
.25	-0.041-i0.264	-0.041-i0.263	-0.042-i0.274	-0.041-i0.275
.5	-0.004-i0.421	-0.004-i0.420	-0.008-i0.438	-0.009-i0.439
1.0	0.383-i0.707	0.383-i0.707	0.382-i0.732	0.380-i0.733

Table 3a. Exact Whitehead Coefficients versus Approximate Values, Type A_A

ζ = 0 degrees, s/c = 1, η = 0

	$\beta_r = 0°$		$\beta_r = 36°$	
k	$\bar{A}_B$- exact	$\bar{A}_B$- approx	$\bar{A}_B$- exact	$\bar{A}_B$- approx
.0	- -	0.305+i0.000	0.801+i0.000	0.800+i0.000
.1	0.301+i0.086	0.301+i0.086	0.691-i0.038	0.693-i0.037
.25	0.282+i0.216	0.282+i0.215	0.540+i0.139	0.542+i0.138
.5	0.213+i0.431	0.214+i0.430	0.409+i0.458	0.410+i0.455
1.0	-0.063+i0.860	-0.061+i0.860	0.068+i1.028	0.068+i1.026
	$\beta_r = 72°$		$\beta_r = 108°$	
k	$\bar{A}_B$- exact	$\bar{A}_B$- approx	$\bar{A}_B$- exact	$\bar{A}_B$- approx
.0	1.005+i0.000	1.005+i0.000	1.173+i0.000	1.173+i0.000
.1	0.951+i0.010	0.951+i0.011	1.134+i0.042	1.135+i0.043
.25	0.803+i0.155	0.805+i0.155	1.004+i0.192	1.005+i0.192
.5	0.619+i0.507	0.620+i0.506	0.796+i0.561	0.796+i0.561
1.0	0.207+i1.187	0.207+i1.187	0.329+i1.320	0.328+i1.320
	$\beta_r = 144°$		$\beta_r = 180°$	
k	$\bar{A}_B$- exact	$\bar{A}_B$- approx	$\bar{A}_B$- exact	$\bar{A}_B$- approx
.0	1.238+i0.000	1.283+i0.000	1.321+i0.000	1.321+i0.000
.1	1.250+i0.060	1.250+i0.061	1.290+i0.066	1.290+i0.067
.25	1.129+i0.219	1.130+i0.219	1.172+i0.229	1.173+i0.229
.5	0.912+i0.601	0.913+i0.601	0.952+i0.616	0.954+i0.615
1.0	0.412+i1.408	0.413+i1.407	0.441+i1.438	0.442+i1.437

Table 3b. Exact Whitehead Coefficients versus Approximate Values, Type A_B

ξ = 0 degrees, s/c = 1, η = 0

	$\beta_r = 0°$		$\beta_r = 36°$	
k	$\bar{A}_c$ - exact	$\bar{A}_c$ - approx	$\bar{A}_c$ - exact	$\bar{A}_c$ - approx
.0	0.000+i0.000	0.000+i0.000	0.000+i0.000	0.000+i0.000
.1	-0.004+i0.011	-0.004+i0.011	0.004+i0.030	0.004+i0.030
.25	-0.023+i0.027	-0.023+i0.028	-0.008+i0.056	-0.008+i0.057
.5	-0.092+i0.054	-0.092+i0.055	-0.086+i0.099	-0.086+i0.098
1.0	-0.307+i0.108	-0.366+i0.110	-0.413+i0.188	-0.410+i0.187
	$\beta_r = 72°$		$\beta_r = 108°$	
k	$\bar{A}_c$ - exact	$\bar{A}_c$ - approx	$\bar{A}_c$ - exact	$\bar{A}_c$ - approx
.0	0.000+i0.000	0.000+i0.000	0.000+i0.000	0.000+i0.000
.1	0.004+i0.047	0.004+i0.047	0.004+i0.060	0.004+i0.060
.25	0.000+i0.093	0.000+i0.093	0.004+i0.125	0.004+i0.125
.5	-0.076+i0.151	-0.076+i0.151	-0.068+i0.199	-0.067+i0.199
1.0	-0.442+i0.270	-0.440+i0.269	-0.460+i0.341	-0.459+i0.342
	$\beta_r = 144°$		$\beta_r = 180°$	
k	$\bar{A}_c$ - exact	$\bar{A}_c$ - approx	$\bar{A}_c$ - exact	$\bar{A}_c$ - approx
.0	0.000+i0.000	0.000+i0.000	0.000+i0.000	0.000+i0.000
.1	0.004+i0.068	0.004+i0.068	0.004+i0.071	0.004+i0.071
.25	0.006+i0.145	0.006+i0.145	0.007+i0.152	0.007+i0.153
.5	-0.062+i0.232	-0.062+i0.232	-0.061+i0.244	-0.060+i0.244
1.0	-0.469+i0.390	-0.469+i0.390	-0.472+i0.407	-0.471+i0.406

Table 3c. Exact Whitehead Coefficients versus Approximate Values, Type A_c

β = 0 degrees, s/c = 1, η = 0

	$\beta_r = 0^\circ$		$\beta_r = 36^\circ$	
k	$\bar{A}_D$ - exact	$\bar{A}_D$ - approx	$\bar{A}_D$ - exact	$\bar{A}_D$ - approx
.0	- -	-0.110+i0.000	-0.361+i0.000	-0.360+i0.000
.1	-0.106-i0.079	-0.106-i0.079	-0.309-i0.031	-0.308-i0.031
.25	-0.083-i0.197	-0.083-i0.197	-0.225-i0.184	-0.224-i0.182
.5	-0.002-i0.394	-0.002-i0.394	-0.109-i0.448	-0.108-i0.446
1.0	0.321-i0.787	0.322-i0.788	0.272-i0.946	0.273-i0.945
	$\beta_r = 72^\circ$		$\beta_r = 108^\circ$	
k	$\bar{A}_D$ - exact	$\bar{A}_D$ - approx	$\bar{A}_D$ - exact	$\bar{A}_D$ - approx
.0	-0.506+i0.000	-0.506+i0.000	-0.627+i0.000	-0.628+i0.000
.1	-0.476-i0.055	-0.476-i0.054	-0.603-i0.073	-0.605-i0.074
.25	-0.385-i0.202	-0.385-i0.201	-0.517-i0.229	-0.519-i0.230
.5	-0.234-i0.503	-0.233-i0.502	-0.346-i0.554	-0.348-i0.554
1.0	0.206-i1.093	0.208-i1.092	0.141-i1.214	0.142-i1.214
	$\beta_r = 144^\circ$		$\beta_r = 180^\circ$	
k	$\bar{A}_D$ - exact	$\bar{A}_D$ - approx	$\bar{A}_D$ - exact	$\bar{A}_D$ - approx
.0	-0.707+i0.000	-0.706+i0.000	-0.735+i0.000	-0.734+i0.000
.1	-0.686-i0.085	-0.685-i0.085	-0.714-i0.089	-0.713-i0.089
.25	-0.602-i0.250	-0.601-i0.250	-0.631-i0.257	-0.631-i0.257
.5	-0.422-i0.590	-0.421-i0.590	-0.449-i0.603	-0.447-i0.602
1.0	0.096-i1.293	0.096-i1.293	0.079-i1.320	0.080-i1.320

Table 3d. Exact Whitehead Coefficients versus Approximate Values, Type A_D

ζ = 0 degrees, s/c = 1, η = 0

	$\beta_r = 0°$		$\beta_r = 0°$	
k	$\bar{A}_A$ - exact	$\bar{A}_A$ - approx	$\bar{\bar{A}}_A$ - exact	$\bar{\bar{A}}_A$ - approx
.0	0.000+i0.000	0.000+i0.000	0.000+i0.000	0.000+i0.000
.1	0.004-i0.043	0.005-i0.043	0.000+i0.000	0.000+i0.000
.25	0.028-i0.107	0.028-i0.107	0.000+i0.000	0.000+i0.000
.5	0.113-i0.213	0.114-i0.214	0.000+i0.000	0.000+i0.000
1.0	0.455-i0.423	0.455-i0.427	0.000+i0.000	0.000+i0.000
	$\beta_r = 36°$		$\beta_r = 36°$	
k	$\bar{A}_A$ - exact	$\bar{A}_A$ - approx	$\bar{\bar{A}}_A$ - exact	$\bar{\bar{A}}_A$ - approx
.0	0.000+i0.000	0.000+i0.000	0.000+i0.000	0.000+i0.000
.1	-0.005-i0.060	-0.005-i0.061	0.028-i0.016	0.028-i0.016
.25	0.005-i0.128	0.004-i0.129	0.030-i0.046	0.029-i0.045
.5	0.085-i0.235	0.084-i0.234	0.017-i0.061	0.016-i0.060
1.0	0.433-i0.453	0.434-i0.451	0.002-i0.063	0.001-i0.065
	$\beta_r = 72°$		$\beta_r = 72°$	
k	$\bar{A}_A$ - exact	$\bar{\bar{A}}_A$ - approx	$\bar{A}_A$ - exact	$\bar{\bar{A}}_A$ - approx
.0	0.000+i0.000	0.000+i0.000	0.000+i0.000	0.000+i0.000
.1	-0.006-i0.083	-0.006-i0.083	0.028-i0.010	0.027-i0.010
.25	-0.015-i0.177	-0.015-i0.178	0.045-i0.040	0.043-i0.040
.5	0.042-i0.294	0.042-i0.295	0.036-i0.072	0.035-i0.070
1.0	0.392-i0.522	0.392-i0.523	0.012-i0.086	0.012-i0.087

Table 4a. Exact Whitehead Coefficients versus Approximate Values, Type A_A

ζ = 45 degrees, s/c = 1, η = 0

	$\beta_r = 108^\circ$		$\beta_r = 108^\circ$	
k	$\bar{A}_B$- exact	$\bar{A}_B$- approx	$\bar{\bar{A}}_B$- exact	$\bar{\bar{A}}_B$- approx
.0	0.000+i0.000	0.000+i0.000	0.000+i0.000	0.000+i0.000
.1	-0.007-i0.101	-0.007-i0.101	0.021-i0.006	0.021-i0.006
.25	-0.026-i0.221	-0.026-i0.222	0.038-i0.027	0.038-i0.027
.5	0.009-i0.359	0.009-i0.361	0.037-i0.057	0.036-i0.057
1.0	0.353-i0.600	0.352-i0.603	0.015-i0.075	0.015-i0.078
	$\beta_r = 144^\circ$		$\beta_r = 144^\circ$	
k	$\bar{A}_B$- exact	$\bar{A}_B$- approx	$\bar{\bar{A}}_B$- exact	$\bar{\bar{A}}_B$- approx
.0	0.000+i0.000	0.000+i0.000	0.000+i0.000	0.000+i0.000
.1	-0.008-i0.113	-0.008-i0.113	0.011-i0.003	0.011-i0.003
.25	-0.031-i0.251	-0.031-i0.251	0.021-i0.014	0.021-i0.014
.5	-0.011-i0.406	-0.011-i0.407	0.022-i0.031	0.022-i0.030
1.0	0.327-i0.658	0.326-i0.659	0.010-i0.043	0.012-i0.044
	$\beta_r = 180^\circ$		$\beta_r = 180^\circ$	
k	$\bar{A}_B$- exact	$\bar{A}_B$- approx	$\bar{\bar{A}}_B$- exact	$\bar{\bar{A}}_B$- approx
.0	0.000+i0.000	0.000+i0.000	0.000+i0.000	0.000+i0.000
.1	-0.008-i0.117	-0.008-i0.117	0.000+i0.000	0.000+i0.000
.25	-0.033-i0.261	-0.033-i0.261	0.000+i0.000	0.000+i0.000
.5	-0.017-i0.423	-0.017-i0.424	0.000+i0.000	0.000+i0.000
1.0	0.318-i0.680	0.317-i0.680	0.000+i0.000	0.000+i0.000

Table 4b. Exact Whitehead Coefficients versus Approximate Values, Type A_B

ξ = 45 degrees, s/c = 1, η = 0

	$\beta_r = 0^\circ$		$\beta_r = 0^\circ$	
k	$\bar{A}_B$- exact	$\bar{A}_B$- approx	$\bar{\bar{A}}_B$- exact	$\bar{\bar{A}}_B$- approx
.0	- -	0.427+i0.000	0.000+i0.000	0.000+i0.000
.1	0.423+i0.112	0.422+i0.112	0.000+i0.000	0.000+i0.000
.25	0.399+i0.281	0.399+i0.280	0.000+i0.000	0.000+i0.000
.5	0.314+i0.561	0.313+i0.560	0.000+i0.000	0.000+i0.000
1.0	-0.027+i1.119	-0.028+i1.119	0.000+i0.000	0.000+i0.000
	$\beta_r = 36^\circ$		$\beta_r = 36^\circ$	
k	$\bar{A}_B$- exact	$\bar{A}_B$- approx	$\bar{\bar{A}}_B$- exact	$\bar{\bar{A}}_B$- approx
.0	0.660+i0.000	0.660+i0.000	0.000+i0.370	0.000+i0.370
.1	0.613+i0.047	0.617+i0.049	0.112+i0.309	0.117+i0.302
.25	0.520+i0.216	0.526+i0.216	0.127+i0.193	0.126+i0.185
.5	0.400+i0.532	0.403+i0.531	0.082+i0.127	0.079+i0.125
1.0	0.038+i1.133	0.038+i1.133	0.034+i0.093	0.034+i0.103
	$\beta_r = 72^\circ$		$\beta_r = 72^\circ$	
k	$\bar{A}_B$- exact	$\bar{A}_B$- approx	$\bar{\bar{A}}_B$- exact	$\bar{\bar{A}}_B$- approx
.0	0.867+i0.000	0.867+i0.000	0.000+i0.308	0.000+i0.308
.1	0.839+i0.057	0.840+i0.058	0.047+i0.293	0.052+i0.290
.25	0.744+i0.202	0.746+i0.202	0.078+i0.242	0.082+i0.234
.5	0.582+i0.524	0.584+i0.523	0.068+i0.183	0.068+i0.177
1.0	0.176+i1.178	0.175+i1.177	0.030+i0.135	0.030+i0.146

Table 4c. Exact Whitehead Coefficients versus Approximate Values, Type A_B

$\mathfrak{F}$ = 45 degrees, s/c = 1, η = 0

	$\beta_r = 108^\circ$		$\beta_r = 108^\circ$	
k	$\bar{A}_B$- exact	$\bar{A}_B$- approx	$\bar{\bar{A}}_B$- exact	$\bar{\bar{A}}_B$- approx
.0	1.041+i0.000	1.041+i0.000	0.000+i0.222	0.000+i0.222
.1	1.021+i0.073	1.020+i0.073	0.020+i0.217	0.022+i0.216
.25	0.937+i0.220	0.937+i0.221	0.038+i0.196	0.040+i0.193
.5	0.762+i0.544	0.762+i0.545	0.038+i0.162	0.038+i0.161
1.0	0.319+i1.237	0.319+i1.237	0.017+i0.124	0.016+i0.139
	$\beta_r = 144^\circ$		$\beta_r = 144^\circ$	
k	$\bar{A}_B$- exact	$\bar{A}_B$- approx	$\bar{\bar{A}}_B$- exact	$\bar{\bar{A}}_B$- approx
.0	1.157+i0.000	1.158+i0.000	0.000+i0.116	0.000+i0.116
.1	1.140+i0.084	1.140+i0.084	0.007+i0.114	0.008+i0.114
.25	1.063+i0.239	1.063+i0.239	0.014+i0.107	0.016+i0.106
.5	0.887+i0.568	0.887+i0.569	0.016+i0.092	0.016+i0.098
1.0	0.422+i1.284	0.423+i1.284	0.006+i0.073	0.006+i0.082
	$\beta_r = 180^\circ$		$\beta_r = 180^\circ$	
k	$\bar{A}_B$- exact	$\bar{A}_B$- approx	$\bar{\bar{A}}_B$- exact	$\bar{\bar{A}}_B$- approx
.0	1.198+i0.000	1.198+i0.000	0.000+i0.000	0.000+i0.000
.1	1.181+i0.088	1.181+i0.088	0.000+i0.000	0.000+i0.000
.25	1.107+i0.247	1.106+i0.246	0.000+i0.000	0.000+i0.000
.5	0.931+i0.578	0.929+i0.578	0.000+i0.000	0.000+i0.000
1.0	0.460+i1.302	0.459+i1.301	0.000+i0.000	0.000+i0.000

Table 4d. Exact Whitehead Coefficients versus Approximate Values, Type A_B

ζ = 45 degrees, s/c = 1, η = 0

	$\beta_r = 0°$		$\beta_r = 0°$	
k	$\bar{A}_c$ - exact	$\bar{A}_c$ - approx	$\bar{\bar{A}}_c$ - exact	$\bar{\bar{A}}_c$ - approx
.0	0.000+i0.000	0.000+i0.000	0.000+i0.000	0.000+i0.000
.1	-0.005+i0.018	-0.005+i0.018	0.000+i0.000	0.000+i0.000
.25	-0.029+i0.046	-0.028+i0.046	0.000+i0.000	0.000+i0.000
.5	-0.115+i0.092	-0.114+i0.091	0.000+i0.000	0.000+i0.000
1.0	-0.459+i0.182	-0.455+i0.182	0.000+i0.000	0.000+i0.000
	$\beta_r = 36°$		$\beta_r = 36°$	
k	$\bar{A}_c$ - exact	$\bar{A}_c$ - approx	$\bar{\bar{A}}_c$ - exact	$\bar{\bar{A}}_c$ - approx
.0	0.000+i0.000	0.000+i0.000	0.000+i0.000	0.000+i0.000
.1	0.000+i0.029	0.000+i0.029	-0.009+i0.007	-0.009+i0.007
.25	-0.016+i0.060	-0.015+i0.060	-0.006+i0.020	-0.004+i0.020
.5	-0.100+i0.108	-0.099+i0.108	0.007+i0.028	0.012+i0.027
1.0	-0.451+i0.206	-0.451+i0.206	0.026+i0.036	0.037+i0.029
	$\beta_r = 72°$		$\beta_r = 72°$	
k	$\bar{A}_c$ - exact	$\bar{A}_c$ - approx	$\bar{\bar{A}}_c$ - exact	$\bar{\bar{A}}_c$ - approx
.0	0.000+i0.000	0.000+i0.000	0.000+i0.000	0.000+i0.000
.1	0.001+i0.043	0.001+i0.043	-0.008+i0.004	-0.010+i0.005
.25	-0.005+i0.091	-0.005+i0.091	-0.009+i0.017	-0.012+i0.020
.5	-0.078+i0.148	-0.077+i0.148	0.004+i0.033	0.003+i0.036
1.0	-0.437+i0.259	-0.436+i0.259	0.033+i0.047	0.035+i0.044

Table 4e. Exact Whitehead Coefficients versus Approximate Values, Type A_c

ζ = 45 degrees, s/c = 1, η = 0

	$\beta_r = 108^\circ$		$\beta_r = 108^\circ$	
k	$\bar{A}_c$ - exact	$\bar{A}_c$ - approx	$\bar{\bar{A}}_c$ - exact	$\bar{\bar{A}}_c$ - approx
.0	0.000+i0.000	0.000+i0.000	0.000+i0.000	0.000+i0.000
.1	0.002+i0.054	0.002+i0.054	-0.005+i0.002	-0.007+i0.003
.25	0.000+i0.119	0.000+i0.119	-0.007+i0.011	-0.010+i0.014
.5	-0.062+i0.191	-0.062+i0.191	-0.002+i0.026	-0.001+i0.029
1.0	-0.426+i0.317	-0.425+i0.317	0.028+i0.041	0.030+i0.039
	$\beta_r = 144^\circ$		$\beta_r = 144^\circ$	
k	$\bar{A}_c$ - exact	$\bar{A}_c$ - approx	$\bar{\bar{A}}_c$ - exact	$\bar{\bar{A}}_c$ - approx
.0	0.000+i0.000	0.000+i0.000	0.000+i0.000	0.000+i0.000
.1	0.002+i0.062	0.002+i0.062	-0.002+i0.001	-0.003+i0.001
.25	0.002+i0.138	0.002+i0.138	-0.004+i0.006	-0.005+i0.007
.5	-0.054+i0.222	-0.054+i0.223	0.001+i0.014	0.000+i0.015
1.0	-0.419+i0.359	-0.420+i0.361	0.016+i0.023	0.016+i0.021
	$\beta_r = 180^\circ$		$\beta_r = 180^\circ$	
k	$\bar{A}_c$ - exact	$\bar{A}_c$ - approx	$\bar{\bar{A}}_c$ - exact	$\bar{\bar{A}}_c$ - approx
.0	0.000+i0.000	0.000+i0.000	0.000+i0.000	0.000+i0.000
.1	0.002+i0.064	0.002+i0.065	0.000+i0.000	0.000+i0.000
.25	0.003+i0.144	0.003+i0.144	0.000+i0.000	0.000+i0.000
.5	-0.051+i0.233	-0.051+i0.234	0.000+i0.000	0.000+i0.000
1.0	-0.416+i0.375	-0.416+i0.376	0.000+i0.000	0.000+i0.000

Table 4f. Exact Whitehead Coefficients versus Approximate Values, Type A_c

$\frac{\pi}{4}$ = 45 degrees, s/c = 1, η = 0

	$\beta_r = 0°$		$\beta_r = 0°$	
k	$\bar{A}_D$ - exact	$\bar{A}_D$ - approx	$\bar{\bar{A}}_D$ - exact	$\bar{\bar{A}}_D$ - approx
.0	- -	-0.184+i0.000	0.000+i0.000	0.000+i0.000
.1	-0.179-i0.101	-0.179-i0.101	0.000+i0.000	0.000+i0.000
.25	-0.151-i0.253	-0.151-i0.252	0.000+i0.000	0.000+i0.000
.5	-0.053-i0.505	-0.053-i0.504	0.000+i0.000	0.000+i0.000
1.0	0.339-i1.009	0.340-i1.008	0.000+i0.000	0.000+i0.000
	$\beta_r = 36°$		$\beta_r = 36°$	
k	$\bar{A}_D$ - exact	$\bar{A}_D$ - approx	$\bar{\bar{A}}_D$ - exact	$\bar{\bar{A}}_D$ - approx
.0	-0.322+i0.000	-0.322+i0.000	0.000-i0.129	0.000-i0.128
.1	-0.294-i0.066	-0.295-i0.066	-0.050-i0.103	-0.053-i0.099
.25	-0.228-i0.220	-0.228-i0.219	-0.061-i0.055	-0.061-i0.050
.5	-0.109-i0.495	-0.108-i0.494	-0.050-i0.028	-0.049-i0.025
1.0	0.299-i1.029	0.299-i1.029	-0.045-i0.016	-0.046-i0.015
	$\beta_r = 72°$		$\beta_r = 72°$	
k	$\bar{A}_D$ - exact	$\bar{A}_D$ - approx	$\bar{\bar{A}}_D$ - exact	$\bar{\bar{A}}_D$ - approx
.0	-0.451+i0.000	-0.452+i0.000	0.000-i0.089	0.000-i0.088
.1	-0.433-i0.075	-0.434-i0.075	-0.023-i0.083	-0.024-i0.081
.25	-0.366-i0.219	-0.368-i0.220	-0.042-i0.063	-0.042-i0.060
.5	-0.223-i0.504	-0.225-i0.504	-0.048-i0.040	-0.047-i0.038
1.0	0.215-i1.080	0.213-i1.080	-0.054-i0.024	-0.052-i0.025

Table 4g. Exact Whitehead Coefficients versus Approximate Values, Type A_D

ξ = 45 degrees, s/c = 1, η = 0

	$\beta_r = 108^\circ$		$\beta_r = 108^\circ$	
k	$\bar{A}_D$ - exact	$\bar{A}_D$ - approx	$\bar{\bar{A}}_D$ - exact	$\bar{\bar{A}}_D$ - approx
.0	-0.561+i0.000	-0.562+i0.000	0.000-i0.055	0.000-i0.054
.1	-0.547-i0.086	-0.548-i0.086	-0.011-i0.053	-0.012-i0.052
.25	-0.486-i0.236	-0.486-i0.236	-0.023-i0.045	-0.024-i0.043
.5	-0.335-i0.528	-0.335-i0.529	-0.033-i0.033	-0.032-i0.031
1.0	0.130-i1.138	0.130-i1.138	-0.044-i0.022	-0.042-i0.022
	$\beta_r = 144^\circ$		$\beta_r = 144^\circ$	
k	$\bar{A}_D$ - exact	$\bar{A}_D$ - approx	$\bar{\bar{A}}_D$ - exact	$\bar{\bar{A}}_D$ - approx
.0	-0.635+i0.000	-0.636+i0.000	0.000-i0.026	0.000-i0.026
.1	-0.622-i0.094	-0.623-i0.094	-0.005-i0.025	-0.005-i0.025
.25	-0.565-i0.251	-0.565-i0.251	-0.010-i0.023	-0.011-i0.022
.5	-0.411-i0.551	-0.412-i0.552	-0.017-i0.018	-0.016-i0.018
1.0	0.070-i1.183	0.069-i1.184	-0.024-i0.012	-0.023-i0.014
	$\beta_r = 180^\circ$		$\beta_r = 180^\circ$	
k	$\bar{A}_D$ - exact	$\bar{A}_D$ - approx	$\bar{\bar{A}}_D$ - exact	$\bar{\bar{A}}_D$ - approx
.0	-0.661+i0.000	-0.662+i0.000	0.000+i0.000	0.000+i0.000
.1	-0.649-i0.097	-0.650-i0.097	0.000+i0.000	0.000+i0.000
.25	-0.592-i0.256	-0.593-i0.256	0.000+i0.000	0.000+i0.000
.5	-0.438-i0.559	-0.439-i0.560	0.000+i0.000	0.000+i0.000
1.0	0.048-i1.200	0.048-i1.199	0.000+i0.000	0.000+i0.000

Table 4h. Exact Whitehead Coefficients versus Approximate Values, Type A_D

ξ = 45 degrees, s/c = 1, η = 0

type	B_2	B_1	B_0	G_1	g_0
A	-0.470	-0.526	0.000	-0.072	0.130
B	0.565	1.229	1.000	-0.244	0.130
C	0.485	0.263	0.000	0.036	0.130
D	-0.595	-1.114	-0.500	0.122	0.130

Moments taken about the leading edge, $\eta = 0.0$, or $a = -1$

Alternate coefficients can also be obtained using the known theoretical two dimensional coefficients together with a rough approximation to the Theodorsen function as $C(p) = (.55\ p + .15)/(p + .15)$. This would result in the alternate coefficients,

type	B_2	B_1	B_0	G_1	g_0
A	-0.500	-0.550	0.000	-0.068	0.150
B	0.500	1.325	1.000	-0.349	0.150
C	0.500	0.275	0.000	0.034	0.150
D	-0.563	-1.163	-0.500	0.174	0.150

Table 5. Transient Theodorsen Coefficients $\eta = 0.0$

k	A_A - exact	A_A - approx	A_B - exact	A_B - approx
.0	0.000+i0.000	0.000+i0.000	1.000+i0.000	1.000+i0.000
.1	-0.012-i0.083	-0.022-i0.087	0.853+i0.003	0.904+i0.005
.25	-0.016-i0.168	-0.027-i0.161	0.737+i0.185	0.773+i0.207
.5	0.050-i0.299	-0.050-i0.280	0.586+i0.548	0.630+i0.555
1.0	0.400-i0.539	0.399-i0.535	0.190+i1.208	0.195+i1.198

k	A_c - exact	A_c - approx	A_D - exact	A_D - approx
.0	0.000+i0.000	0.000+i0.000	-0.500+i0.000	-0.500+i0.000
.1	0.004+i0.042	0.008+i0.044	-0.423-i0.051	-0.449-i0.052
.25	-0.006+i0.084	-0.002+i0.080	-0.351-i0.213	-0.367-i0.229
.5	-0.087+i0.150	-0.088+i0.140	-0.215-i0.524	-0.237-i0.527
1.0	-0.450+i0.270	-0.450+i0.270	0.218-i1.104	0.215-i1.098

$$l = 2\pi\rho U^2 b \left\{ A_A \frac{\bar{h}}{b} + A_B \bar{\alpha} \right\} e^{i\omega t}$$

$$m = 2\pi\rho U^2 b^2 \left\{ A_c \frac{\bar{h}}{b} + A_D \bar{\alpha} \right\} e^{i\omega t}$$

Table 6. Exact Theodorsen Coefficients versus Approximate Values, $\eta = 0.0$

β_r	Mode	Amount of Mode Present at Flutter Point		
		Tuned	Blade "0" Mistuned	"Alternate" Mistuning
0°	$\cos j\beta_0$	0.00	0.15	0.14
40°	$\cos j\beta_1$	1.00	0.59	1.00
	$\sin j\beta_1$	1.00	0.52	0.91
80°	$\cos j\beta_2$	0.00	0.86	0.32
	$\sin j\beta_2$	0.00	1.00	0.15
120°	$\cos j\beta_3$	0.00	0.40	0.31
	$\sin j\beta_3$	0.00	0.32	0.16
160°	$\cos j\beta_4$	0.00	0.30	0.62
	$\sin j\beta_4$	0.00	0.08	0.30

Table 7. Multiblade Modes Present at Flutter

N = 9, γ = 45 degrees, s/c = 1, η = 0.5

N = 9

The engine order n will excite the structural modes $\sin j\beta_r$ and $\cos j\beta_r$ as follows:	
n	r
0, 9, 18, 27,.....	0
1,8,10,17,19,26,28,.....	1
2,7,11,16,20,25,29,.....	2
3,6,12,15,21,24,30,.....	3
4,5,13,14,22,23,31,.....	4

Table 8. Structural Modes Responding to Engine order Excitation - Tuned Rotor, N = 9

		$\mathcal{J}_A$					
k	1/k	β_r = 40 degrees		β_r = 80 degrees		β_r = 120 degrees	
		exact	approx	exact	approx	exact	approx
.1	10	-0.1682	-0.1722	-0.1561	-0.1588	-0.0886	-0.0889
.25	4	-0.0078	-0.0083	-0.0084	-0.0082	0.0008	0.0008
.5	2	0.0011	0.0009	0.0013	0.0013	0.0034	0.0032
1.0	1	0.0011	0.0010	0.0012	0.0011	0.0015	0.0015

$\Xi = 45^\circ \quad s/c = 1 \quad \nu = 86.2 \quad \eta = 0.5$

Table 9. Exact Aerodynamic Damping versus Approximate Values

$$\underset{\sim}{P} = \begin{bmatrix}
1 & 1 & 0 & 1 & 0 & 1 & 0 & 1 & 0 \\
1 & .7660 & .6428 & .1736 & .9848 & -.5000 & .8660 & -.9397 & .3420 \\
1 & .1736 & .9848 & -.9397 & .3420 & -.5000 & -.8660 & .7660 & -.6428 \\
1 & -.5000 & .8660 & -.5000 & -.8660 & 1 & 0 & -.5000 & .8660 \\
1 & -.9397 & .3420 & .7660 & -.6428 & -.5000 & .8660 & .1736 & -.9848 \\
1 & -.9397 & -.3420 & .7660 & .6428 & -.5000 & -.8660 & .1736 & .9848 \\
1 & -.5000 & -.8660 & -.5000 & .8660 & 1 & 0 & -.5000 & -.8660 \\
1 & .1736 & -.9848 & -.9397 & -.3420 & -.5000 & .8660 & .7661 & .6428 \\
1 & .7660 & -.6428 & .1736 & -.9848 & -.5000 & -.8660 & -.9397 & -.3420
\end{bmatrix}$$

See equations (2-39) and (2-42)

Table 10. Values of Basic $\underset{\sim}{P}$ Matrix for N = 9

β_r	B_2	B_1	B_0	G_1	g_0	$\tilde{B}_2$	$\tilde{B}_1$	$\tilde{B}_0$	$\tilde{G}_1$
0°	-.069	-.134	.243	0	0	0	0	0	0
40°	-.063	-.128	.346	-.090	.188	0	-.015	-.240	.188
80°	-.063	-.127	.429	-.155	.313	0	-.017	-.209	.144
120°	-.062	-.124	.493	-.198	.390	0	-.012	-.142	.087
160°	-.060	-.120	.528	-.221	.427	0	-.005	-.050	.030
Isolated airfoil	-.015	-.148	.500	-.158	.130	0	0	0	0

Values interpolated from general Table 2 for pitching about midchord ($\eta = .5$) and for N = 9

Table 11. Transient Whitehead Coefficients for Torsional Flutter Analysis. Type D, N = 9, $\xi = 45^0$, s/c = 1, $\eta = .5$

i	$(E_2)_{i0}$	$(E_1)_{i0}$	$(E_0)_{i0}$	$(H_1)_{i0}$	$(g_0)_1$	$(H_2)_{i0}$	$(g_0)_2$	$(H_3)_{i0}$	$(g_0)_3$	$(H_4)_{i0}$	$(g_0)_4$
5	-.001	-.001	-.002	.005	.188	-.006	.313	.005	.390	-.002	.427
6	-.001	0	.007	-.026	↓	.045	↓	-.044	↓	.019	↓
7	0	.002	.020	-.045	↓	.021	↓	.039	↓	-.033	↓
8	-.001	.006	.049	-.042	↓	-.038	↓	.005	↓	.044	↓
0	-.063	-.126	.426	-.020	↓	-.034	↓	-.044	↓	-.049	↓
1	-.001	-.011	-.174	.012	↓	.026	↓	.039	↓	.049	↓
2	0	-.002	-.048	.038	↓	.043	↓	.005	↓	-.042	↓
3	-.001	-.001	-.024	.046	↓	-.011	↓	-.044	↓	.030	↓
4	-.001	-.001	-.011	.033	↓	-.047	↓	.039	↓	-.015	↓
Isolated airfoil	-.015	-.148	.500	-.158	.130	0	0	0	0	0	0

Table 12. Moment at Blade i due to motion of Blade 0.

N = 9, $\xi = 45^0$, s/c = 1, η = .5 (midchord)